Spinal Fusion and Computer Methods: An FEA study into Ovine Lumbar Vertebrae Fusion

A Master of Engineering Thesis

Sebastian Jones

72957752

Abstract

Spinal fusion is a surgery undertaken to relieve pain or degeneration in the spine. This involves the fixing together of two or more vertebrae and the promotion of bone growth to fuse the vertebrae together. Diagnosis time for spinal fusion surgery averages 4 months and the economic costs of lost productivity are significant. The ability to measure the process of spinal fusion in real time would have the potential to reduce the diagnosis time by half as the fusion mass created during the spinal fusion healing process is strong enough to support normal activities before it becomes visible on medical imaging methods. Implantable sensors would allow for the loads through the spine to be measured, allowing doctors to give their patients a shorter recovery plan based on how their spine is fusing.

Sheep are an ideal analogue for human spinal implant development as they have a spine structure that closely matches the human spine, and thus spinal implants can be tested on sheep for verification of design to ensure that human trials have a higher likelihood of success. A large research gap found was the lack of sheep models that allow the virtual prototyping of spine implants before an animal study is required.

This thesis discusses the construction of such a model from CT imaging to CAD to the construction of an FEA model. The FEA model considers the effect of material strength changes in the bone healing zones (fusion mass) and how load transference though the spine is affected. The model shows that with gradual increase in bone strength and stiffness, strain through the pedicle rods is reduced. This thesis also discusses the development of methods to measure stiffness changes on fused sheep spines. The mechanical testing apparatus was partially verified by testing sheep spines subjected to simulated spinal fusion.

Acknowledgments

Firstly, I would like to thank Dr Debbie Munro for providing this project and the advice that went along with it. I really could not have done this project without your help. I would like to thank Julian Phillips and Oscar Torres for your support in bringing together hardware and software for the lab work required for this project. Thank you to Digby Symons for FEA related advice. Thank you to Nadia, Sam and Martin out at Lincoln for the CT imaging. Special mention to Simon Blue, and Nina Pernus for discussing ideas and keeping me sane. And finally, a thank you to Nuts & Bolts Café for keeping me caffeinated.

Contents

Table of Figures

Table of Tables

Glossary

ACRONYM	DESCRIPTION
BHZ	Bone healing zones, also. known as the fusion mass.
CAD	Computer aided design.
FEA/FE	Finite element analysis/Finite Element.
CT	Computed tomography.
STL	CAD file type based on triangular mesh.

Chapter 1. Background and Introduction

1.1 What is spinal fusion?

Spinal fusion is the surgical process of fixing two or more vertebrae relative to each other and promoting bone growth between vertebrae to ensure permanent fusion [6]. This is done primarily to resolve the pain associated with degenerative spinal diseases such as spondylolysis, arthritis, or degenerative disc disease as a last resort treatment option [7]. Spinal fusion surgery is also used for stabilisation of the spine in cases of structural degeneration. The leading theory to the success of these surgeries is that a reduction of movement between vertebrae reduces the irritation and impingement of nerves leading from the spinal canal and causes a reduction in the pain felt by the patient [6].

There are two primary methods of spinal fusion undertaken: Intervertebral fusion, where the intervertebral disc is partially or wholly removed and a weight-bearing cage implanted to provide structure for morselised bone to grow around [8]; and posterolateral fusion, where the intervertebral discs are left intact, and the fusion area is located between the transverse processes of the adjacent vertebrae [9].

According to one study, patient outcomes vary with non-union observed in approximately one out of 10 cases and a minimum of 20% of surgeries considered unsuccessful in treating the original issue [10]. In the USA alone, upwards of 200,000 spinal fusion surgeries are performed per year. This results in considerable economic cost due to the surgery itself and additionally the lost productivity due to a recommended healing time of up to 6 months [10].

1.2 How is it tested/modelled in FEA?

Modelling spinal fusion involves procuring a geometric model of the spine, building a model for an FEA (finite element analysis) solver such as Abaqus or ANSYS [11]. To best build a model, CT imagery is acquired and converted into a usable CAD format. This model is then optimised for import into an FEA solver. A mesh, material properties, and boundary conditions are applied. The model is then run and solved for a particular desired stress, strain, load response. For the process of spinal fusion an area of fusion, the “fusion mass” also needs to be created [12]. The influence of the fusion mass (thus how the model handles the healing process) can either be controlled with specified size changes or by variation of material properties. Both approaches can potentially be used at once in well-informed modelling cases. Ideally, the analysis incorporates features that are measurable for physical verification studies. Further enhancements could include instrumented pedicle fixation applied digitally to the model that match typical vertebral fixation methods.

1.3 Use of sheep as an analogue for human lumbar spine

Sheep are an ideal domesticated species that are frequently used for research into spinal fusion, and sheep are an important species as their spine shape and size are similar to the human spine [13,14]. The bone growth rate is also similar. On average sheep, vertebrae are longer but narrower than the average human vertebrae, but are similar in volume, structure, and level of articulation. Because of this similarity, surgical techniques and implant designs for spinal fusion are often developed on sheep before being sanctioned for use on humans. Sheep are used to prove viability, which often takes 6 months or more for the process of healing to fully complete. The largest advantage scientifically is that sheep can be euthanised at certain points post treatment for comprehensive analysis to be undertaken. This is especially important in the development of fixation methods such as pedicle screws, where otherwise the only way to observe progress would be through medical imaging such as Computed Tomography (CT). Highly invasive analysis such as this cannot be done with human patients for clear ethical reasons.

1.4 Identified Gap

The easiest and cheapest method of testing is virtually. Through a model of the spine, methods and implant designs can be tested to achieve the best outcomes before there is a need to fabricate components or prepare a surgery. There are several good FEA models for the human spine that have been verified with cadaver studies. Because sheep are frequently used in research and development in this field, an ovine spine model would be useful because it could remove some of the need or extent of animal studies. However, there are no models that model the process of spinal fusion, nor are there available models of the ovine lumbar spine that have the fidelity needed for modelling spinal fusion. The existence of an ovine spine FE model that considers the structural and material changes that occur in spinal fusion would be highly useful for the development of implants and techniques for the spine and would allow better understanding of the process of spinal fusion.

1.5 Thesis statement:

This thesis aims to increase understanding of spinal fusion and how the strength of the spine changes over the healing process. It aims to create a finite element model of the ovine lumbar spine that incorporates the strength changes of the bone in the fusion mass during the healing process in a way that is measurable and verifiable.

1.6 Content of this Thesis

This thesis discusses the digital recreation of a sheep's lumbar spine using CT scans, spinal instrumentation models, and the use of a variety of modelling tools to create a functional FEA model of a sheep spine. This model was then used for simulating different levels of bony fusion and correlating strain in spinal instrumentation. Development of testing methods for the mechanical validation of this model is then discussed.

Chapter 2 Methods

The research undertaken in this thesis can be grouped into several primary activities:

1. A literature review into the following areas: Spinal FEA and modelling techniques, comparative studies between sheep and human vertebrae, the current state of implantable sensors, and material properties of bone and other tissue types present in the bone healing process.
2. The processing of CT imagery to a CAD model stable and comprehensive enough for import into an FEA solver.
3. Building and running of a Finite Element study (FEA).
4. The development of test methods and equipment for the verification of the FEA spine model.

Each subtopic of this thesis is its own chapter, starting with the literature review and continuing through CAD model development, FEA study, mechanical testing, etc. The methods section below summarises the key methods used for each part of the thesis.

2.1 Literature review

The literature review was grouped into several parts: research into previous methodologies and FEA studies of the spine (and other bone structures were applicable), research into bone and other tissues for their material properties, and research into the state of implantable measuring devices and other methods. The literature review can further be grouped into two main sections: Initial research into spinal fusion, implantable sensors and suitability of sheep as a spinal research analogue undertaken initially for the research proposal, and research primarily into material properties of bone and other materials for use in the FEA models (as well as FEA modelling approaches for the spine).

2.2 CT to CAD process

To make a model of the ovine lumbar spine, a geometric model had to be obtained. This was done through the conversion of a CT image set of a Romney ewe with several pieces of software: 3D Slicer, ITK Snap, MeshLab, Meshmixer, GeoMagic Freeform, and SolidWorks. To do this a CT scan of a sheep vertebrae was acquired from the Lincoln University's Johnstone Research Station and a higher resolution set of scans from the MARS Institute. The conversion process began with taking a segmentation of the CT scans with the contrast number associated with bone. This produced a spine vertebrae STL type geometry. This vertebral model was then cleaned with a set of programs before import into SolidWorks where it could be modified with spinal fixation and prepared for import into an FEA solver.

This process took several iterations and experiments with certain software suites to find the best workflow and cleanest results. The facet joints of the spine proved to be a difficult feature to resolve correctly.

2.3 FEA studies

This portion of the research discusses the iterative process of FEA modelling the lumbar spine. It shows the development from models that served as validation checks for freshly imported geometry using default mesh and material settings to comprehensive studies that show the slow change of material properties during healing. There are two main models discussed: The Basic model, an early model for development purposes and the Advanced model. The Advanced model contains the most up to date material properties and geometry and uses the research into material strengths to

educate the model. Within the Advanced model there are two main iterations with the main difference being the material set used with each one.

2.4 Development of testing procedures

To verify the findings of the FEA studies, a test setup needed to be developed to mechanically test ovine spines. This was to be for the mechanical testing of ovine spines in varying states of fusion harvested during an intended sheep study. The ongoing effects of the COVID-19 pandemic prevented this sheep study from occurring. However, the methods and tooling for mechanical spine testing were developed, nevertheless. The test apparatus was designed around National Instruments' LabVIEW software and related NI hardware because of its versatility. This setup was able to be used with an unpowered drill press for verification of its function. Later, an Instron ElectroPuls E3000 test stand will be used for programmable and precise mechanical testing. The drill rig test setup included two rotary encoders, a button load cell, and a spinal rod-mounted strain gauge as well as a series of mounts and adapters. This setup was used to experiment with a 3D printed ABS and rubber simulation spine and again with an explanted sheep spine. While there were accommodations that had to be made to fit the drill press apparatus, simulated spinal fusion was undertaken and showed the sensors would respond to a simulated increase of spine stiffness.

Chapter 3 Literature Review

3.1 Introduction and aims:

The overall aim of the literature review was to research and summarise previous work done into the strength of the bone healing process, specifically the healing process during a posterolateral fusion (fusion of transverse processes). Research was conducted in the following areas:

- Existing mechanical data on the bone healing process
- Similar studies, implants and FEA work
- Species comparative studies into the lumbar spine
- implantable sensors

Many studies covered some of these topics but rarely all topics in detail. The literature that was most useful and influential detailed:

1. The mechanical properties of tissues and specifically the types of bone, cartilage, and tendons.
2. Patents and the use of implantable strain sensors for orthopaedic strain measurement.
3. Live and cadaver studies involving bone fusion or healing. The most useful articles contained information of the sheep trials of products and procedures intended for humans such as intervertebral cages and other fixation methods.

3.2 General tissue properties

3.2.1 Bone and tissue healing properties

Osteoclasts and osteoblasts remove and form bone, respectively. This happens quickly at first and forms a calcium and collagen matrix that is considered a bone equivalent of scar tissue called woven bone. This new bone then remodels over time to optimise its strength and shape [15]. New bone generally becomes visible via X-ray when it begins to remodel. The strength of woven bone is of interest because of the potential for it to be mechanically strong enough to support the normal loads of the upper body [16]. Proving this would allow for a reduced recovery period post spinal fusion surgery.

Spinal fusion surgery is primarily done to immobilise a set of vertebrae to prevent pain and pressure on the nerves leading from the spine [6]. In a posterolateral spinal fusion, morselised bone is laid down between the transverse processes of adjacent vertebrae. The vertebrae are fixed with pedicle screws and rods and the bone begins to grow into a callus, fusing the two vertebrae together. The lumbar vertebrae, which this thesis models, take most of the load of the torso and upper body. As the bone fuses and strengthens, it slowly relieves the pedicle fixation of its load [16].

The major assumptions about a single-level, lumbar spinal fusion surgery is that the vertebrae and surrounding joints are separate before the surgery and fixed after the surgery, acting as a single (large) vertebral body. As a rule of thumb, tissues between the vertebrae can be considered as soft tissue (ligaments, tendons, cartilage, and muscle) before the surgery and solidified bone afterwards. However, in cases where the intervertebral disc is not removed, there is always some movement across the fusion site. Healing tissues progress from soft tissues to a woven bone that is then remodelled to lamellar and cancellous bone. This process takes about two years.

While the mechanical strengths of some types of tissue are adequately documented, the strengths of bone healing at various stages are not documented as well. It was found that final tissue strengths are better documented as proper testing can be achieved from cadaver studies. Several other

species have similar lumbar spines and bone physiology to humans. Sheep and deer are used as spine research platforms for spinal products and methods intended for humans. Sheep are the preferred species for this as they are more readily available, and their physiologies are better understood due to the larger degree of domestication.

Table 3.1: Final strengths of spinal tissues [3]. This study compared the cervical spine of sheep and humans. The lumbar spine has similar properties but a larger geometry.

Material	Young's modulus (MPa)		Poisson's ratio		Cross-sectional area (mm^2)	
	SCS	HCS	SCS	HCS	SCS	HCS
Cortical bone	12,000	12,000	0.29	0.29	–	–
Cancellous bone	450	450	0.29	0.29	–	–
Posterior element	3500	3500	0.29	0.29	–	–
Endplates	2000	2000	0.4	0.4	–	–
Annulus grounds	5 (Anterior region)	3.4	0.45	0.4	–	–
	2.5 (Posterior region)		0.45		–	
	1 (Lateral region)		0.45		–	
Nucleus	1	1	0.49	0.49	–	–
ALL	5.77 (≦11%, 12.84 (>11%)	30	0.3	0.3	14.42	6.1
PLL	1.62 (≦27%, 28.264 (>27%)	20	0.3	0.3	7.46	5.4
CL	2.87 (≦32%, 33.19 (>32%)	20	0.3	0.3	109.06	50.1
LF	1.89 (≦27%, 40.78 (>27%)	1.5	0.3	0.3	24.15	46.6
ISL	1.22 (≦15%, 58.74 (>15%)	1.5	0.3	0.3	28.98	13.1
PEEK	3600		0.4		–	
Graft bone	3500		0.29		–	

ALL anterior longitudinal ligament, *PLL* posterior longitudinal ligament, *FL* flaval ligament, *CL* facet capsular ligament, *ISL* interspinous ligament, *PEEK* polyetheretherketone

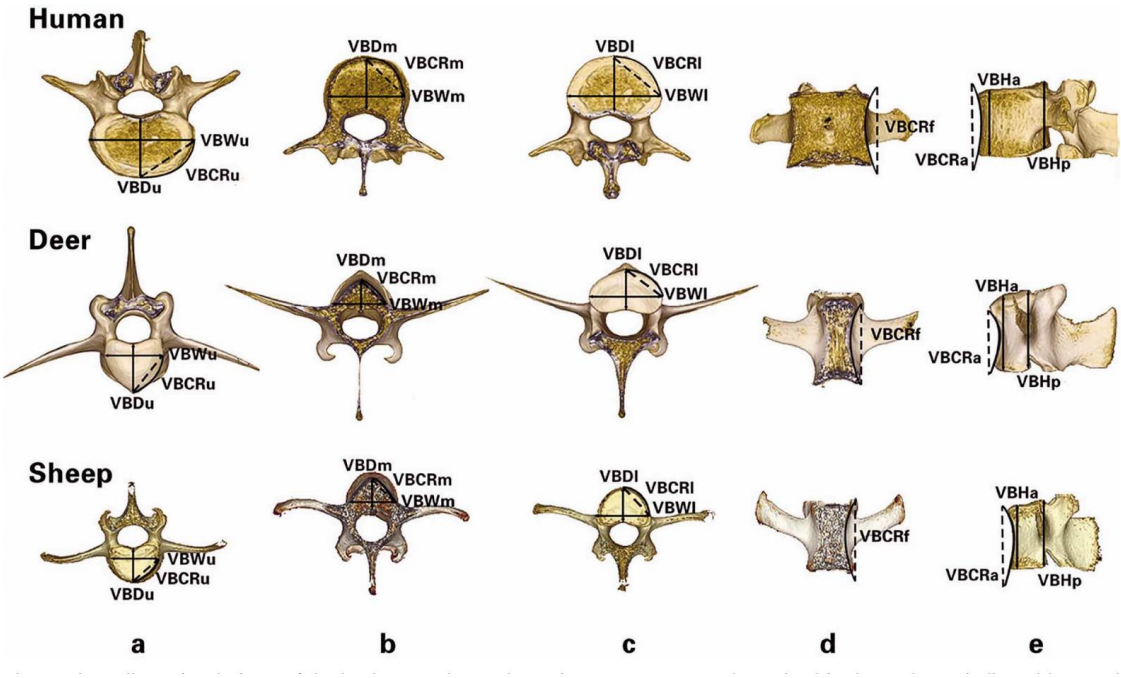

Figure 3.1: Three-dimensional views of lumbar vertebrae from various species showing similarities and differences. The various measurements used are common for describing vertebral dimensions and how these compare across vertebral types.[3]

3.2.2 Spinal fusion FEA studies

A finite element model of spinal fusion and biomechanics have been used for the design and optimisation of implants/fixation methods and how they interact with bone, and working FEA bone and muscle models of the human spine can be purchased commercially. However, these models do not feature fractures, fusions or other conditions. Specific studies often detail specific fixture options to stabilise a fracture and have FEA results for that case.

FEA work involving the sheep spine is rare. The sheep lumbar and cervical spine is similar in size to their human counterparts so are often used to test devices intended for spinal fusion. Despite the use of them as a similar testbed for trials of spinal medical devices, there is limited literature on how the spine behaves with fusion over time during healing. Most studies on the subject are either cadaveric sheep or concerned with the safety and effectiveness of the product used. In one study [17], flat edge and curved intervertebral cages were used for cadaver tests in human and sheep cervical spines to compare similarities and suitability of the cages in sheep and then FEA models of the human spine. Results were then verified with cadaveric sheep models. Although focused on the cervical spine, this study was useful as it discussed verifying FEA work or sheep spines using cadaver studies.

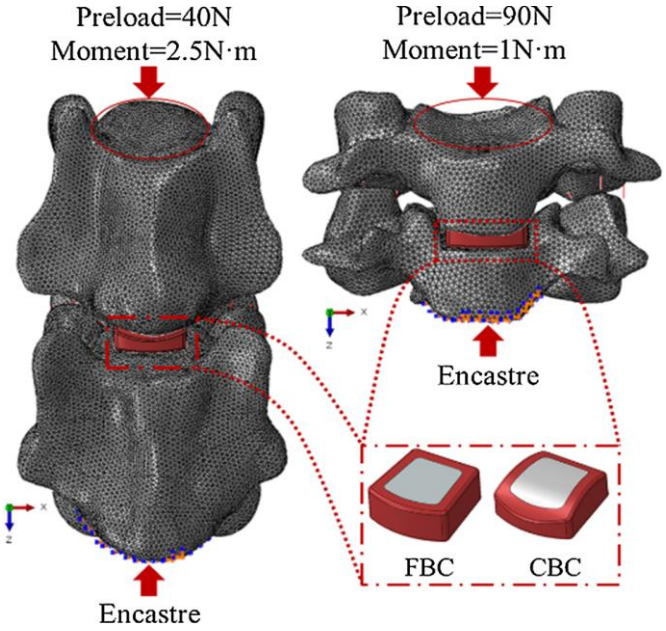

Figure 3.2: FEA modelling of intervertebral cages for the thoracic spine shows the potential and complexity of problems that can be analysed. This style of analysis is also easily applied to the lumbar spine region.[15]

FEA often is just a tool used for informing a design. Software suites like ANSYS are used for FEA and can be used for topology optimisation such as in the design of compliant intervertebral cages [4]. Implants like these are designed for human use and verified with cadaver testing or other compliant testing methods like Sawbones™ spine models. A study on cervical cages[3] highlighted early FEA and its ability to assist in design.

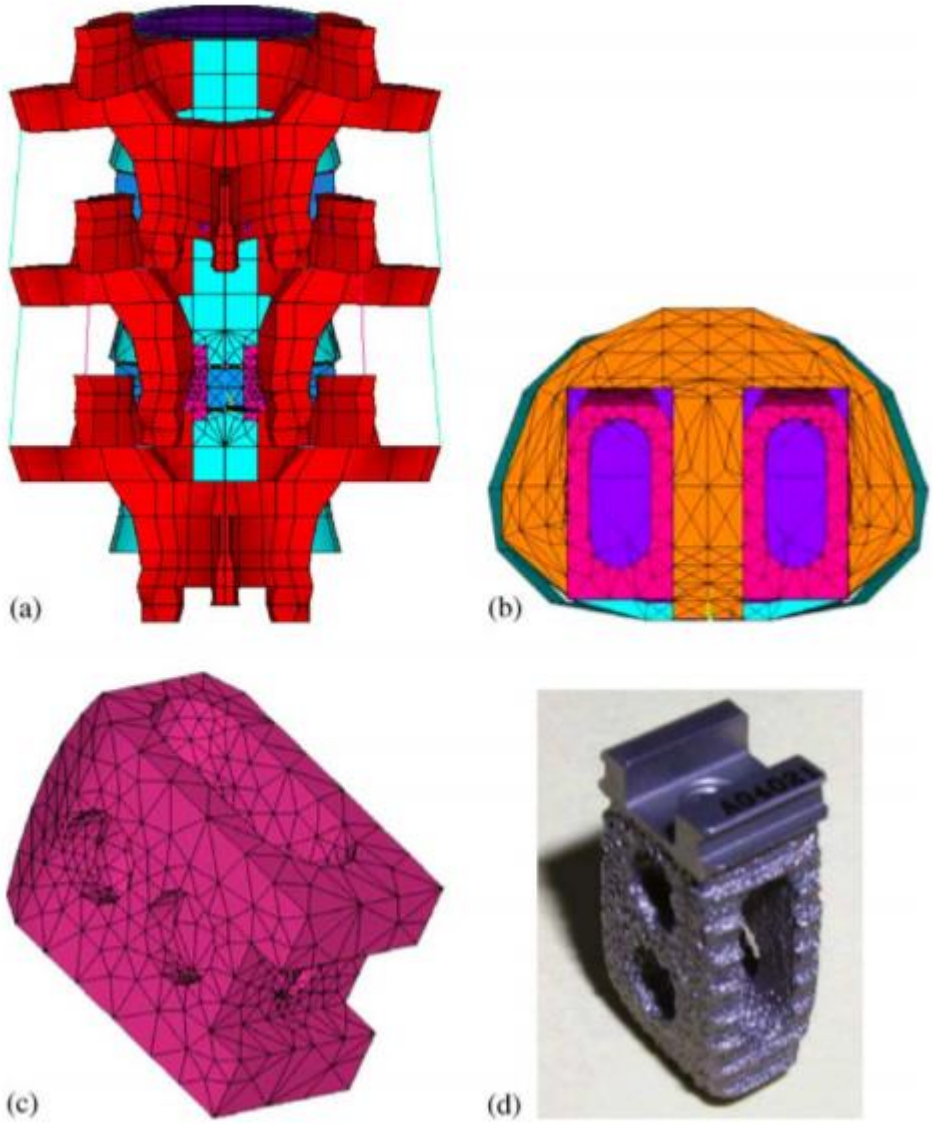

Figure 3.3: Early FEA of spine and resultant intervertebral cage design [4].

More modern software offers more refined mesh handling and allows better resolution for FEA results, and thus modern studies more realistically match what is observed in real life. The biomechanics of the spine are a great application of FEA due to the complexity in geometry, boundary conditions and design challenges involved. Due to a large amount of variation between individual spines, producing a general bone model that fits all cases is challenging. In one study, in order to produce an average set of spine characteristics (rotation angles, change in stress during certain movements, etc), multiple FEA models were run on 5 different human spines from L1-L5 to account for variation [18]. Results were averaged and compared to a range of experimental results and

literature. In general, the larger the participant pool of a study, the more accurate the results are likely to be. Xu's study[16] highlighted how to produce a modern FEA model as shown in Figure 3.4 and 3.5.

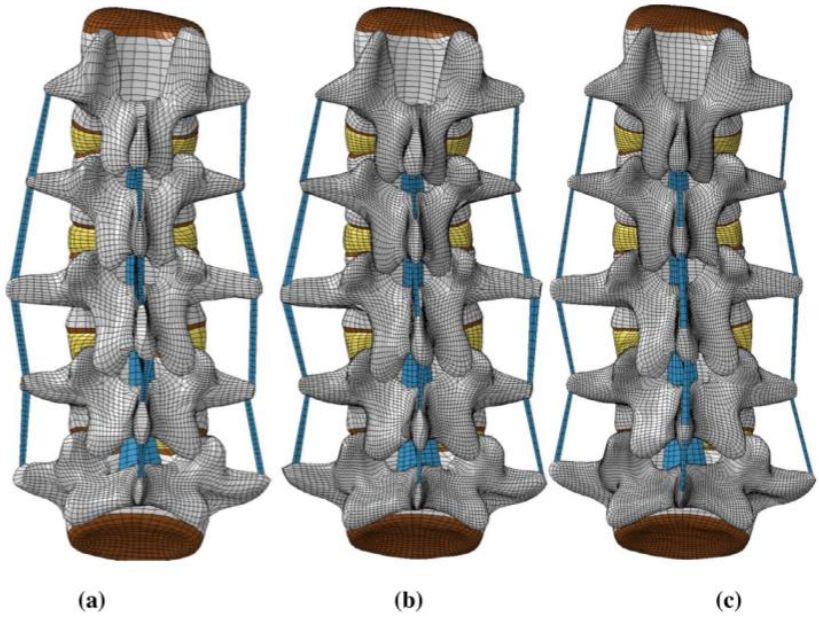

Figure 3.4: Xu study showing the possible resolution of modern FEA methods.

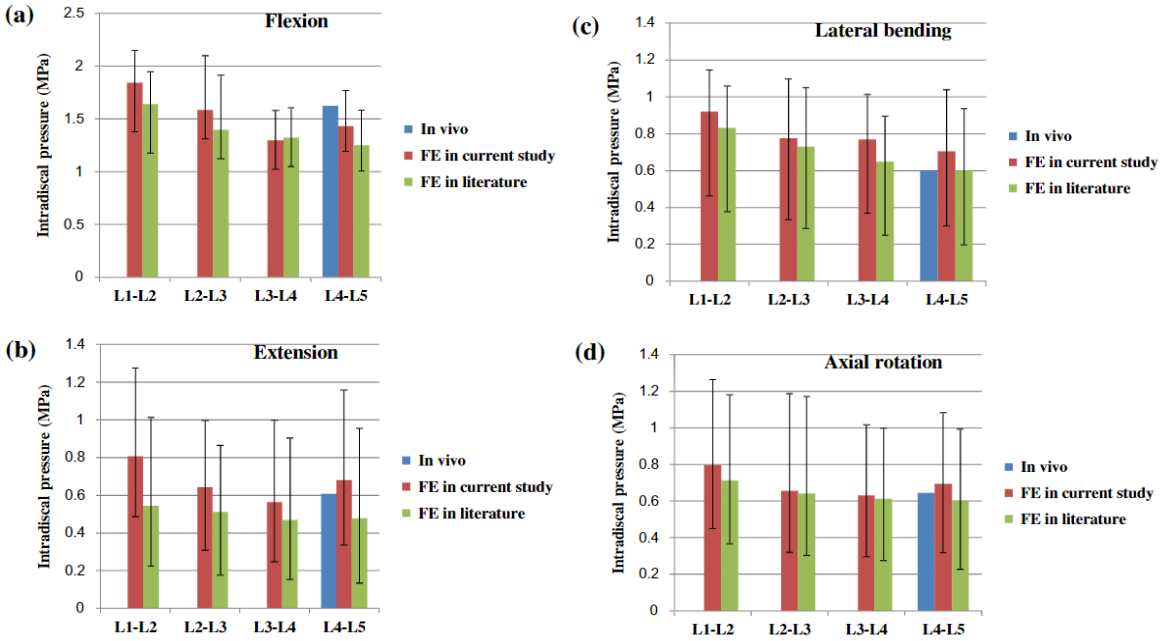

Figure 3.5: Stress changes of the intervertebral disc at the prescribed movement condition of the spine.

3.3 Studies on implants

For studying implants, mechanical strain gauge devices are a great candidate for this purpose. Mechanical strain devices require little training to use beyond the radiology analysis skills common for doctors, surgeons, and radiologists. The devices require no electronics and therefore are easier to calibrate and sterilise. One example of such a device is shown in Figure 3.6 for femur fixation [3]. This sensor was proven workable during a cadaver study.

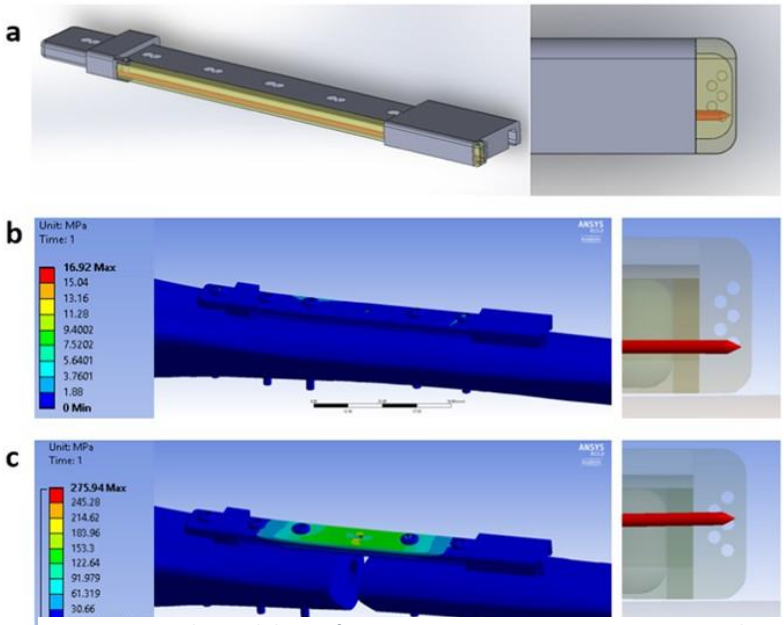

Figure 3.6: Mechanical device for measuring strain via X-Ray images and associated FEA study of the internal stresses for this process [3].

Another example for strain data capture is the use of nanogels. These can be implanted anywhere in the body during minimally invasive procedures and can be used with bone, tissue, and cartilage. In Figure 3.7, Zinc Oxide granules were added to a nanogel matrix and this was then attached to cadaveric tissue samples through sutures or medical adhesive [5]. The strain experienced was visible on X-ray and ultrasound imaging by the change in length and width/diameter of the gel implant.

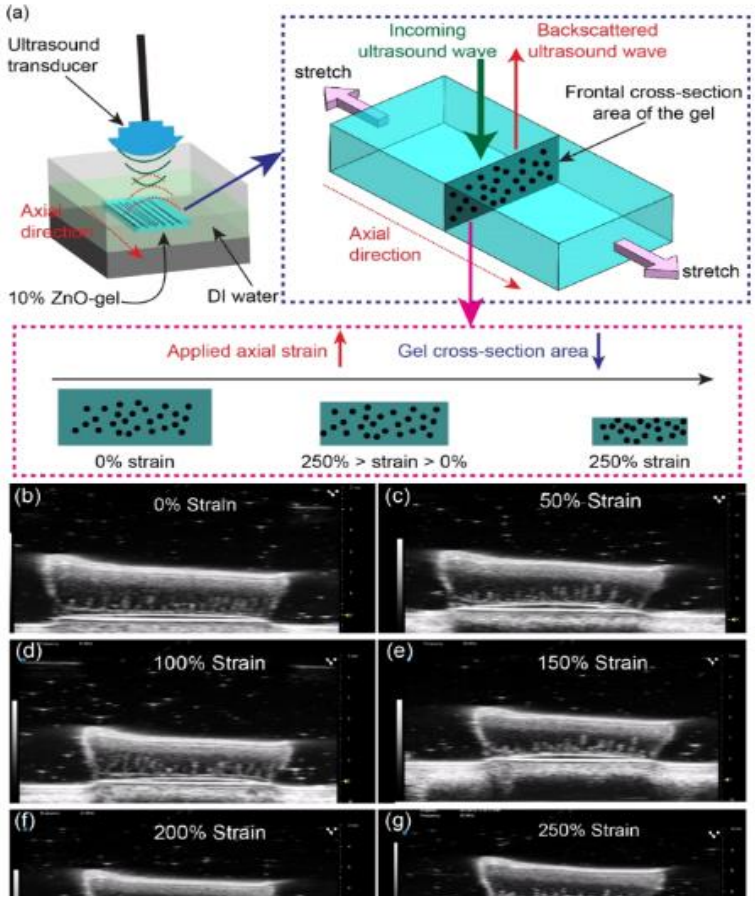

Figure 3.7: nanogel strain measuring system for ultrasound monitoring showing how the ZnO particles reflect ultrasound and how this arrangement changes due to strain [5].

Several patents exist for wirelessly powered implantable sensors for directly measuring strain. Among these are designs that clip onto the existent spinal rods [1], and those that have the sensors integrated within the rod and housing [19] (Figure 3.8). In addition, implantable pressure sensors are used for internal pressure readings such as blood pressure in the aorta or cranial fluid pressure. Pressure sensors could perhaps read spinal stresses if implanted into the intervertebral discs. The sensors patented by Dr Munro use a custom strain sensor and associated electronics in a wireless battery-free design that is integrated with the spinal rod [19] (Figure 3.9). A version of this has already been used for a sheep study run by Dr Munro while at UC Davis. This version of the sensor required an implanted battery pack to provide the voltage for wireless transmission. The present sheep study planned for this thesis will use a fully wireless version of Dr Munro's sensor that can power on inductively. By removing the battery, the sensor and spinal fusion surgery to implant It will be less complex and less likely to fail.

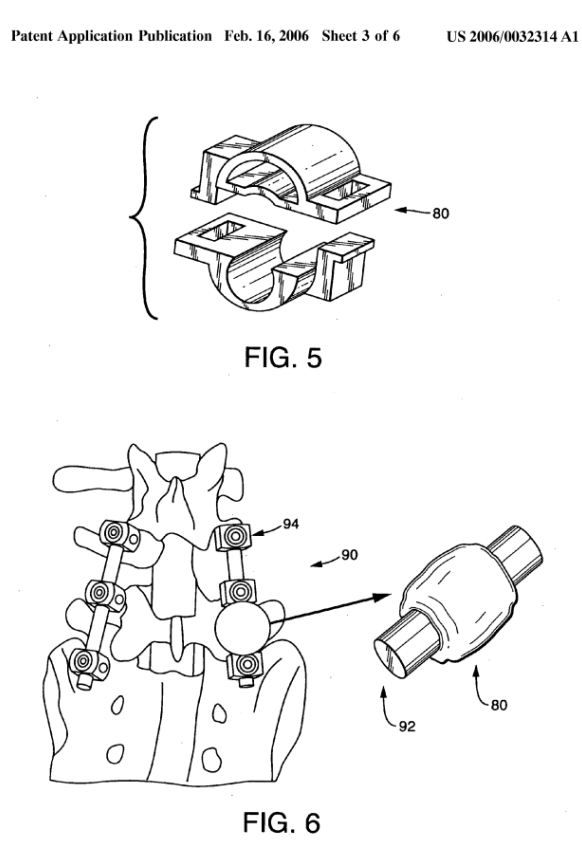

Figure 3.8: Patent for a strain sensor that attaches to pedicle fixation [1].

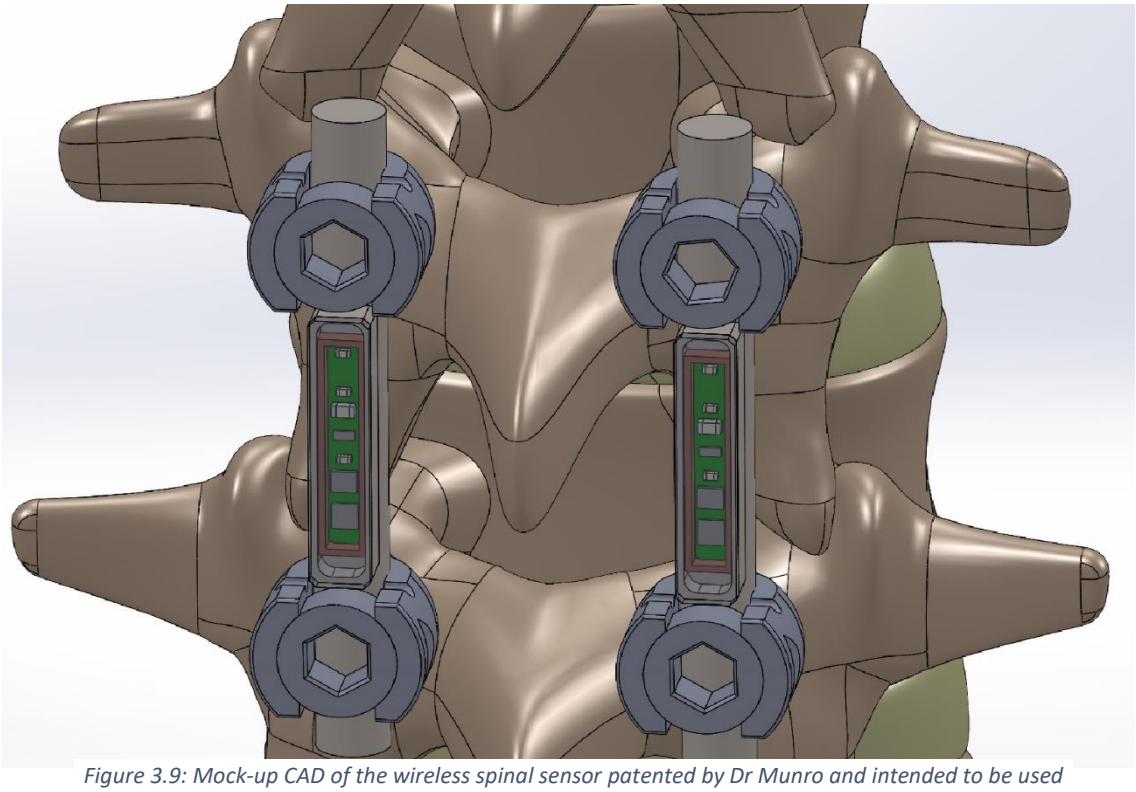

Figure 3.9: Mock-up CAD of the wireless spinal sensor patented by Dr Munro and intended to be used in the sheep study run by the University of Canterbury and Lincoln University.

Chapter 4 Tissue Properties

4.1 Overview of bone healing

To begin to understand the change in stiffness during fracture healing, it is necessary to understand that bone healing is a process that begins at a fracture with the formation of a hematoma around the fracture site [20]. This hematoma forms from blood clotting around haemorrhaged blood vessels in the bone severed by the fracture. Injury to bone also triggers the release of pro-inflammatory cytokines and other factors from the bone marrow. These releases of factors increase cellular activity around the wound site. Capillaries soon form which allow transport of cells that remove necrotic tissue and allow the formation of granulation tissue, a fibrin-dense matrix of collagen, elastins and various growth factors [21]. This matrix improves fracture stability and is the first cell type to form during the conversion of the hematoma to a soft callus. Following and during formation of the granulation tissue, mesenchymal stem cells are transported to the fracture site and differentiate into osteoblasts (bone forming cells), fibroblasts (connective tissue forming cells), and chondroblasts (cartilage forming cells). These cells work to lay fibrous down connective tissue to the two fractured ends, further stabilising the fracture. The hematoma becomes a rounded area of fibrous tissue called a soft callus. Over the next few days to weeks, osteoblasts migrate to the callus and begin to lay a bone matrix. This matrix is called woven bone and it provides stability to the fracture. Bone healing can be seen with medical imaging only after mineralisation is present in woven bone [20]. In the weeks to months to years after a fracture, the bone remodels the callus to return the bone to its pre-fracture state. This process of removing bone and adding it where strength is required is called bone remodelling. Osteoclasts cut through and remove the areas where strength is not required, and osteoblasts lay down bone where strength is required [15] (Figure 4.1). This way the structure of bone self-optimises in the months after a fracture [15]. Due to the process of remodelling, bone is the only tissue in the body in which healed tissue is indistinguishable to the original tissue.

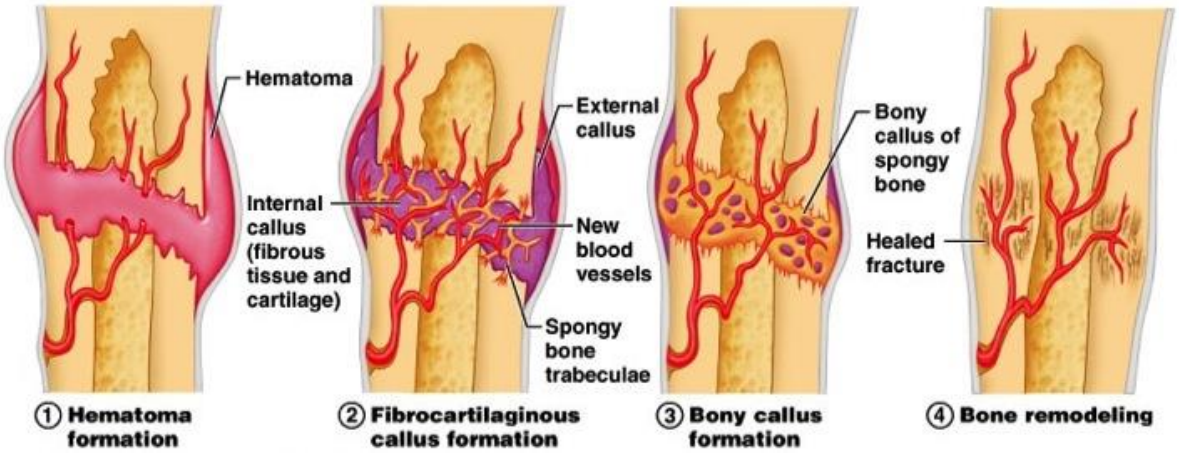

Figure 4.1: Process of bone healing [22].

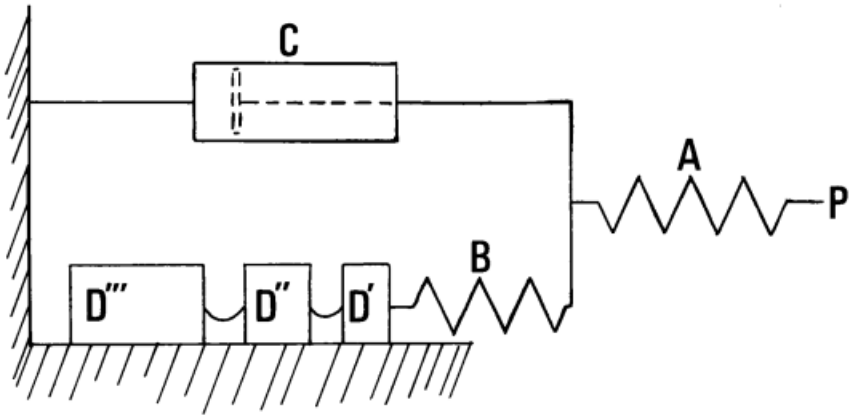

Figure 4.2: model for visco-elastic behaviour of bone [23].

In spinal fusion the bone remodelling process differs as the goal of fusion is to initiate a bone healing response between vertebrae in areas where bone normally does not form. This is achieved by introducing morselised bone from either an autograft (bone transferred from the same individual, usually from the pelvis), allograft (bone transferred from another individual), or a synthetic bone graft with bone growth factors [7]. The presence of stem cells triggers the bone healing response where a soft then hard callus form[24]. The spinal fusion area then remodels over time and permanently joins the vertebrae. It can be modelled as shown in Figure 4.2.

4.2 Materials

This section outlines the material choices used to build the sheep spine FEA model. Some materials were available in existing ANSYS and SolidWorks material databases while all bone, ligament, and other tissue materials needed to be researched to obtain a viable set of material properties. The properties necessary for FEA were: Young's (Elastic) modulus (E), Poisson's Ratio, yield, ultimate and compressive strengths, and strain at failure. Research was undertaken into the properties of trabecular bone, cortical bone, woven bone, hard callous, soft callous, and cartilage for the purposes of this thesis.

4.3 Anatomical differences between sheep and humans (and other species)

Sheep spines make an excellent substitute for humans for *in situ* and cadaveric testing as well as during development of new spinal hardware. Much research and testing is performed in sheep because sheep have a spine shape and volume that is similar enough to a human spine to be applicable for the same surgical techniques and fixation methods with equivalent size hardware used for spinal fusion surgery in humans [25]. Ovine vertebrae are generally longer and narrower than the human spine but have an approximately equal height while human vertebrae have a vertebral width of around twice the length in most sheep vertebrae [25 14 13]. The evolutionary basis of this difference is the biomechanical requirements of a horizontal vs vertical posture of sheep versus humans[25].

Human and sheep spines act in a similar load-bearing manner. In sheep, the spine is a beam having a high stiffness in the thoracic and lumbar regions to allow for efficient force transfer during normal gait of the animal [26 13]. Most herbivorous quadrupeds, such as goats and deer, have a similar spine structure. In contrast to the lumbar sheep spine, human lumbar spines have high mobility to allow for the bending and rotation of normal human activities, and human upright posture requires the spine to be directly load bearing with this load increasing down the spine, with the lumbar spine being both a very mobile vertebral unit and bearing the weight of the entire upper body. As such, the human lumbar vertebrae are larger and denser than most comparable size mammals [25]. Another

adaptation of the human spine to assist in load bearing while maintaining mobility is the increased diameter of the spinal canal [14].

This combination of mobility and high loading means that humans have more incidents of slipped discs, pinching of nerves, spondylosis and other degenerative diseases[6]. The long age and sedentary lifestyle of some humans may contribute to this fact.

Deer lumbar spines make an excellent substitute for the human lumbar spine for similar reasons as the sheep lumbar spine [25]. They are a similar size, shape, and strength. Being slightly larger than ovine lumbar vertebrae, the deer lumbar vertebrae are debatably a better analogue to the human lumbar spine for the purpose of testing fixation methods. However, the skittish nature of deer [27] coupled with the fact that sheep are more available and better researched internationally leads to the higher usage of sheep for the above purpose [25] (Figure 4.3)

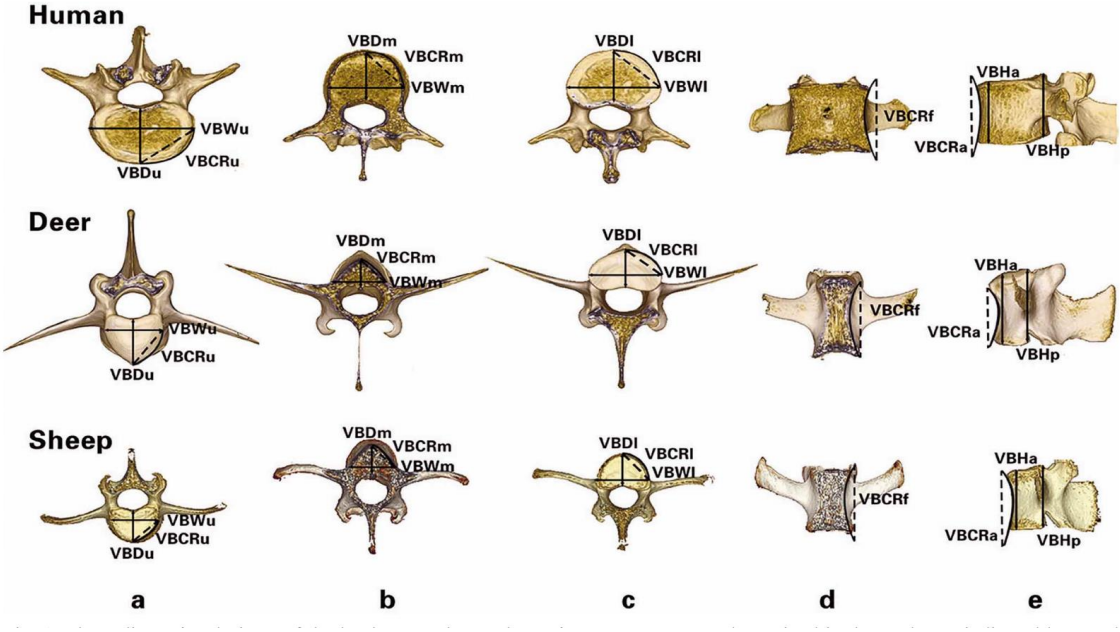

Figure 4.3: Differences in spine size and shape between human deer and sheep [25].

4.4 Other species

Bone strength and growth rate are not a constant between species. Because bone is a self-optimising material, it is only as strong as it needs to be. Often this means that bone strength in lower mass animals has a lower density and lower elastic modulus. In practice this results in a range of materials properties for the same tissue type. There are overlaps in the upper and lower bounds of these properties between species, which is why sheep can be used as an analogue for spinal fusion in humans; the bone properties are similar enough to be used in modelling and testing. Many of the studies researched obtained bone properties from rabbits, rats, horses, and pigs.

4.5 Sourcing of information

A range of studies outlining the strengths and elastic material properties of bone were sourced. These varied in publishing date from 1962 to the present. The properties and areas researched included studies into each of the main bone tissue types: compact/cortical bone, spongy/cancellous/trabecular bone, woven bone, cartilage, and granulation tissue.

To model the intervertebral discs between adjacent vertebrae, tissue properties of the annulus fibrosis and nucleus pulposus were also required. The primary goal of this research was to obtain a realistic set of mechanical material properties that could be input into the FEA models. Most studies focused on a certain property or set of properties. This meant that often a useful study would outline one material aspect and how this was affected by a specific variable. As such, a large combination of studies into bodily tissues were required to provide the full set of material properties. Sometimes, a literature summary paper could be found regarding a particular material. A study into the full set of properties of compact bone was one such study, and it further provided information about the annulus fibrosis [28]. A 1970 study into general bone properties was another good resource utilised for this study [23]. However, for a more comprehensive set of material properties, the information found was averaged across multiple species. Any information regarding ovine tissue properties was noted and weighted accordingly. With the large amount of tissue variability present in bone healing, any information to aid in building tissue properties was useful.

4.6 Structure of bone and other tissues

Bone is made from a variety of different material types. In long bones there are at least two different types of bone present, most notably compact and spongy bone. In a fracture situation woven bone is also present. The structure of bone is primarily based on a matrix of type I collagen and hydroxyapatite [29]. The density of this matrix is directly related to strength of the bone. Additionally, cartilaginous, marrow, muscle and other tissue types are located within and anchored to bone. A fusion mass in a rabbit spine is shown in Figure 4.4. In Figure 4.5a and b, the structure of a sheep vertebra is shown in further detail.

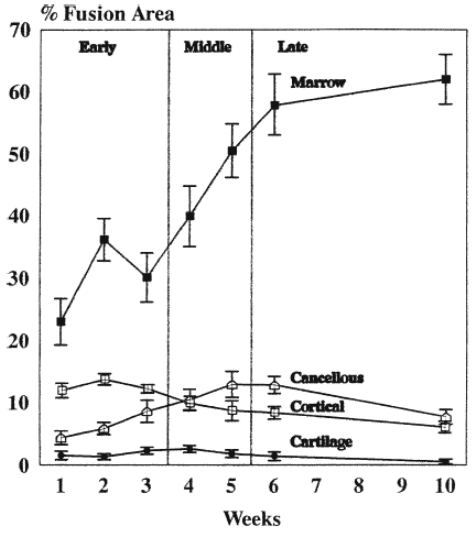

Figure 4.4: Tissue proportion in fusion mass during bone healing in fused rabbit spines [2].

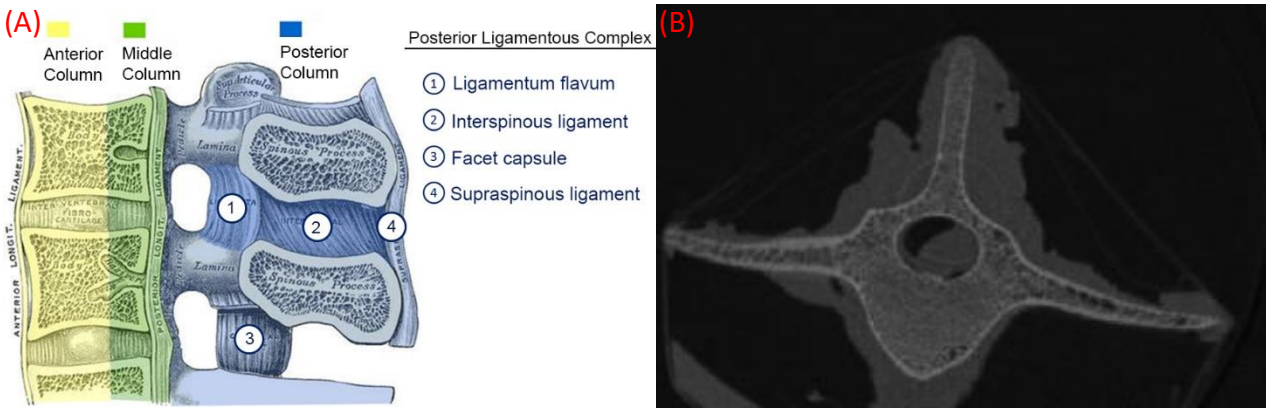

Figure 4.5: Internal structure of the human spine (A) and lateral CT cutaway of a sheep lumbar spine (B). Note thicker bone externally and hollow spongy bone internally.

4.7 Compact bone

Cortical or compact bone is generally the strongest type of bone in the body and is located in the surface features of most bone. The further the distance from the neutral axis, the greater the influence of bone strength on bone stiffness. Hence bone increases its density and strength at the bone surface for maximum strength in bending [30]. In long bones such as the femur, this high stiffness is achieved at the lowest weight, and thus lowest cell count, possible. Compact bone is relatively uniform in strength and density across the body. The makeup of vertebrae are no different. Compact bone is found on the exterior surfaces of vertebrae and provide most of the strength of the bone, especially in bending. Finding properties for compact bone was straightforward as several studies interpret the bulk properties of bone as being the average material properties for the bone as a whole. This makes sense as compact bone does contribute to a large portion of overall bone strength. In long bones, Compact bone can make up 80% of total bone mass [30]. Also, spongy or trabecular bone has the same material properties as compact bone, but is simply less dense.

The stiffness of compact bone varies from species to species. For humans the Young's (elastic) modulus of compact bone is usually between 12-18 GPa [23]. In oxen and cows this can be up to 24 GPa [23]. In sheep, the compact bone Young's modulus is in a similar range to human bone. Smaller animals such as rabbits, ferrets and rats can have a Young's modulus range of 5-10 GPa [23]. Being much lighter animals, their bones have no need to be as strong or dense compared to human or sheep compact bone. Rats and mice are light enough that they do not remodel their bones to repair microfractures the way larger mammals do.

A literature review study by J.D Currey [23] was one of the more useful sources of information for material properties as it summarised a variety of bone strength characterisation studies across a variety of species and characterisation techniques. For this thesis, all properties found were averaged across all species with the highest and lowest values removed. This produced a complete set of material properties able to be used in FEA.

Table 4.1: Mechanical properties used for compact (cortical) bone.

Material Property	Value
Poisson's ratio	0.14
Young's modulus, E	1.4 GPa
Yield strength in compression	80 MPa
Yield strength in tension	185 MPa
Ultimate compressive strength	107 MPa

The above table does not fully represent the properties of bone due to its nature as a directional and strain rate dependent material. For simplicity when modelling, bone was assumed to have isentropic strength properties.

4.8 Spongy Bone

Spongy bone, also known as cancellous bone or trabecular bone, is roughly equivalent in strength per mass to cortical bone, as stated earlier. This bone is more porous and similar in structure to a kitchen sponge, or an open cell foam. The gaps between the bony structures are home to bone marrow and blood vessels and assist the bone structure in withstanding compressive loads while reducing mass. Spongy bone's properties are directly related to the density of the three-dimensional lattice structure and how large the internal cavities are [30]. The bone lattice will be denser where

there is a higher requirement for strength such as closer to the bone surface and near absent where additional bone would make no difference to the overall stiffness of the bone structure.

In the vertebrae, spongy bone plays the important role of resisting high compressive and bending loads. The density of the trabecular lattice is high throughout the central axis of the vertebrae and lower towards the spinous and transverse processes [31]. This is to provide a high compressive stiffness between the vertebral endplates while the processes, being muscle and ligament anchor points, are loaded predominantly in tension and thus don't require the same density.

Table 4.2: Material properties averaged for spongy (trabecular) bone

Material Property	Value
Poisson's ratio	0.14
Young's modulus, E	1.67 GPa
Yield strength in compression	30 MPa
Yield strength in tension	2.5 to 26 MPa

4.9 Soft and Hard (Bony) Callus

Significant fracture stabilisation begins with the formation of a soft callus. The process begins with the infiltration of fibroblasts and chondroblasts into the granulation tissue. These cells begin the formation or fibrocartilage, stabilising the fracture site. With a more stable fracture, osteoblasts can lay bone matrix material down effectively. The fibrocartilage of the soft callus has been modelled in several studies, and diffusion-based FEA studies have modelled the change in material type and strength over the healing process [32]. Good results have been obtained by treating this material as isentropic and linear-elastic, especially in static loading scenarios, such as this thesis [18] [17].

Recent studies have rebuilt the callus from CT imagery and assigned each element a Young's Modulus and Poisson ratio value in a piece-wise fashion based on CT contrast values. A similar approach is possible through the BoneMat freeware [33], which creates element-wise strength variation across a CT-derived bone geometry, with the contrast differences in CT imaging used to create the geometry[34]. Another approach has been to treat the strength of the callus as a diffuse material where particles representing osteoblasts and similar cells move through the bone [32]. For these studies, bone strength was assumed to follow the diffusion of these particles in the direct modelling of the change in callus strength from granulation tissue to a bony callus. This study[32] was useful because it outlined the full set of materials present in the callus over the time frame of healing. The geometry of the simulated callus was based on the fracture healing behaviour of long bones in a body and resembled the soft callus formed on the femur or tibia for humans, goats and sheep.

Woven bone is the first mineralised tissue produced during the bone healing process. In essence, it is the progressive mineralisation of the fibrocartilage that forms the soft callus. Osteoblasts travel through the fibrocartilage matrix and lay down a woven bone matrix. At this stage, the fracture becomes much more stable as the newly formed bone matrix allows the structure to withstand compressive loads more effectively than the tissues found in the soft callus [35]. This form of bone is weak compared to mature bone as its biological function is to create a permanent structure at speed.

With most studies found, the most comprehensive data was for human soft callus tissue. Ovine soft callus tissue materials were generally derived from human tissue properties with key alterations

such as strength changes. Additionally, the callus strengths were usually based on studies detailing the soft and hard callus present in the healing of long bones as these are easy to visualise and measure due to their size and clarity during imaging. Limited study has been undertaken into the strengths of the soft and hard callus formed specifically during spinal fusion. Research undertaken so far has related strength to radio density (Hounsfield Unit) due to the opacity of mineralised bone and its increase of density during the bone healing process.

A wide range of mechanical values for the hard and soft callus were used/obtained/derived in various studies with various methods across various species and various anatomical locations. As such, the provided mechanical properties had a large range dependent on the above factors. To provide a reasonable set of material properties that were usable in FEA, material properties for all researched studies were added to the materials database and then averaged across all samples. As the formation of woven bone was a key variable in the present research, the material properties of the callus and woven bone were varied to simulate a stiffening fusion.

4.10 Granulation tissue

Granulation tissue or annulus grounds are one of the first tissue types to form within a hematoma, and it forms in 3-7 days following a fracture. Granulation tissue is a low strength support matrix that provides structure for the transport of cells to and from a fracture site while filling any free space within the hematoma [20]. It is packed with capillary blood vessels that assist in this measure. Ovine granulation tissue has not been characterised for mechanical properties. Human granulation tissue has been characterised, but its properties vary drastically depending on the timeframe of healing [36]. As time elapsed since fracture increases, this tissue becomes stiffer as it transitions to a soft callus with the laying down of resilient extracellular matrix materials like collagen. This material is difficult to model due to its rapidly changing strength. The transition of strength has been treated as a diffusing material previously [32]. However, for most FEA studies researched that used granulation tissue, it was been treated as a linear-elastic material or omitted entirely [37] [12] [17]. The properties of the granulation tissue used were determined though averaging the highest and lowest values given across the studies researched. An upper and lower value were used to represent the variation inherent across studies into this tissue type.

Table 4.3: Mechanical properties for granulation tissue.

Material Property	Value
Poisson's ratio	0.39
Young's modulus, E	0.001 to 2 MPa

4.11 Intervertebral Disc

The intervertebral discs are composed of two parts: the annulus fibrosis and the nucleus pulposus. The gel-like nucleus pulposus is the main load bearing element in the intervertebral discs, with the annulus fibrosis serving as an outer sheath to constrain the area the nucleus is in [38]. The annulus fibrosis is highly fibrous and directional [39]. The fibre orientation is circumferentially around the nucleus pulposus while the nucleus can be considered an isentropic material [39].

There are many approaches to modelling the intervertebral disc; several studies used an approach where the fibrous annulus was modelled as a directional material with the nucleus pulposus as an isentropic material. One study [40] modelled the annulus fibrosis of a human spine with a multi-segment annulus fibrosis that was given hyper-elastic properties and treated the nucleus pulposus as a viscous fluid. The simplest FEA analysis of the intervertebral disc assumed it was one body with

the isentropic properties of the annulus fibrosis [37]. Several studies used material properties derived from a different species to the spinal geometry used. An example being the use of human disc mechanical properties on an ovine lumbar geometry [14].

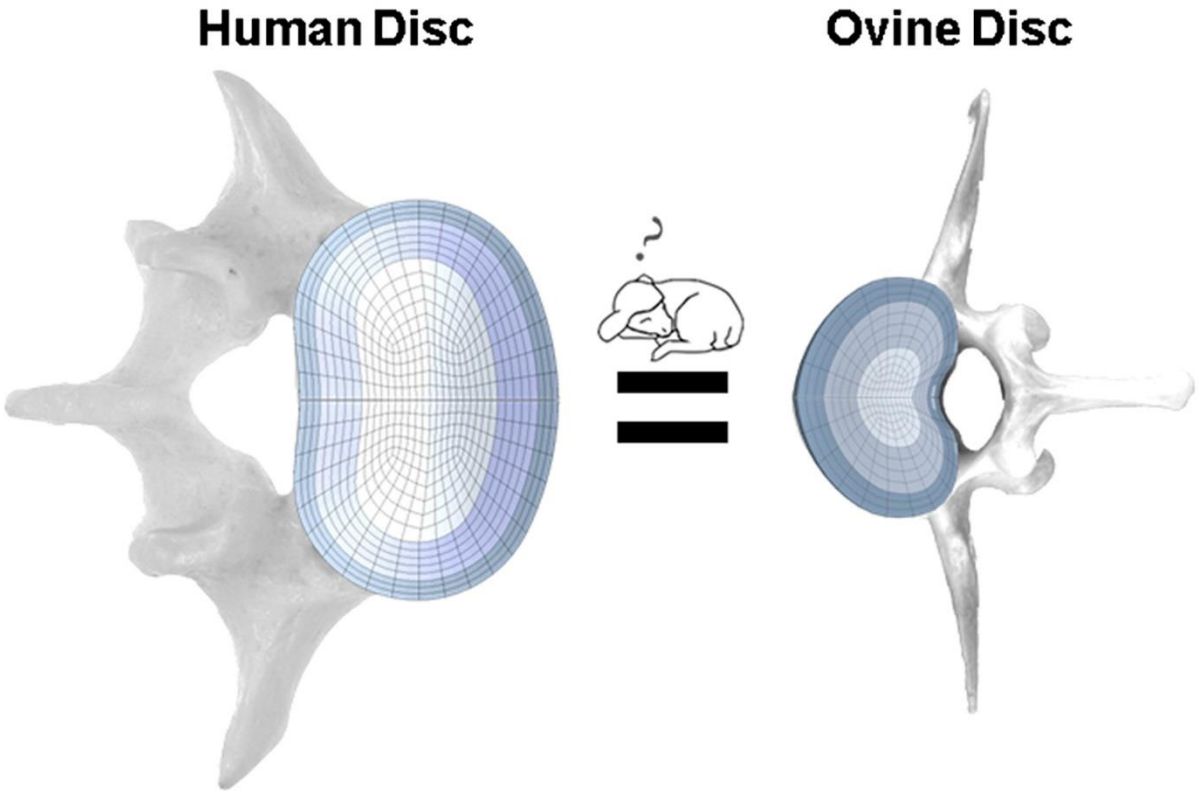

Figure 4.6: Size and FEA mesh comparison between human and sheep intervertebral discs [14].

For simplicity in modelling, isentropic material values are better for FEA, as it is easier to construct and specify. As the present FEA model was intended to study the influence of the change in stiffness of the bone healing zones (BHZ), fully realised intervertebral disc geometry, materials and boundary conditions were deemed unnecessary. Studies that showed the full properties of intervertebral discs (both annulus fibrosis and nucleus pulposus mechanical properties and dimensions) in human FEA studies and then again with ovine intervertebral disc were the most useful [14,17,34]. Two studies [28,39] that outlined the complete properties of the annulus fibrosis in a literature review format were particularly useful. While this body of work only outlined human annulus fibrosis properties, it was nevertheless used due to its level of completeness.

Nucleus pulposus modelling was approached with several methods using several research papers in this area. The biomechanical role of the nucleus pulposus is to support the load through the spine. It consists of an elastic jelly-like material that is predominantly water held within a collagen matrix [41]. As such, it is a largely incompressible material. Several FEA studies took advantage of this fact and simplified the elements of the nucleus pulposus as an incompressible fluid [11]. While successful, this approach is limited by the FEA software and the solving mode used. Additionally, while largely water by mass, the nucleus pulposus will hold its shape in a similar fashion to soft rubbers or gels (hydrogels, silicone, or other). Studies detailing FEA in human spine specimens treated the nucleus pulposus as a hyper-elastic, hyperplastic material with set Koen values [14 42]. These values were derived from experimental studies [43 44]. Information for specific mechanical property values in the sheep spine are near non-existent. Studies modelling the ovine spine often used human properties for the annulus fibrosis and nucleus pulposus [17].

As with all other tissue types, the annulus fibrosis and nucleus pulposus were averaged across studies and species for a most complete set of mechanical properties. The resultant numbers used are shown below.

Table 4.4: Material properties used for annulus fibrosis.

Material Property	Value
Poisson's ratio	0.44
Young's modulus, E	4.3 MPa
Tensile yield strength	2.7 MPa
Strain at failure	0.97

4.12 Approach to modelling

For ease of modelling, it was decided to represent the materials used as linear-elastic. This was for ease of interpolation and comparing the slow changes of stiffness over the healing process. While the intervertebral disc was suitable for configuration as hyper-elastic and directional, studies that treated this material as linear-elastic achieved sufficient results. The focus of this thesis was to determine the effects of BHZ on overall spine load sharing and how strain in pedicle fixation changed over time during healing. As such, linear-elastic material properties sufficed.

Several studies were used to determine mechanical properties to use in FEA. The most valuable resource used was the Granta biomaterials database [45]. Bone, cartilage, muscle and ligament properties as well as the cellular building blocks of collagen and elastin are available in the database. Notably, granular tissue, annulus fibrosis, and nucleus pulposus materials are absent. Soft and hard callus material characterisation was not expected to be in the Granta database due to its transitionary nature, and this assumption was correct.

Studies containing necessary mechanical information were located that had the relevant properties recorded. Materials were categorised into types of bone or tissue (cortical bone, annulus fibrosis, etc). Then, source study, species, tissue source location, and tissue strength determination method were noted. All properties planned for use with FEA were averaged across tissue type. This also averaged results from different species and determination methods. The large variation in tissue properties required this action. Averaged material results were then compared to the Granta database value, where applicable, for a gauge of accuracy (Figure 4.7). Five bone types were initially created with varying Young's (Elastic) moduli as shown in Table 8.2. These were used in the initial modelling efforts, called the Basic model.

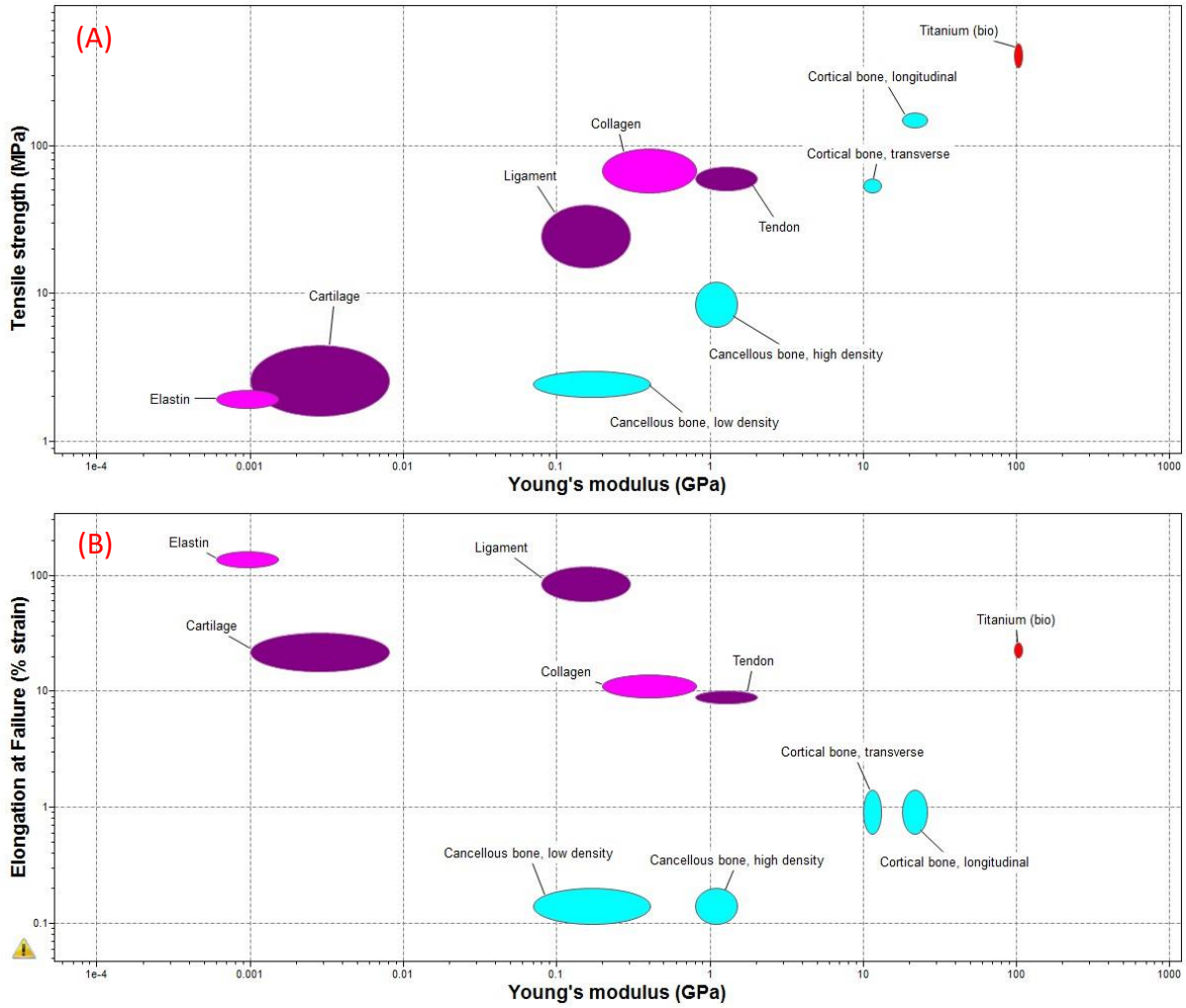

Figure 4.7: Granta materials database showing tensile strength (A) and elongation at failure (B) [45].

Version two of the Advanced model used bone values that were interpolated to provide more range, thus expanding the table to eight bone types. This was primarily to provide more range of material values to see a more gradual change of stiffness, especially for the low strength materials such as granulation tissue. The values used are shown in Table 8.3.

Chapter 5 Sheep study planning

5.1 Sheep study

As discussed in an ethics-approved proposal, Dr Munro has developed a diagnostic implantable sensor system for spinal fusion and wishes to test this technology in a large animal model. Lincoln University has surgical expertise and knowledge of normal and disease sheep models to assist. The surgical procedure will consist of four pedicle screws placed posterolaterally on two adjacent lumbar vertebrae and then spanning the pedicle screws with titanium spinal rods, one of which will have a wireless, implantable sensor attached.

The sheep study aims to provide world-first data to validate the sensor designed by Dr Munro and refined at the University of Canterbury. If successful, this will result in the live reading of strain in the spinal rod the sensor is mounted to and provide data on how the strain changes over time.

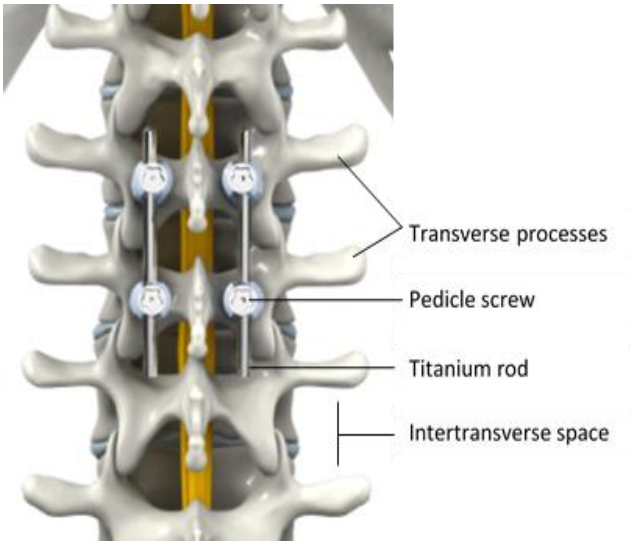

Figure 5.1: Diagram of the standard fixation used for spinal fusion surgeries. This arrangement will be near identical for the sheep study with one of the spinal rods replaced by the sensor rod and housing.

Formerly, it was thought the sheep study would be completed in 2021, and the FEA model could have been validated against the sheep study, but due to numerous delays, this part of the project was not completed.

5.1.1 Objective

The objective of the sheep study was to evaluate the effectiveness of the sensor to detect spinal fusion (the level of bone growth/healing *in situ*) and compare this to the current standard assessment protocol of radiography

Chapter 6 Cadaver study

Although the live animal study could not be started, a cadaver study into surgical techniques and utilisation of an instrumented prototype sensor rod was undertaken at Lincoln University Johnstone Research Station Veterinary Theatre. Dr Brent Higgins performed a posterolateral fusion (fusion of adjacent transverse processes) on a 7-year-old Romney ewe cadaver. An instrumented spinal rod (sensor rod) was used in this surgery to gain insight into the strain during preload of the pedicle nuts and during simulated weight bearing motions.

The cadaver sheep was CT imaged before the surgery to allow for insight into how the surgery would be undertaken regarding screw locations and bone harvesting for a fusion mass. Practice of anesthetising the sheep and wound sealing was done to simulate surgery with a live animal. Typical pedicle fixation methods and tooling were used for the fusion itself. The pedicle screws, manufactured by Ossability, were supplied with their own tooling.

The instrumented sensor rod was a titanium 3D-printed prototype manufactured by Rodin Cars. This rod was subsequently instrumented by Angus Malcolm of ABI with strain gauges and a development board for obtaining a digital output. The sensor rod and placement are shown in Figure 6.3.

The cadaver surgery was as realistic as possible. This was necessary as the cadaver study was used as training for the planned sheep study surgeries. Preparation consisted of the shaving of the animal's back, applying surgical dressings and antiseptic. Finger palpations were done by Dr Higgins to locate the exact area he wanted to fuse. It was determined that the L4-L5 vertebrae were best for fusion. One incision was made along the spine above this point. Muscle was then separated down to the transverse processes on the left. The spinous process was trimmed with a bone burr and pilot holes were drilled for the pedicle screws. The holes were widened, then pedicle screws were installed with the supplied hand-crank tool. The sensor rod and standard spinal rod were installed (Figure 6.2). Strain preload was measured before the cadaver sheep was lifted and manipulated by hand to replicate a sheep's gait. The sensor rod and standard rod were then swapped places to measure side to side differences in preload and simulated gait loading on strain. Another incision was then made on the hip to allow for extraction of iliac crest bone with an osteotome and then was morselised. In a live spinal fusion this morselised bone would be inserted around the spinal rods and pedicle screws to initiate a fracture healing response for the fusion mass. Bone from the host is known as an autograft. If insufficient bone mass can be obtained from the sheep's iliac crests, allograft or a bone growth factor would be needed.

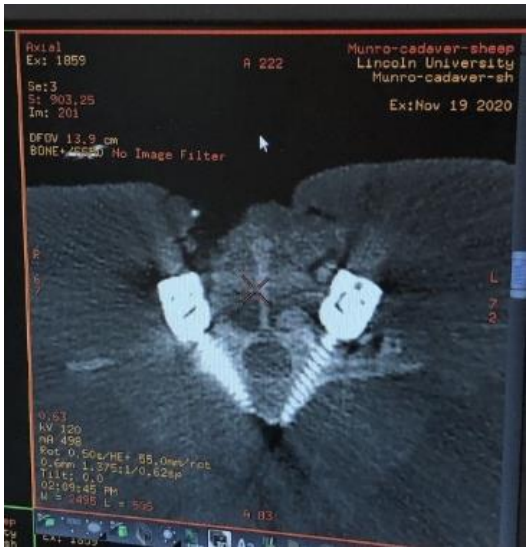

Figure 6.1 Close-up of pedicle screw placement

The sheep was then CT imaged a second time to verify the location of the pedicle screws. Figure 6.1 and 6.3 show correct location of the screws as well as the development board and damage from the iliac crest bone harvesting. Following scanning, the pedicle screws and rods were removed and cleaned and the cadaver sheep discarded.

This cadaver study was successful in providing a practice scenario for live sheep spinal fusion surgery and an opportunity to fine tune the surgical process.

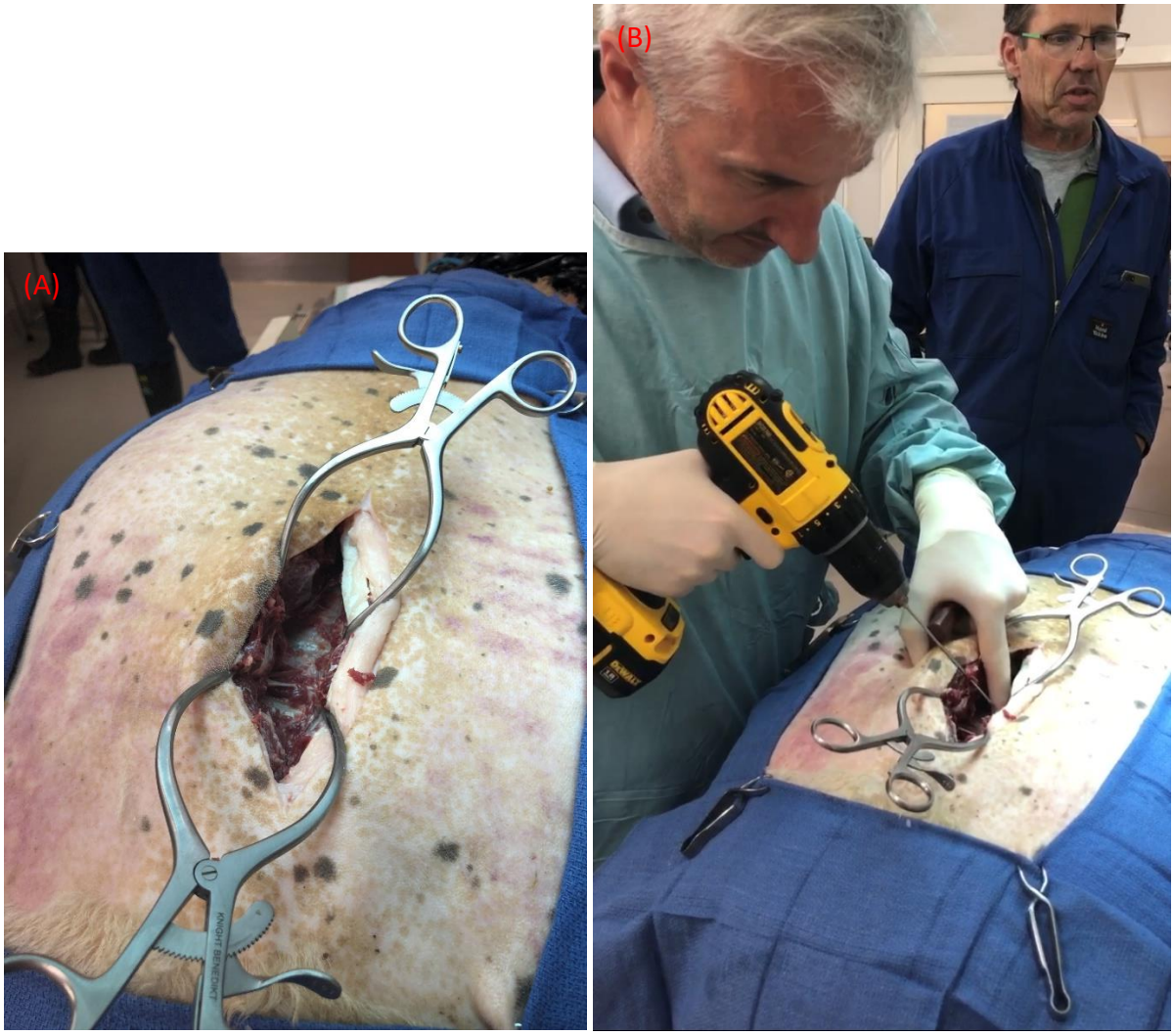

Figure 6.2A: incision down to the spine held open by retractors and Figure 6.2B Brent Higgins drilling the holes for pedicle screws.

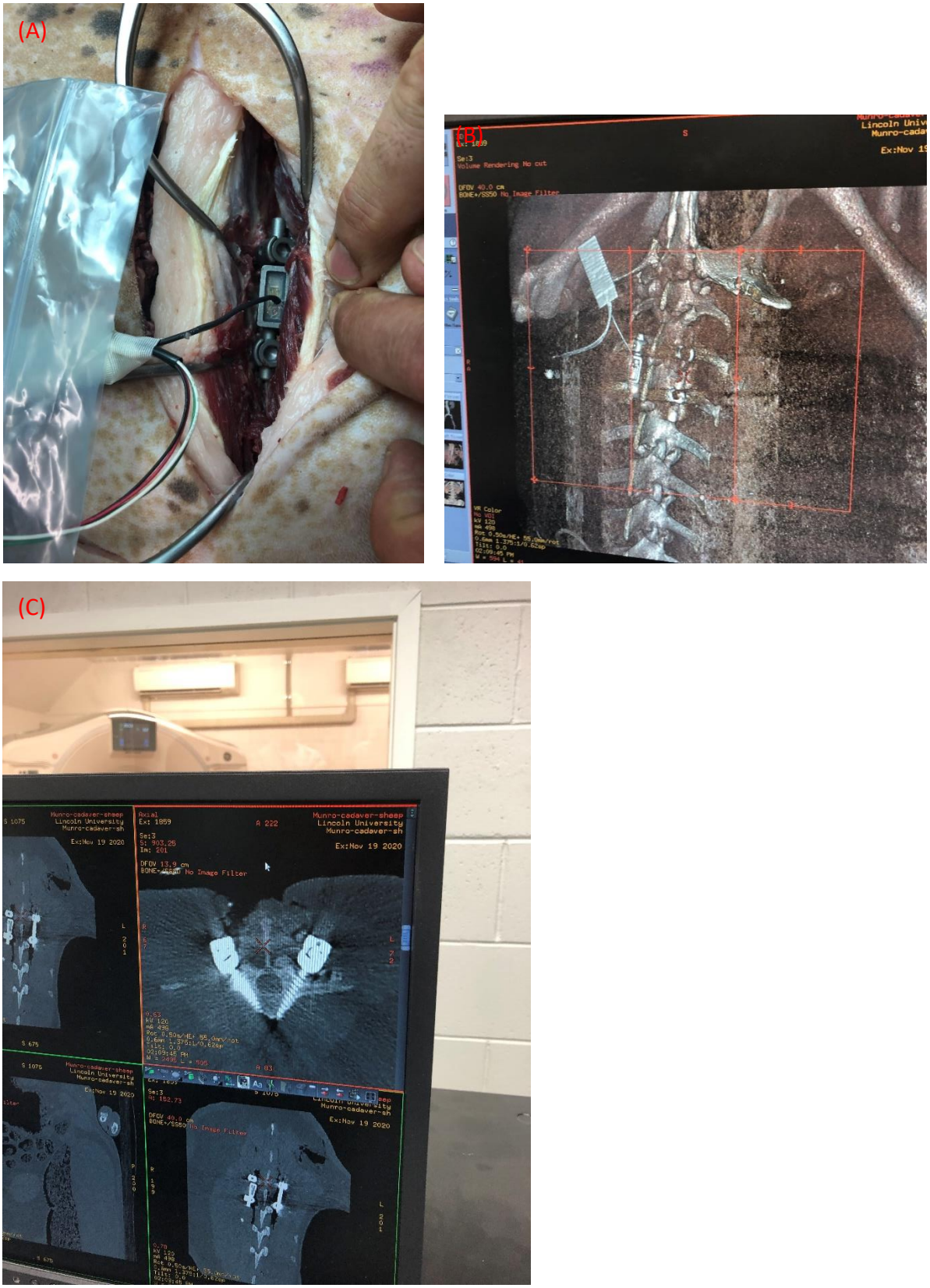

Figure 6.3 A,B,C: Sensor rod installed in position on the spine. A zip-lock bag protects the development board. CT scans show position of spinal and sensor rod and pedicle screws.

Chapter 7 CAD Model Development

7.1 Introduction

A cornerstone of this thesis was producing a finite element analysis (FEA) model of the sheep spine and how it changes in stiffness over time. To produce an FEA model, a valid geometry to base it from was required. Two main geometries were produced: a "Basic" model—to develop analysis techniques, material combinations, and boundary conditions with a simple geometry, and an "Advanced" model—which took lessons from the Basic model and applied them on a higher-detail geometry of the sheep lumbar spine. These models were produced using CT scan data from Lincoln University and MARS Bioimaging [46], respectively. The CT scan data was transferred as images via a standard Digital Imaging and Communications in Medicine(DICOM) protocol and was subsequently processed with 3D Slicer [47] for the Basic model and ITK-SNAP [48] for the Advanced model. Post processing of the models was done in MeshLab [49], Autodesk Meshmixer [50],3D Systems GeoMagic Freeform [51] to reduce polygon count to a usable level. Final model editing and assembly was conducted in SolidWorks 2020 [52] prior to importing the geometry into SolidWorks Simulation (an inbuilt FEA software tool) and then ANSYS Mechanical 2021 [53].

7.2 Scanning methods

To produce an FEA model of a sheep (ovine) spine, a CAD model of the spine needed to be produced. There are two main ways to produce a spine model: freehand using a point cloud in CAD as reference geometry, or by converting medical images, such as a CT scan of a spine, into a form that can be loaded into CAD software. Using medical imaging ensures that the resultant geometry is essentially identical to the structure of the bone in question. Two sources of CT imagery were used to create the geometry for this project: Lumbar spine regions of sheep undergoing CT imaging at Lincoln University's Johnstone Memorial Laboratory using their GE Prospeed CT [54], and individual ovine lumbar vertebrae scanned with the MARS Microlab 5X120 [55] housed at the University of Otago's Christchurch campus. The Lincoln CT scanner was large enough to scan an entire sheep (or human), while the MARS colour CT scanner was only large enough to hold an ovine lumbar vertebra with the transverse and vertebral processes shortened to fit in its 125mm diameter by 450mm length. Once a full DICOM image was obtained from either scanning method, it was loaded into a DICOM viewer that had the ability to segment areas of the geometry and convert them into a stereolithography STL-type geometries (consisting of point cloud based tetrahedral meshes, where all surfaces are triangulated) [47,48].

7.2.1 Lincoln University CT Scanner

The Johnstone Memorial Laboratory at Lincoln University has a GE Prospeed CT scanner owned and operated jointly by the Otago University Medical School, the University of Canterbury, and Lincoln University. Its main purpose is for assisting with animal research of human ailments. This CT scanner was used for our preliminary scanning efforts and provided the geometry for the Basic model. The

initial DICOM imagery used for the Basic model was obtained from a full helical scan of a sheep dated 16 August 2018.

The GE Prospeed CT scanner can scan an entire sheep and thus the entire skeleton was available for our use; however, the scanner could not provide a resolution fine enough to show the separations between the vertebra's facet joints. However, for early work, the resolution was sufficient for our purposes. This scanner was also used for verification of correct pedicle screw location when preparing spine specimens for mechanical testing (Figure 7.1).

CT images from this scanner were usable, but the lower resolution helical scans (Figure 7.2) resulted in fused facet joints during segmentation, which carried through to the STL geometry and proved difficult to separate in CAD. The facet joints were thus manually "cut" in SolidWorks; however, to accurately (and digitally) cut the fused spine geometry in a way that was biomechanically accurate to the original sheep spine was not possible with the software tools available.

Figure 7.1: Example of spine DICOM slice derived from Lincoln University CT scans.

7.2.2 MARS Bioimaging Multi-Spectral CT Scanner

The MARS Bioimaging company is a medical start-up based at the University of Canterbury that aims to revolutionise medical imaging with their CT scanner that looks at multiple wavelengths of x-rays across the spectrum to produce high-resolution, colour CT scans. For example, the internal sponge like structure of bone is clearly defined into the 0.1mm range. The processing of our sheep lumbar vertebrae reportedly took 1-2 hours each.

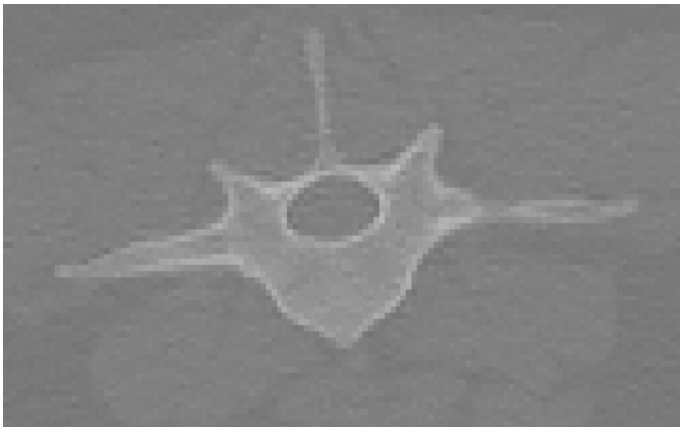

Figure 7.2: Sheep ready for scanning (a). Resultant image from helical scanning run.

The MARS team scanned both intact lumbar sheep spines and individual sheep vertebrae at a range of power levels varying from 35 KeV to 80+ KeV. The resultant data was incredibly dense and generated massive files, with the DICOM series per vertebrae averaging 60 GB for a full set at varying power levels.

This high resolution DICOM series was used for producing the Advanced model (Figure 7.3). The detail available was significantly higher than the Basic model and allowed the internal structure of the vertebrae to be viewed in sub-millimetre detail. When processed with 3D slicer and converted into STL geometry, each lumbar vertebra regularly approached 1GB in size with up to 5 million vertices. The size of these files, coupled with the internal structure, made the geometry unusable, as many CAD programs would not accept a shape with so many triangulated faces. Reduction of the geometry was therefore necessary. Additionally, the faces of the internal structure added unnecessary detail that often would cause meshing to fail, so this geometry data needed to be removed.

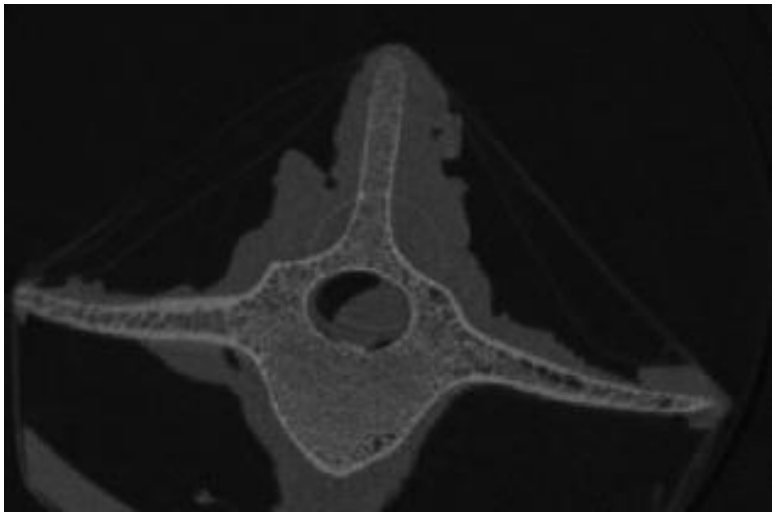

Figure 7.1: Example of DICOM slice derived from MARS imaging process.

7.3 Initial Modelling Work – requirements for FEA

To produce an FEA model of the ovine lumbar spine, valid CAD geometry needed to be created. An early priority of this thesis was obtaining geometry of a sheep lumbar spine from a viable source. Suitable models online or available for purchase were either limited in their resolution or were subpar for what was required in terms of model quality. Attempts to track down an existing sheep spine model through GrabCAD[56], Embodi3D[57] and similar online CAD libraries proved unsuccessful. Human lumbar spine models were easily found online; however, ovine models of the spine with the fidelity needed were impossible to source. Most scientific papers that involved a digital model of the ovine lumbar spine had produced their own models from CT scans. It was determined that the easiest method to obtain a valid spinal geometry was to build it from CT scan data. These scans could be converted from DICOM medical images into a 3D model that could then be refined in CAD software and manipulated until suitable to run in FEA software

The first attempt at a model was produced from a full helical CT scan of a sheep used for other research purposes at Lincoln University. DICOM data (a generic file type used for CT scan output) was obtained and processed using Embodi3D's online slicing tool. The output geometry left much to be desired, as the resolution and meshing obtained were too poor to allow for any FEA results to be generated. Better geometry was produced from the same CT data using the tools within 3D Slicer. The lumbar spine geometry was segmented using a technique known as contrast mapping with a cut-off value of approximately 250 pixels of light intensity (Hounsfield Units). This segmentation was saved as an STL body and imported to SolidWorks where it was processed and modified for use in FEA.

A basic FEA study was run within SolidWorks Simulation to ensure the geometry would mesh without error. Initial FEA work was then carried out with the material set to a default material (mild steel) and boundary conditions of the fully-constrained lowest visible endplate and a 100N vertical load acting on the top vertebral endplate of a four-vertebrae geometry (more detain in FEA chapter – will link). This method yielded useful information regarding how successful an FEA model was

going to be with the Basic geometry. The main drawbacks of the model were that the intervertebral discs were entirely absent and needed to be fully reconstructed within CAD and the fact that the vertebrae had “digitally” fused through the facet joints and in some vertebrae, through the space the intervertebral discs normally occupied. These unwanted fusions made the initial scans unusable for this research project, as the output geometry would require significant and unrealistic cuts applied to the model.

As such, higher resolution CT scans of sheep lumbar spines were sourced from the MARS scanner, and when processed, these scans produced a high-quality geometry used for the Advanced model.

7.3.1 Early Models and Progress

The vertebral model used is that of a skeletally mature ewe. The model currently in use for preliminary work was produced from a spiral capture CT scan of a 5 y/o ewe from the Lincoln university research flock. CT scans often have trouble showing areas of cartilage such as joint surfaces, intervertebral discs, and tendons/ligaments without a contrast agent. Because of these limitations, the CT model may be supplemented with laser topology scans of vertebrae and intervertebral discs acquired from sheep spine dissection. This was to make it easier to make and segment models to work from as there would be no difficulty in separating a large mesh based on contrast methods (Figure 7.4).

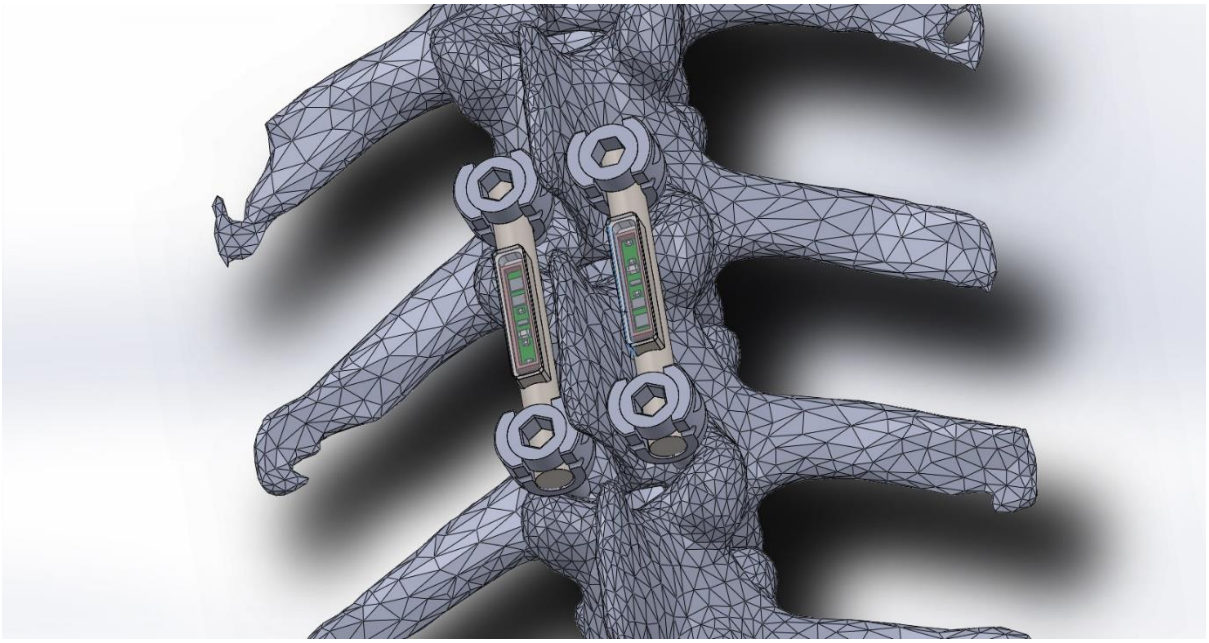

Figure 7.2: CAD mock-up of the sheep spine and wireless sensor. The Sheep spine model was produced from a CT scan that was processed into an STL file in 3D slicer, an open-source medical imaging software package.

7.4 Model Overview and CAD Iterations

7.4.1 Initial CAD Work

The first working iteration of the Basic model was created from a full helical scan of an adult ewe dated to 16 Aug 2018. This set of DICOM images were provided by Lincoln University.

The first attempt at segmentation was by using thresholding methods with a cut-off value of around 250-pixel opacity within 3D Slicer software. Since a sample area was not selected, the whole sheep skeleton was converted, which was then cut down within SolidWorks to contain just the lumbar vertebrae. For the second attempt, a boundary box set around the lumbar spine was used for segmentation. This yielded similar results, but was more manageable. The second spine model was then imported to SolidWorks where the inbuilt FEA suite (SolidWorks Simulation) was used to apply static boundary conditions of a 100N load at one end of the spine and the other end constrained. As the purpose of this model was to test the concept, realistic loads and materials were not needed, thus the material used was default mild steel. The imported FEA geometry is shown in Figure 5a.

Under the described conditions, the Basic model of the lumbar spine successfully meshed, compiled, and ran, producing results almost immediately. The points of highest stress were located at the incorrectly fused facet joints or where the vertebral endplates had inadvertently fused. Figure 5b shows how the vertebrae were separated (Figure 7.5).

The Basic model spine geometry was then imported into ANSYS SpaceClaim CAD modelling software [ref https://www.Ansys.com/products/3d-design/Ansys-spaceclaim version 2021) and analysed in ANSYS FEA software under similar default mesh and boundary conditions. With default material selections, the SolidWorks Simulation FEA results were comparable to the ANSYS FEA results.

Figure 7.5: A) Basic model CAD on import and B) slices made to separate model into bodies.

The Basic spine model required the spine to be separated at the facet joints for all levels and the vertebral end plates for some levels as shown in Figure 5b. For the purposes of the Basic model, this separation could be rough and not as biomechanically accurate as required for further analysis. The Advanced model would be used for higher resolution, correct material analyses. Separation of the lumbar vertebral body was achieved in SolidWorks with a set of extruded cuts: at a rough diagonal across the fused facet joints for separation of bodies and between vertebral end plates for cleaning the vertebral end surfaces prior to the creation of intervertebral discs. As the desired model only required four vertebrae, L2 to L5, the newly formed L1 and L6 bodies were then deleted. Intervertebral discs were then created by using the SolidWorks loft feature to create a new body between vertebral endplates. Having flattened each vertebral endplate meant that a loft could be applied directly from surface to surface.

This process created more space between vertebrae than exists in a sheep spine but was acceptable for creating an early working geometry that became the Basic model. After separation, a variable block of material was added between the transverse processes of vertebrae L3 and L4 to represent bone healing zones, as shown in Figure 7.6.

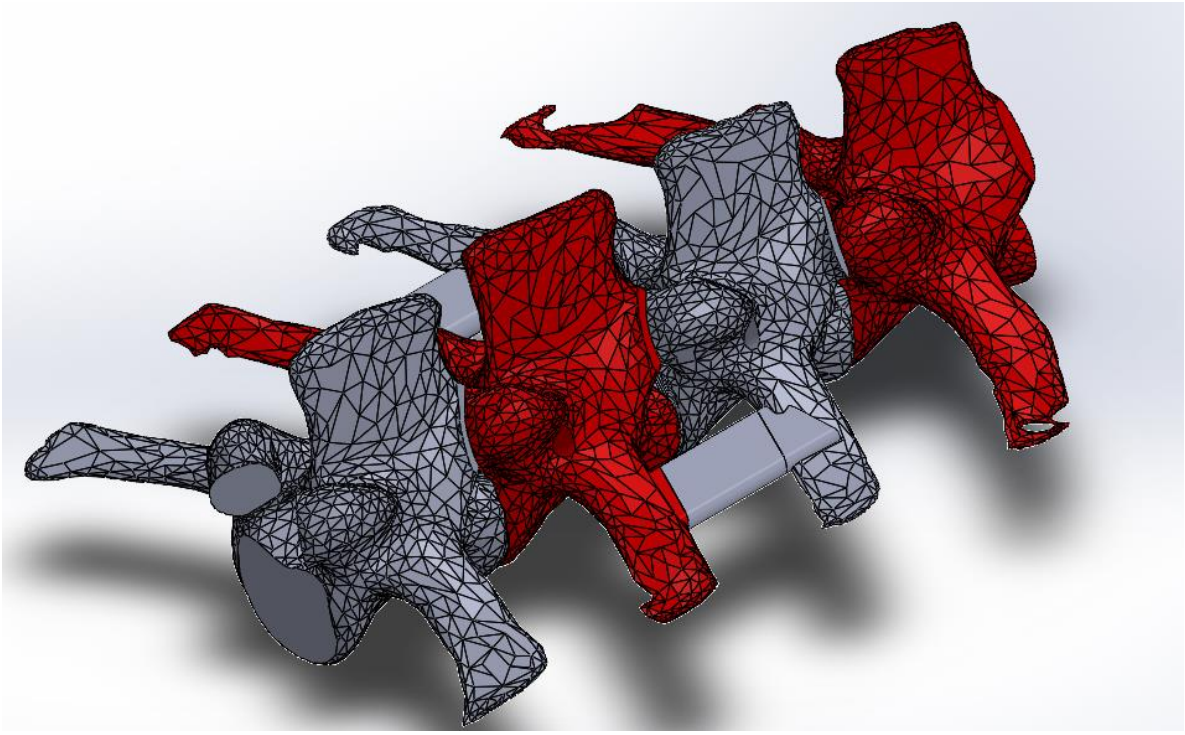

Figure 7.6: Final Basic model geometry with bone healing zones.

7.4.2 Advanced Model Creation

The biomechanical inaccuracies of the basic spine model around the facet joints called for a more advanced geometry. The facet joints in sheep contribute significantly to torsional stiffness of the spine; hence, a version of the spine that retained these features was required for accurate FEA modelling. Due to the low resolution of the CT scans from Lincoln University, the facet joints were perceived as a single entity by the slicing software and therefore tended to fuse most vertebrae into a single body. It was concluded that better DICOM image quality or processing techniques were required to achieve better results.

MARS Bioimaging has a multi-spectral CT scanning technology with the needed capabilities. First, they had a scanning resolution high enough to show, and thus process, all major and minor structures of the vertebrae, and second, they were able to scan both complete lumbar spine sections as well as individual lumbar vertebrae. This allowed the creation of individual vertebrae models that could be digitally re-assembled back into a spine with the outline of the intact sheep spine to guide the process. This process was hindered by the very high levels of detail that the MARS scanning methods could output (generally upwards of 1 million vertices per vertebrae). With this level of detail, the average size of the MARS DICOM file used to produce a 3D geometry was 12GB and the output STL file was approximately 1GB. This was problematic because the maximum size file SolidWorks would accept as an editable item was 200 MB. Thus, the 3D geometry files had to be reduced significantly.

Initially, Autodesk Meshmixer was used as a decimation filter to reduce the sampling frequency and thus mesh size of the vertebral bodies, however it struggled significantly with the large file sizes. MeshLab was then selected for initial decimation as it was well optimised for handling very large STL files and other point cloud types of data. The vertebral body STL's were imported into MeshLab and then an isentropic explicit (constant entropy) decimation filter was applied. This reduced the vertex count of the mesh by 80%. Quadric edge collapse decimation, which preserves boundary and normal faces, was repeatedly applied to reduce the mesh count further. At this stage, the resultant geometry could be re-imported into Autodesk Meshmixer with significantly reduced geometry, noise, and complexity. However, internal cavities, while reduced in complexity, remained. This is shown in Figure 7.7a.

The presence of internal cavities resulted in the early versions of the Advanced model failing mesh checks because of the size and shape of these often-small internal faces. Further work was required to reduce and remove these internal faces as the software suites used did not provide a satisfactory result when processing the MARS-derived geometry. Thus, a more powerful STL processing suite was required to further clean the geometry.

7.4.3 Final Geometry Processing

Correspondence with industry representatives led to 3D Systems GeoMagic Freeform being recommended as a CAD suite that would suit itself well for our purpose. GeoMagic normally provides a digital manipulator arm with tactile response to drive the full features of Freeform and is used extensively within the medical community for its ability to easily shape geometry to nonstandard shapes very quickly.

A two-week free trial of this software was obtained and several capability tests were done, including importing an STL post-MeshLab-processing file and importing a raw, full-resolution MARS scan STL file. Freeform works by representing the geometry as a virtual “clay” and has embedded tools that add or remove material from the geometry. The main digital tool used for geometry cleaning was the “hot wax ball.” This tool was used to push around “clay” and smooth the more troublesome areas of the vertebral body mesh. A powerful feature used in conjunction with this hot wax tool was “cavity filling.” When a hole in the model was filled over and disconnected from the “air” the cavity was deleted in the geometry. A large portion of internal cavities were deleted upon import of STL geometry into Freeform this way, which reduced the quantity of error-prone mesh faces significantly. The surface complexity was also smoothed automatically during the import process. The simplified the geometry was thus quicker and easier to process for further altering operations as shown in Figure 7.7c.

For the lower bone density regions on the vertebrae’s transverse processes, it was more straightforward to simply remove the transverse process tips than to fix all the cavities., which was acceptable as the tips of these bone sections are not relevant to spinal fusion.

The final step of the Freeform cleaning process was further reduction of the STL mesh density while keeping the shape of the model for each vertebra from L2 to L5. This reduced the triangle count by a further 50%. Freeform was able to optimally increase the mesh density around areas such as the facet joints and processes while simultaneously removing excess mesh density where undesired. The direct import MARS geometry and the post-MeshLab-processed

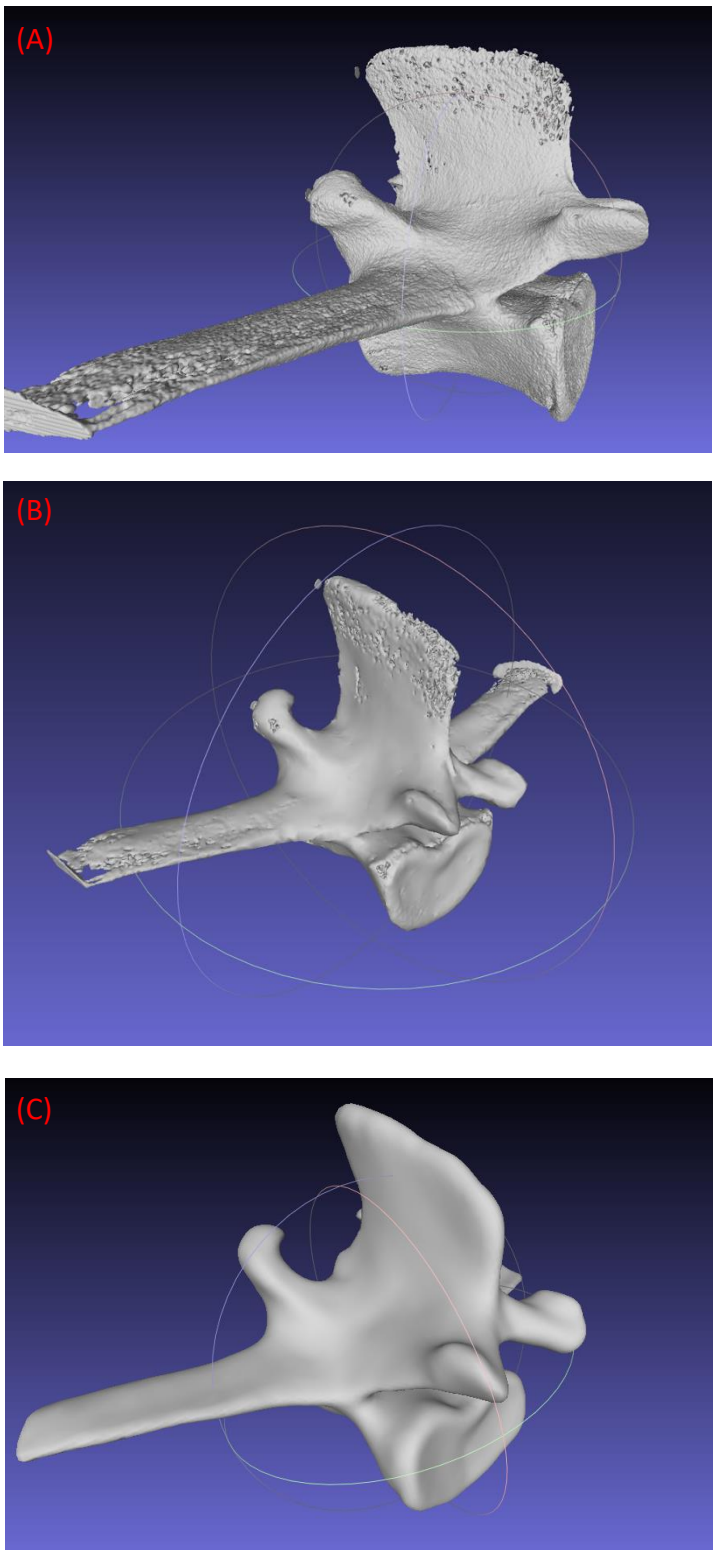

Figure 7.7: (A) Raw STL at full resolution at import from ITK Snap. (B) Mesh having been fully processed in GeoMagic Freeform. (C) Mesh having been fully processed in GeoMagic Freeform.

geometry were thus nearly indistinguishable to the eye after cleaning in Freeform.

7.5 Assembly of the Complete Model

Vertebrae by themselves do not constitute a spine. To provide a useful model for analysis, the processed vertebrae were assembled along their Cartesian planes within SolidWorks. Intervertebral discs were created, then the bone growth regions were created, and then pedicle fixation was added. Finally, the assembled spine model could be imported to ANSYS for stress analysis using FEA.

7.5.1 Assembly of Individual Vertebrae

Before placement of vertebrae took place in the SolidWorks CAD assembly, each vertebra was individually repositioned and aligned along its Cartesian planes. Realignment was done in GeoMagic Freeform[51] or Autodesk Meshmixer[50]. Once aligned, the vertebrae were arranged parallel to each other and were manually dragged into a rough tolerance of their final position. Once vertebral bodied L2 to L5 were roughly placed, a mesh outline of the Basic model was overlaid over the assembly. This allowed the spacing of the vertebrae to be matched to the approximate spacing of an intact spine. The crucial spacing of the facet joints was determined by trial and error. The vertebral placement would often match the overlay spine but on inspection with a cross section, the facet joint volumes would be overlapping and thus would cause issues downstream in FEA. To fix this, small movements and rotations of the vertebrae were manually applied. Contrast to better show separate vertebrae was also added by the way of changing saturation as seen in the cross section on Figure 7.8. Exact matching of spacing could not be achieved, but the model is very close to anatomically correct.

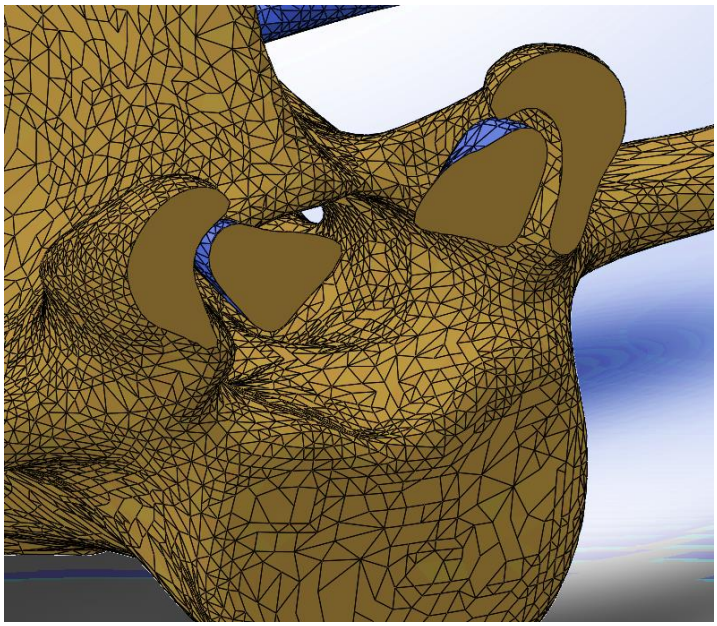

Figure 7.8: Cross-section showing detail of facet joint placement and differential colouring.

7.5.2 Creation of Intervertebral Discs and Bone Healing Zones

With the arrangement of the spine finalised, intervertebral discs were lofted between the vertebral endplates. This involved outlining a profile for each endplate, then lofting this profile to the matching vertebral endplate on the next vertebrae. The loft was done in two stages for each intervertebral disc--once for the outer annulus fibrosis (a fibrous ring on the periphery) and again for the nucleus pulposus (a gelatinous core) as shown in Figure 7.9.

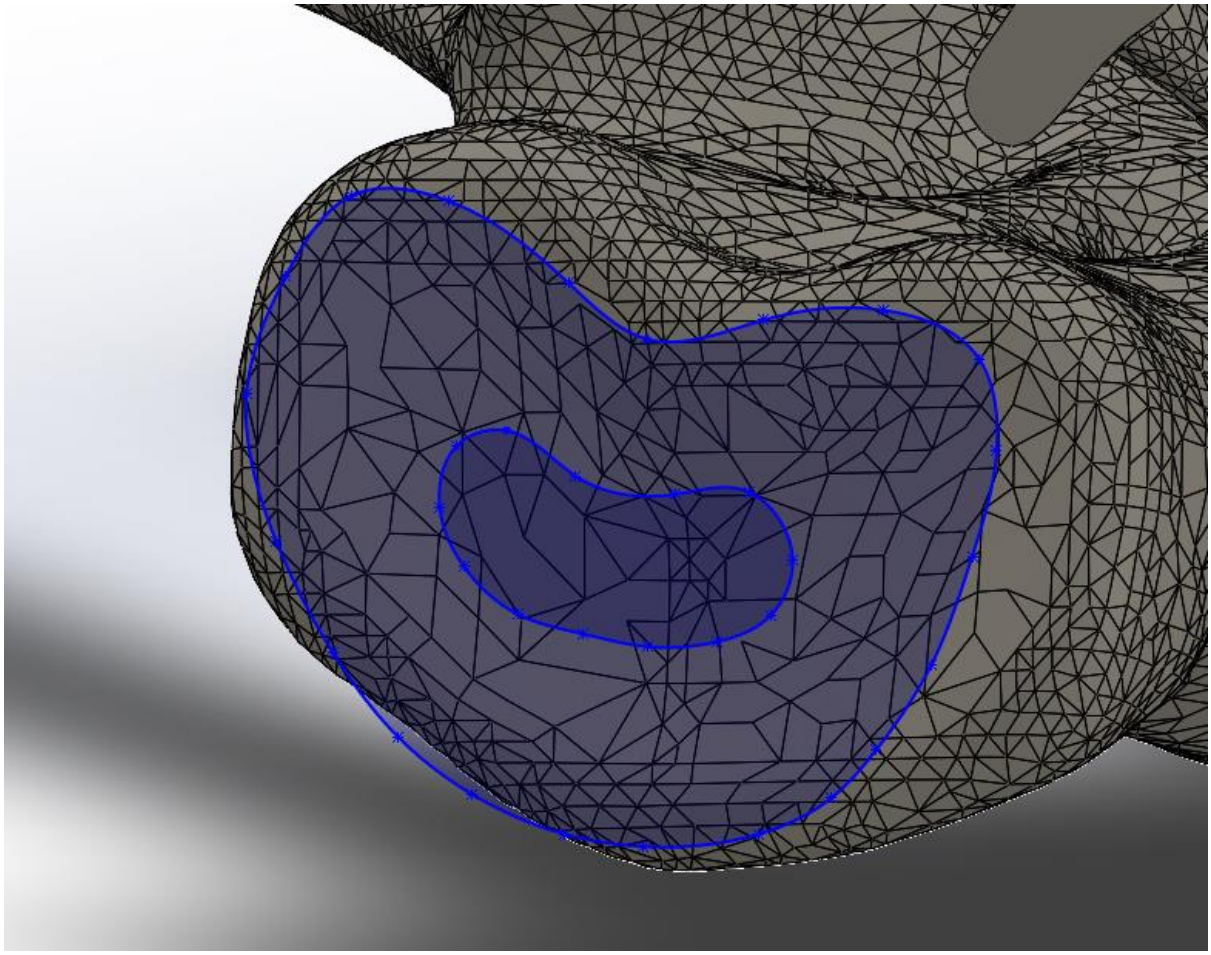

Figure 7.9: Profile of the L2-L3 intervertebral disc. One section was extruded to become the annulus fibrosis, while the inner section became the nucleus pulposus.

The addition of a bone healing zone was carried out with a similar technique. Sketches were created roughly bisecting the transverse processes of adjacent vertebrae. A volume loft was applied between the processes, connecting L3 and L4 and “fusing” them. The newly created bone growth zone and L3/L4 vertebrae were then separated back into separate parts via surface cuts. This resulted in a separate body for each bone growth zone and the L3 and L4 vertebrae being separate again as shown in Figure 7.10.

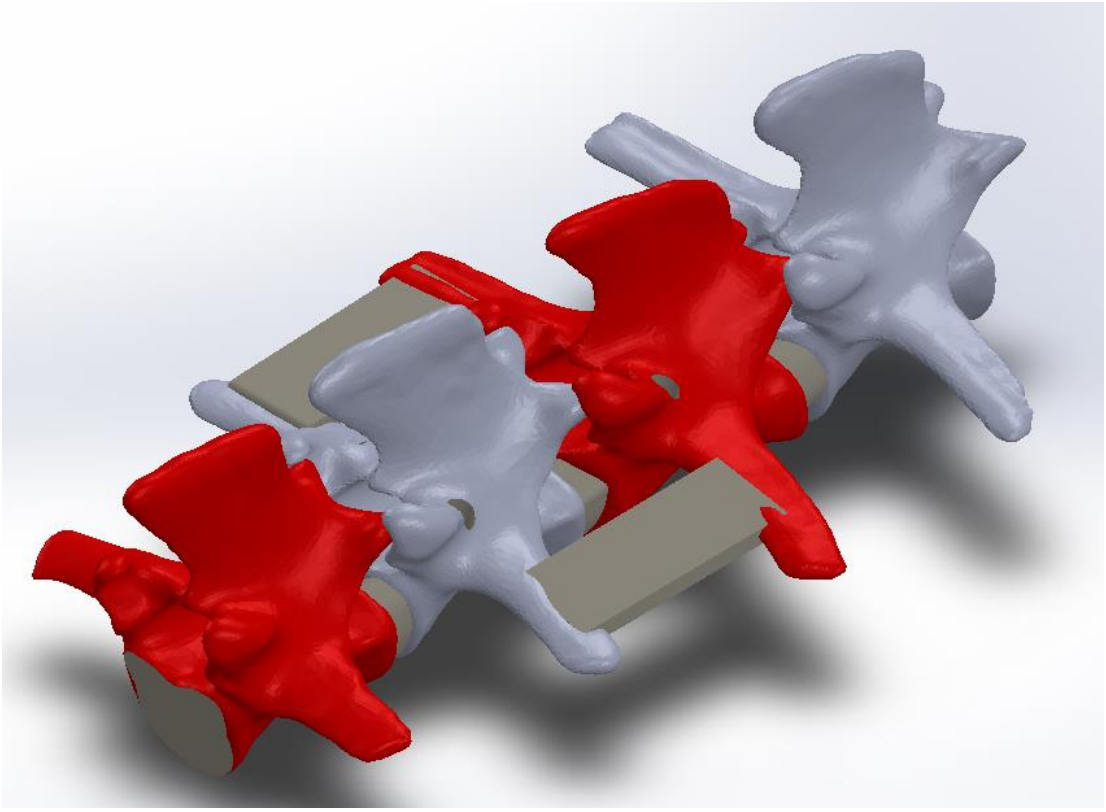

Figure 7.10: Completed Advanced model including bone growth zones.

7.5.3 Inclusion of Spinal Instrumentation

The final step in the CAD assembly of the sheep lumbar spine was the addition of spinal instrumentation with pedicle fixation. Extruded cuts were made in the L3 and L4 vertebrae in matching locations, diameters, and angles seen in CT scans (Figure 7.11) to mimic the holes created when positioning pedicle screws during a spinal fusion surgery. CAD models of the pedicle screws were inserted into the holes, and spinal rods were then bridged between two pedicle screws on either side of the spine and fastened with pedicle nuts. All spinal instrumentation was given a titanium material type in the CAD model. The resulting assembly is shown in Figure 7.12.

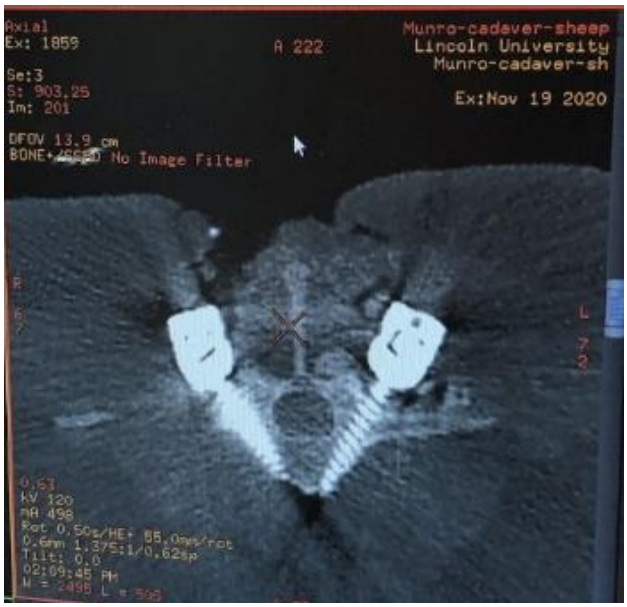

Figure 7.11: Correct angle of pedicle screw drilling as performed by Dr Brent Higgins.

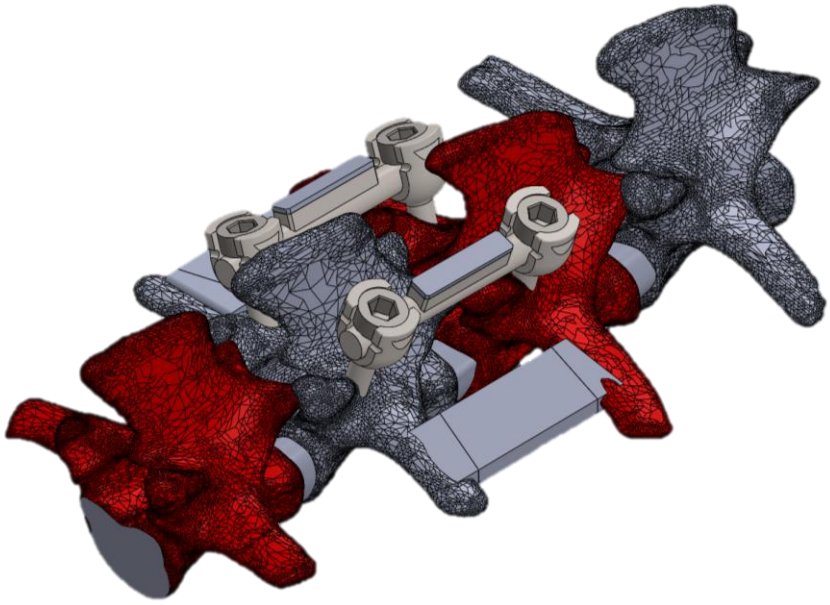

Figure 7.12 Finished Advanced model with pedicle fixation.

Once satisfied with placement of all necessary parts in CAD, the completed Advanced model was imported to ANSYS where FEA could begin.

Chapter 8 FEA – Analysis of Spinal Fusion

8.1 Introduction

This chapter introduces and covers one of the primary objectives of this thesis: modelling a sheep spine that replicates what is seen in real life and configuring that model to simulate a growing bony fusion. The first step of this process involved running static FEA studies on individual vertebrae to verify mesh quality and then continued to full-scale FEA modelling that considered the changing strength of the bone healing zones (BHZ).

The structure of bone in and around the spine has a very complex geometry, making traditional methods of calculating stress and strain very difficult. This is compounded by the fact that bone is structured to be optimised in how it carries load. Cortical bone contains a dense aligned cell structure and is close to the surface where stress is the greatest. Bone also has a spongy core that is optimised to carry directional loads with a minimal mass. A finite element study can overcome most of these limitations with the ability to numerically calculate solutions to a wide range of loads, mesh, boundary, and material conditions at once. This is important in a structure with a wide and changing range of properties such as healing bone post spinal fusion.

Multiple FEA studies were run, each with slightly different properties of bone at the fusion site to model how the bone forms a callus, takes load, and remodels. Loads and boundary conditions could be kept nearly identical once set up, streamlining the process. It was intended that data gathered from the live sheep study would be used to validate the model and provide basis for fine tuning. However, this never eventuated.

Two main models were used; a Basic model with basic geometry to develop processes and test boundary conditions and materials, and an Advanced model that closely replicated sheep lumbar spine anatomy. Both models featured the addition of healing zones where bone strength was altered from the stiffness of cartilaginous (woven) bone for a soft bony callus during early spinal fusion to the full stiffness of healed and remodelled cortical bone.

8.2 Basic Model and Initial Work

The first FEA work that was carried out involved validation checks on multiple lumbar spine parts, assemblies, and geometries for their compatibility with meshing and boundary conditions.

8.2.1 Basic model validation checks

The bone models, as described previously, were developed from CT imaging; there was a need to test these models for their ability to mesh and be able to run in an FEA simulation. The Basic model was imported into SolidWorks, the end faces trimmed to be flat, and a preliminary study performed using the SolidWorks Simulation inbuilt FEA solver (Figure 8.1). One flat end of the geometry was constrained and a 10 N to 100 N load was applied to the other end as seen in Figure 8.2; a metal alloy was used as the default material. If this simple study could be meshed and run, the imported spine geometry was valid.

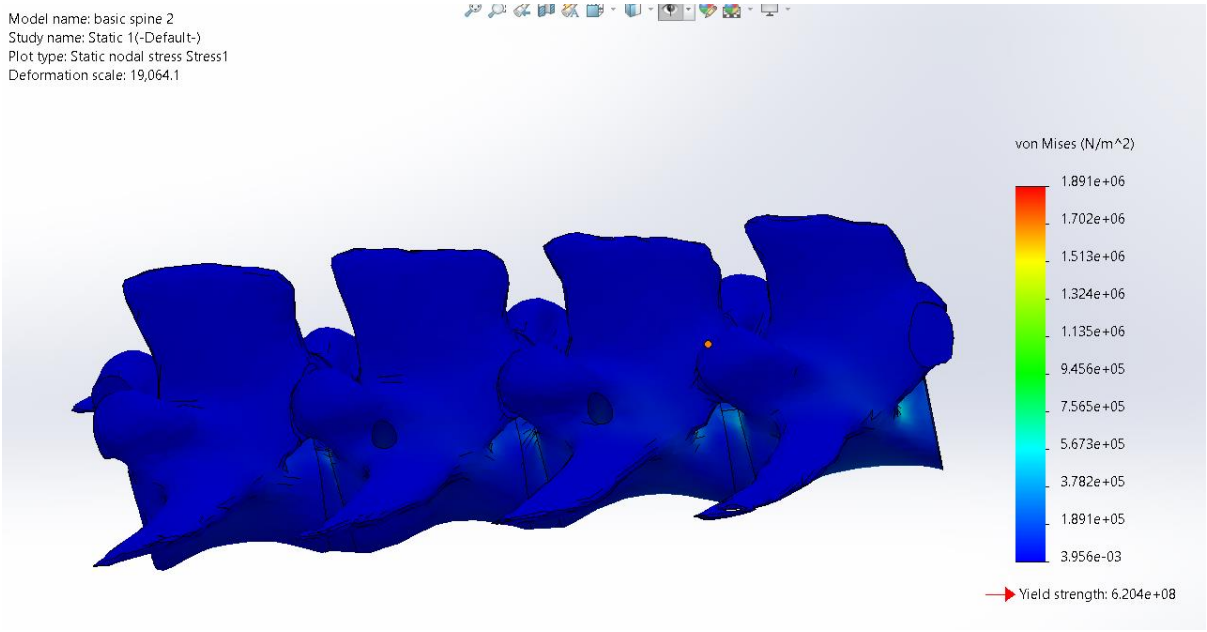

Figure 8.1: Example of validation meshing and FEA in SolidWorks.

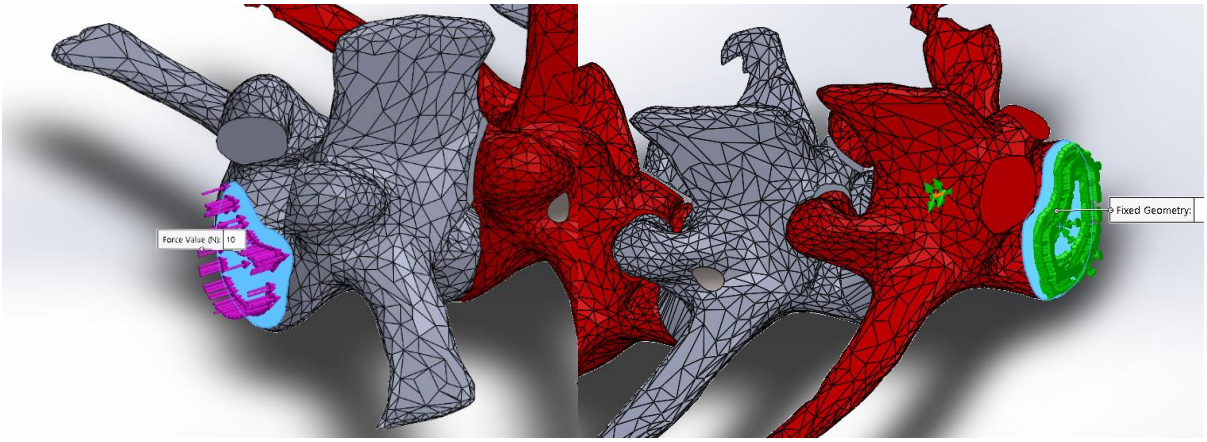

Figure 8.2: A) Compressive load applied on L2 flat end. B) Fixed constraint condition on L5 end.

On successful validation, the basic model was further built upon in CAD; however, with the addition of the spinal instrumentation at the pedicle landmarks on the spine, the model became too large to mesh and run in SolidWorks Simulation. A more powerful solver was required. ANSYS Mechanical was selected as the FEA solver due to its powerful inbuilt meshing, ease of use, and ability to chain multiple studies together within ANSYS Workbench, a graphical user interface tool. Two versions of the Basic model were created: one with bone healing zones and one without. Most static analyses were conducted on the model with BHZ, while the other model was used for transient analysis because it more closely matched a 3D printed plastic spine used for mechanical testing. During the early stages of analysis, a selection of metals and plastics were used to emulate the difference between bone and cartilage-like materials, such as found in the intervertebral disc and other non-bone areas. Typical material selections for the Basic model are shown in Figures 8.4 and 8.5, with the bone modelled as steel and the intervertebral disc as ABS plastic. Figure 8.5 further illustrates how the BHZ were modelled as PVC plastic. Later versions of this model used a range of softer to stiffer plastics and rubbers in the BHZ to give some representation of healing bone.

In reality, there is muscle between the transverse processes of each vertebrae, and bone healing is initiated with a bone growth factor, usually morselised bone harvested from the iliac crest on the

pelvis of the sheep. The morselised bone is sprinkled around the spinal rods and screws and grows in an organic, nonlinear manner, as seen in Figure 8.3. These CT scan images were generated from a prior study on lumbar spinal fusion in a sheep model. The BHZ in the current thesis were simplified to rectangular cross-sections to facilitate FEA modelling.

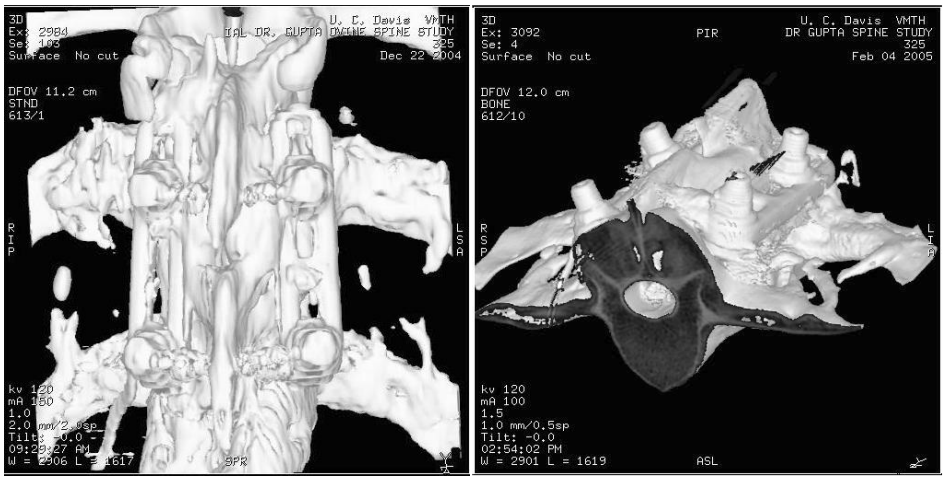

Figure 8.3: CT scan images showing bone growth occurring 17 weeks after spinal fusion surgery.

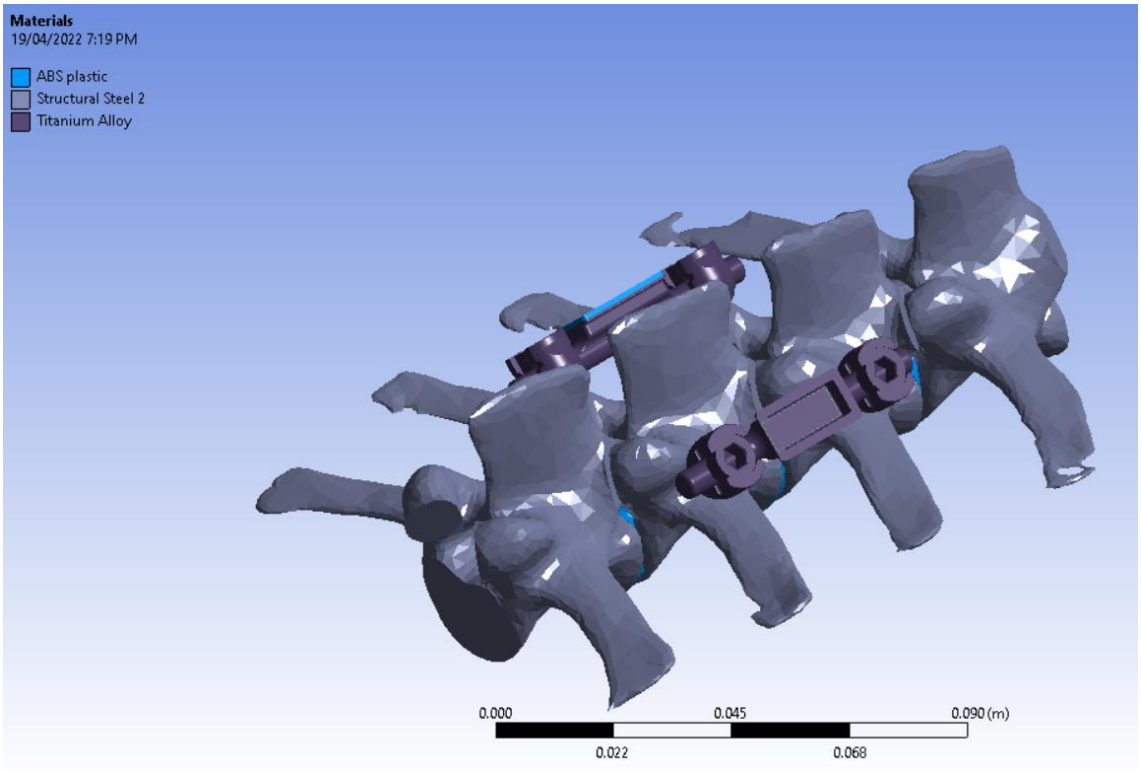

Figure 8.4: First version of Basic model without BHZ showing material choices in ANSYS Mechanical.

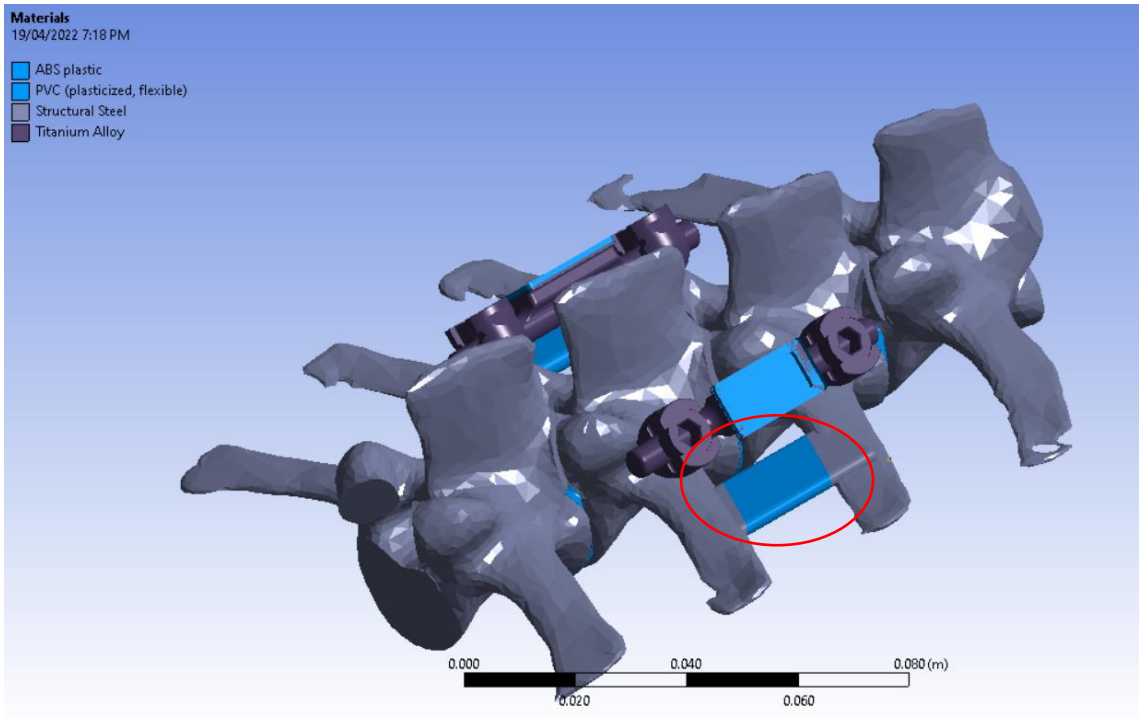

Figure 8.5: Material scoping of basic model with BHZ (circled).

8.2.2 Boundary conditions

The primary loading condition was a 100 N axial compression load applied to the L2 upper vertebral flat end of the lumbar spine. The lower L5 flat end was fully constrained in all degrees of freedom, as shown in Figure 8.2. These were not representative of physiological loading in a sheep but were suitable for developing the FEA model.

All initial contacts were considered fully bonded and parts did not move independently. Automatic contact detection was set to off, because with the material choices and loading magnitude used, self-contact was not an issue as deformations were not large enough to require recalculation of the model with each load step. However, later versions of this model that included BHZ increased computation time considerably and necessitated use of the large deformation mode turned on to account for deformation between load steps.

8.2.3 Advanced model validation checks

The Advanced model required the use of ANSYS for FEA checks because the MARS-derived vertebral bodies were too large and complex for SolidWorks FEA to mesh without failure. Similar to the Basic model, but at a more granular level, one end of each lumbar vertebrae was constrained and the other end had an axial load applied as shown in Figure 8.6 for vertebrae L3.

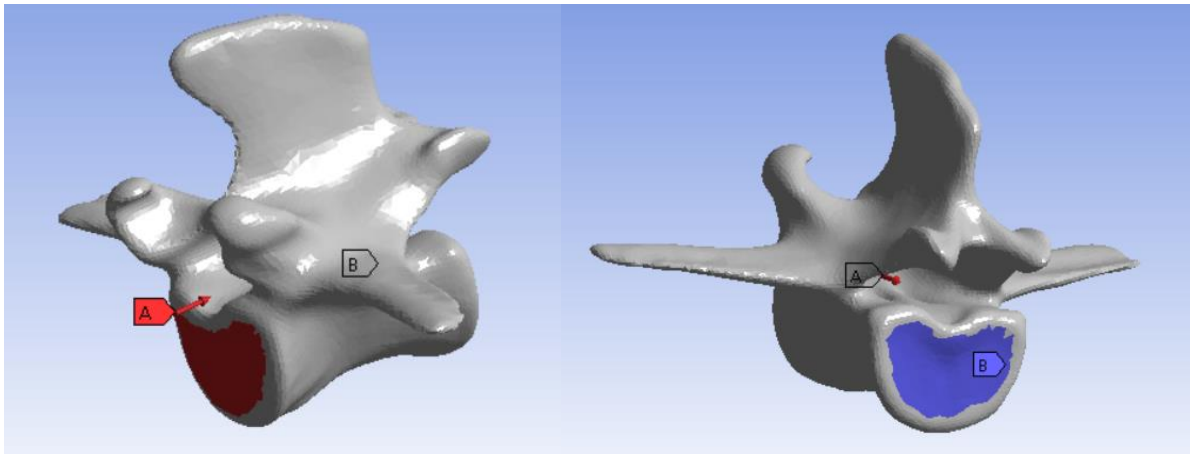

Figure 8.6: Placement surface for loading (A, red) and fully fixed constraint (B, blue) areas on L3 vertebrae for validation checks in ANSYS.

This was repeated for each vertebra to ensure that the FEA simulation would run when all vertebrae were assembled and intervertebral discs generated. Metal alloys were used for the bone material when checking the mesh integrity (Figure 8.7). The loading was a 100 N axial compressive load.

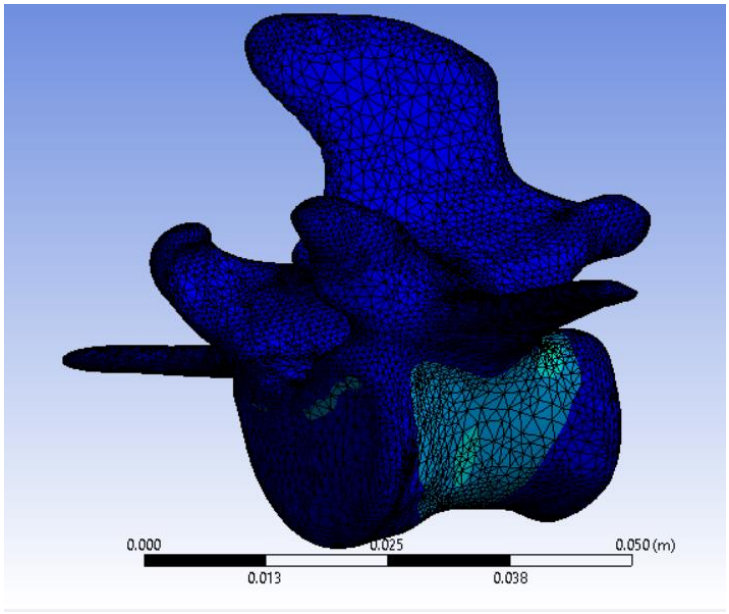

Figure 8.7: Output of validation check for L3 vertebrae in ANSYS.

Once all individual lumbar vertebral bodies were determined to be functional in FEA, the Advanced model of the lumbar spine was assembled in CAD, with intervertebral discs, spinal instrumentation, and BHZ added. The model was then imported to ANSYS in its entirety and run with basic boundary conditions of one constrained end and one axial load at the opposite end. Once it was ascertained the full lumbar spine assembly would mesh and run, more representative materials, like bone and a soft annulus fibrosus for the intervertebral disc, were introduced.

8.2.4 Limitations of models

The linear properties of the materials used for the Basic model analysis resulted in predictable load-to-stress and -strain outputs; however, real bodily tissues are viscoelastic. A complete material library would need to be used to obtain more accurate results, so these were incorporated in the Advanced model.

In addition, the introduced BHZ required a longer solve time to process; however, if the geometry would mesh, the model would run. Importing the CAD model from SolidWorks generally meant that there were no mesh errors during the meshing and analysis steps for ANSYS, and while there were improvements that could have been made, such as filleting edges where stress concentrations were found, the Basic model ran well and served its purpose.

The Basic model was mainly set aside when the Advanced model's geometry became functional and stable; however, the Basic model proved more useful for a transient analysis, as the Advanced model was much slower and less efficient for this process.

8.3 Transient Model

For the benefit of another researcher, a transient model of spinal movement was developed to create data for training a computer science machine-learning model of spinal fusion. The setup of this FEA simulation was based on the Basic model of the sheep lumbar spine. The goal was to produce a transient load case that approximated a sheep's gait to create output data that was usable in predicting the state of spinal fusion via machine-learning algorithms.

8.3.1 Model setup

Setup of this model involved linking the static structural study from ANSYS to a transient, time-dependent analysis. Setup data from the Basic model was shared directly into the transient study. This way, the mesh and materials were common between the two FEA studies. Then, the static mechanical loading was replaced with time steps to show the side-to-side motion of sheep gait. The ANSYS Workbench interface allowed for easy sharing of data between analysis modes as well as study linking. The structure of the Basic model is shown in Figure 8.8 for a 5-second analysis and a transverse load. A virtual strain probe was applied to the recessed face of one of the spinal rods for comparison to mechanical testing data.

The initial version of the transient model omitted BHZ for simplicity, but later versions included them in the analysis. This systematic approach mirrored the setup for the static Basic model. For the boundary conditions, the fully constrained and loaded faces of the transient Basic model matched the static Basic model. The primary difference between static and transient was the direction and magnitude of the primary load (from compressive to shear).

8.3.2 Gait Simulation

To approximately simulate the side-to-side gait cycle of the ovine lumbar spine, a sinusoidal 100 N peak amplitude load was applied over a 5 second period. This was discretised into 40 time-steps with variable time-step length dependent on the load rate of change. The load was applied in the z-direction from the L2 upper flat end and is shown in Figure 8.8 near its final time-step.

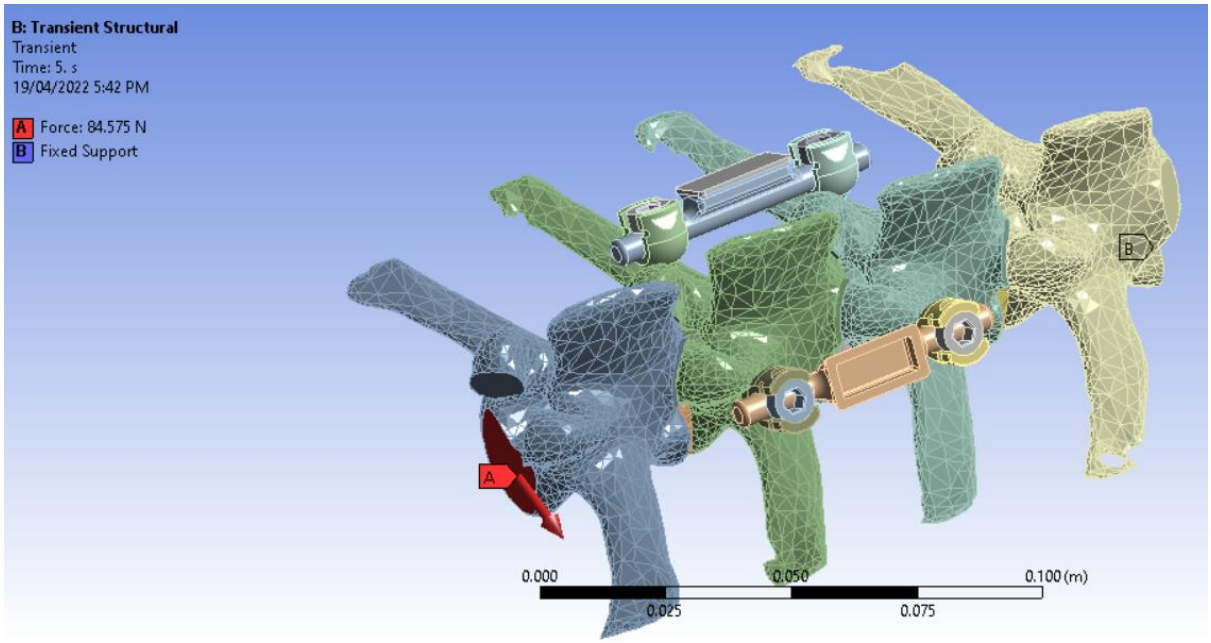

Figure 8.8: Basic model setup for transient analysis. The opposite face (B) is fully constrained.1.3.3 Outcomes

The transient model proved successful for creating data for the other researcher's machine-learning algorithm. Further simulations with more realistic bone and tissue materials would have been beneficial in creating a more valid model, but the Basic transient model was useful for understanding how the change in stiffness of the BHZ affects the load going through the spinal instrumentation and its corresponding influence on strain in the lumbar spine.

8.4 Advanced Model

The Advanced model was developed to provide a more accurate FEA model of the sheep lumbar spine and bone healing during spinal fusion. The primary differences between the Advanced model and the Basic model included: anatomically correct facet joints, anatomically correct intervertebral discs with the inclusion of the annulus fibrosus as an outer ring and the central nucleus pulposus as a region of gelatinous material, and the use of a full bone, ligament, and cartilage library compiled as a database for this thesis. The Advanced model was designed to be used for comparison with an ovine lumbar spine prepared for mechanical testing. The loads used matched the expected load for mechanical testing of a 5 Nm moment applied through a 4-vertebrae spinal column undergoing flexion in a test jig.

8.4.1 Initial work

The first version of the Advanced model was created by importing the MARS-derived geometry from SolidWorks into ANSYS Mechanical. This model had anatomically correct facet joints and improved fidelity. The same validation checks used in the Basic model were used to check the geometry for its ability to mesh and run in FEA.

The first version of the Advanced model consisted of two spinal rods with sensor housings, a single material for the intervertebral discs, and extruded bone growth zones as shown in Figures 8.9 as a solid and Figure 8.10 with meshing.

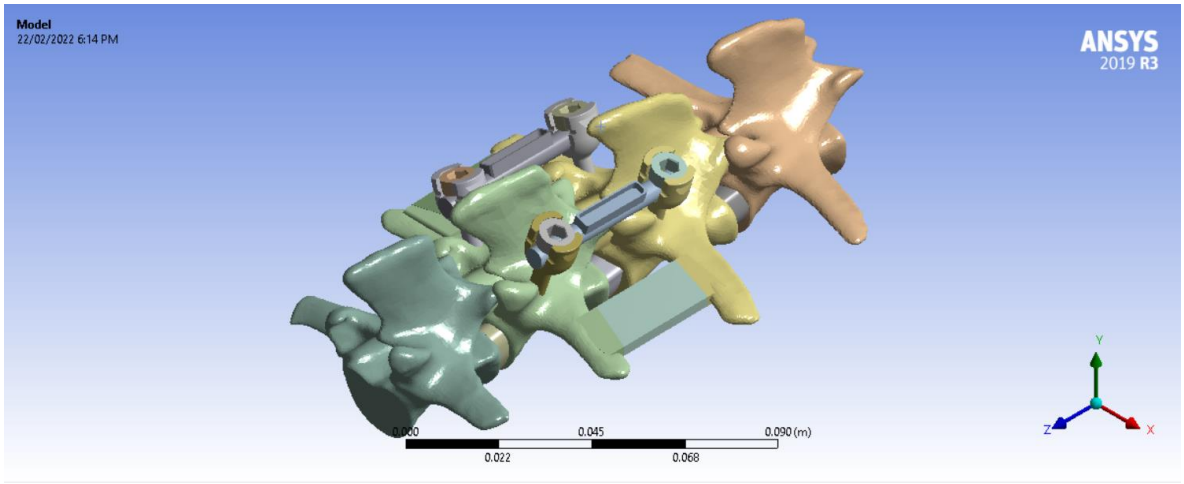

Figure 8.9: First version of Advanced model.

Like with the Basic model, the L5 lower end was fully constrained in all degrees of freedom. This constraint was active for all analysis modes and studies for this thesis. For the L2 upper end, initially a 100 N axial load was used for verification work on the FEA model. This was then replaced with a 5 Nm moment around the X axis acting on the L2 upper end. This simplified loading did not accurately represent the loading present in an actual sheep's spine but was of the correct magnitude and direction; however, artefacts of the chosen loading and boundary conditions altered the location of the measured stresses and strains in the sensor housing, as well as the BHZ.

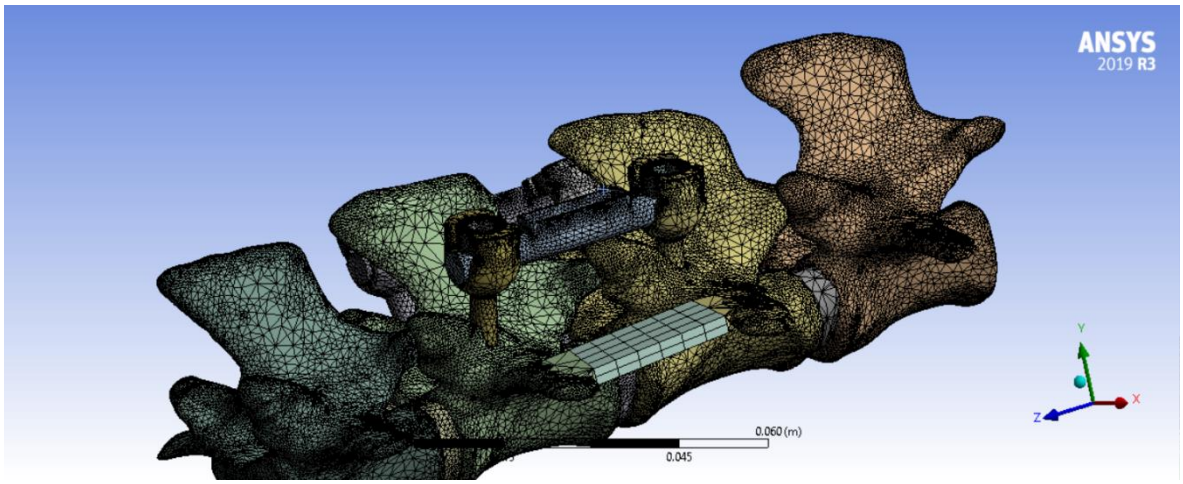

Figure 8.10: Initial mesh of Advanced model.

8.4.2 Materials for spinal construct

Materials were initially set to use the same set of plastics as the Basic model (PVC and ABS). Using a created tissue library, materials were set for each body as described in Table 8.1.

Table 8.1: Material selection for each body.

BODY	MATERIAL
L2 VERTEBRAE	Bone Type 1
L3 VERTEBRAE	Bone Type 1
L4 VERTEBRAE	Bone Type 1
L5 VERTEBRAE	Bone Type 1
D2 INTERVERTEBRAL DISC	Annulus Fibrosus (Approximation)
D3 INTERVERTEBRAL DISC	Annulus Fibrosus (Approximation)
D4 INTERVERTEBRAL DISC	Annulus Fibrosus (Approximation)

SPINAL ROD WITH HOUSING	Titanium
PEDICLE SCREW	Titanium
PEDICLE NUT	Titanium
LID FOR HOUSING	LCP injection-moulded plastic
BONE HEALING ZONES	Bone Types 1 – 5

Standard materials were provided in the ANSYS-supplied Gravita Engineering Toolbox Library. Bone Types 1 through 5, cartilage, and intervertebral disc materials were generated as an average determined from a clinical literature review regarding these tissue types, which is discussed in detail in the chapter on materials. Bone 1 corresponded to healthy trabecular/cortical bone. This was the stiffest of the biological materials used. Bone 5 corresponded to the soft callus (scar tissue-like woven bone that forms around fractures and stabilises the healing bone) and was the least stiff biological material used. Bone types 2, 3, and 4 represented intermediate stiffnesses as the woven bone is mineralised to become cortical, fully fused bone. Properties of these materials, as well as the bulk annulus fibrosus (for the intervertebral disc), properties are shown in Table 8.2 as well as Figure 8.11.

Table 8.2: Biological tissue mechanical properties used in first Advanced model.

TISSUE	E LASTIC MODULUS (GPA)	POISSONS RATIO	YIELD STRENGTH IN COMPRESSION (MPA)	YIELD STRENGTH IN TENSION (MPA)	ULTIMATE COMPRESSIVE STRENGTH (MPA)	ULTIMATE TENSILE STRENGTH (MPA)
BONE 1	12.0	0.14	140	80	185	107
BONE 2	6.64	0.24	84	48	111	176
BONE 3	4.86	0.27	65	37	86	199
BONE 4	3.97	0.28	56	32	74	211
BONE 5	1.29	0.33	28	16	37	245
ANNULUS FIBROSUS	0.988	0.33				245

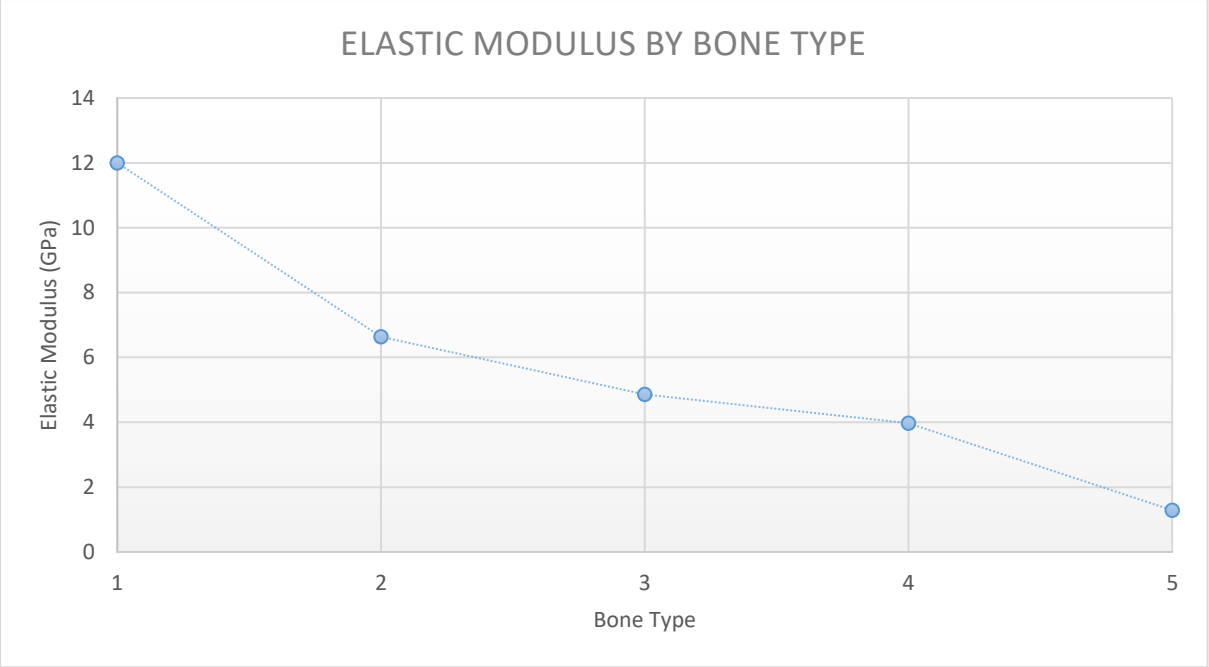

Figure 8.11: Elastic modulus per bone type. Bone 1 representative of healthy intact cortical or trabecular bone. Bone 5 is representative of soft callus tissue formed during healing.

8.4.3 Outcomes of initial Advanced model

The FEA model produced several strong trends with the simulated change of bone stiffness over time. The 5 Nm moment acting on the L2 vertebrae was held constant for all analyses. As bone stiffness in the BHZ increased: strain through the BHZ decreased, stress through the BHZ increased, and the stress and strain response of the spinal rods (both types) decreased. The full response of the lumbar assembly is seen below in Figure 8.12. The maximum stress and strain values seen in the entire model were found in the intervertebral discs because of the way the 5 Nm moment was applied at L2.

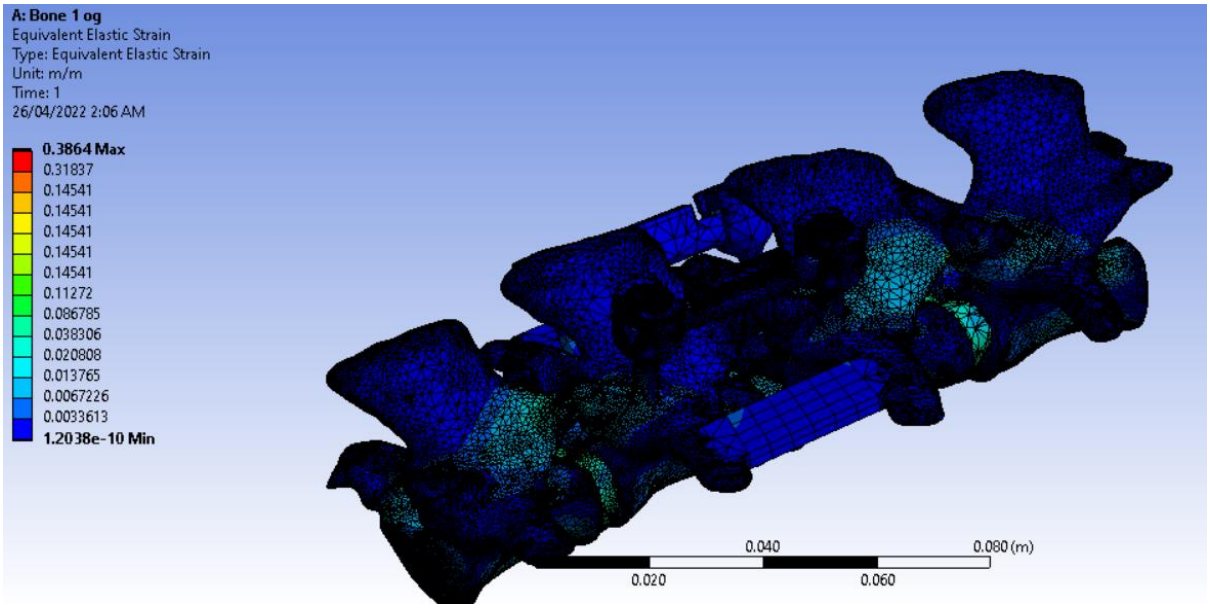

Figure 8.12: Basic model whole unit strain response for Bone Type 1 in BHZ. The highest strains were found within the intervertebral discs.

The main area of interest for this study was the strain on the spinal sensor rod with its integrated housing as a function of stiffening in the BHZ. It was found that the stress and strain response for the sensor rod was inversely proportional to the stiffness of the BHZ, as shown in Figure 8.12. From the posterior, the spinal rods with integrated housings were identified as left and right. The maximum stress and strain were measured in the housing recess on the flat face, as this is where the actual strain sensor would be mounted in live animal studies. Results are shown in Figure 8.13.

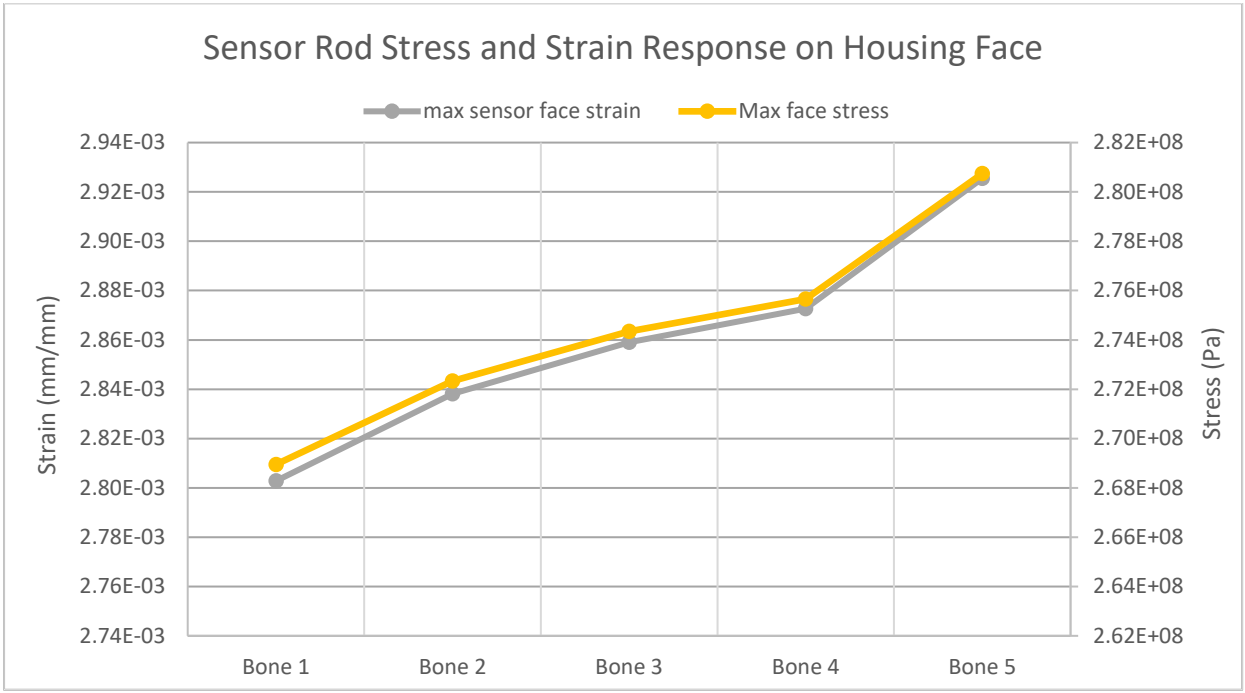

Figure 8.13: Stress and strain response through the sensor rod on the flat face of the housing.

BHZ.

8.4.4 Refinements to Advanced model

Using the same geometry as before, the Advanced model underwent some key changes (Figure 8.14) to better represent both the anatomical structure of the intervertebral discs and to better replicate the intended mechanical test setup with only one spinal rod including an integrated sensor rod.

- One of the spinal rods was replaced with a standard rod (typical 5.5 mm titanium spinal rod).
- Both BHZ had fillets applied to their square edges to reduce stress concentrations in the previous analyses.
- The base geometry was edited to eliminate a pedicle nut pretension issue by altering the pedicle nut mating type in SolidWorks from a surface contact to a tangential mate.
- Mesh resolution was increased in key areas to provide a more accurate strain response.
- Automatic contact finding was also activated because of large observed displacements on the facet joints during loading at higher load steps.

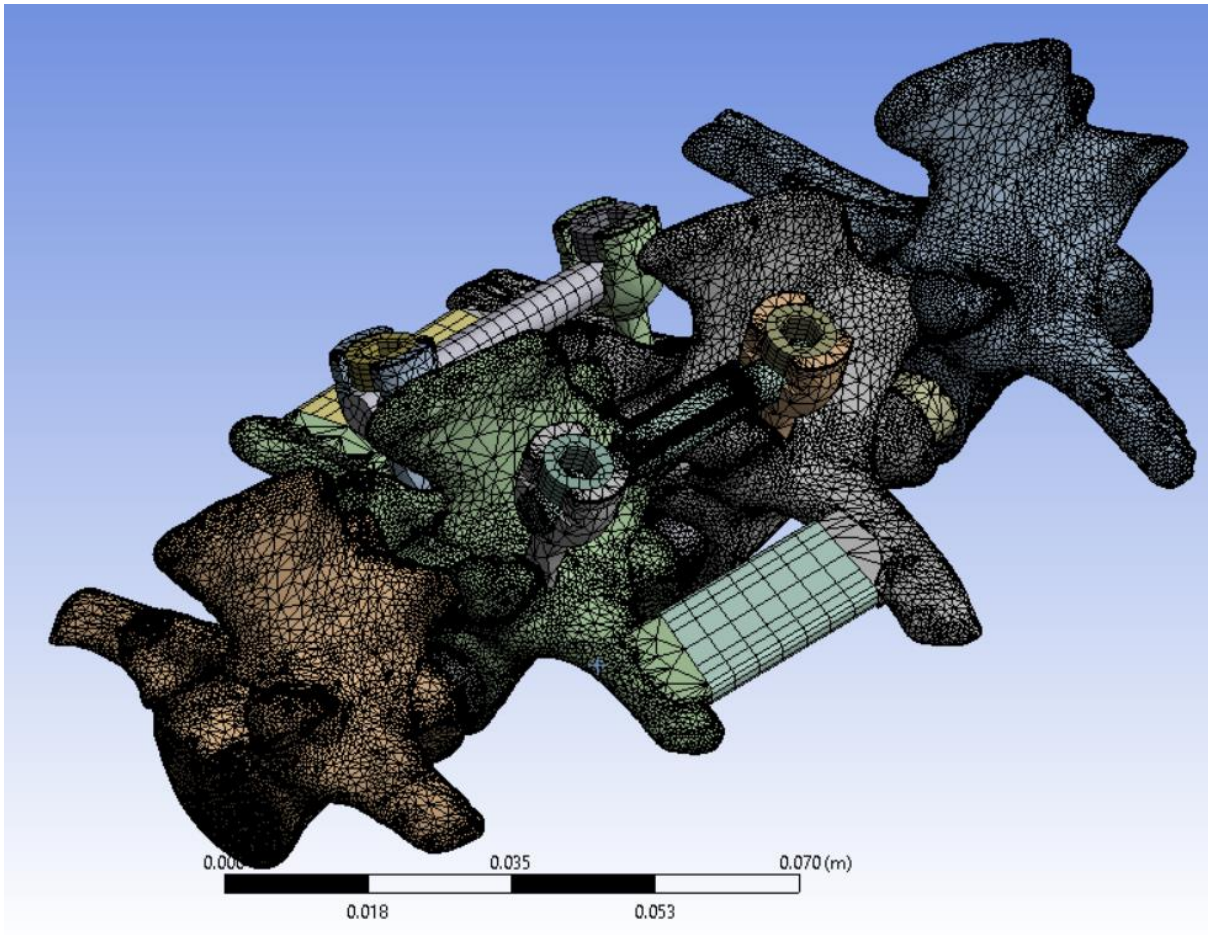

Figure 8.14: Fully meshed refined Advanced model. A standard spinal rod was used on left side and a sensor rod was used on right side of spine.

Upon review of the bone material set used for previous analyses, it was decided it did not adequately match the strengths and stiffnesses of healing tissues before the soft callus stage, particularly “granulation tissue” which forms to help stabilise a fracture. The bone material library was therefore expanded to incorporate this change for the refined Advanced model. The number of data points for bone was increased from 5 types to 8 types (Table 8.3 and Figure 8.15). This helped show the smaller changes of bone stiffness which correspond to early bone healing. The setup of other materials was identical to the initial Advanced Model with the exception that a Shore 35 PVC elastomer was applied as the core material within the intervertebral discs due to its similarity in properties to the nucleus pulposus. This material was sourced through the Gravita material library.

Table 8.3: Bone properties used for simulating the strengths of bone from fracture stabilisation to remodelling in refined Advanced Model.

Tissue	Represents	Young's modulus, E (GPa)	Poisson's Ratio	Yield strength in compression (MPa)	Yield strength in tension (MPa)	Ultimate strength in compression (MPa)	Ultimate strength in tension (MPa)
Bone 1	Fully remodelled bone	12	0.14	140	80	185	107
Bone 2	Partially remodelled bone	2.1	0.20	~	~	~	~
Bone 3	Woven bone	1.6	0.40	252	144	333	368
Bone 4	Hard callus	0.99	0.33	168	96	222	245
Bone 5	Intermediate callus	0.50	0.44	94.5	54	111	123
Bone 6	Soft callus	0.0031	0.40	21.0	12	~	~
Bone 7	Intervertebral disc	0.002	0.40	18.9	11	~	~
Bone 8	Granulation tissue	0.00099	0.40	16.8	9.6	~	~

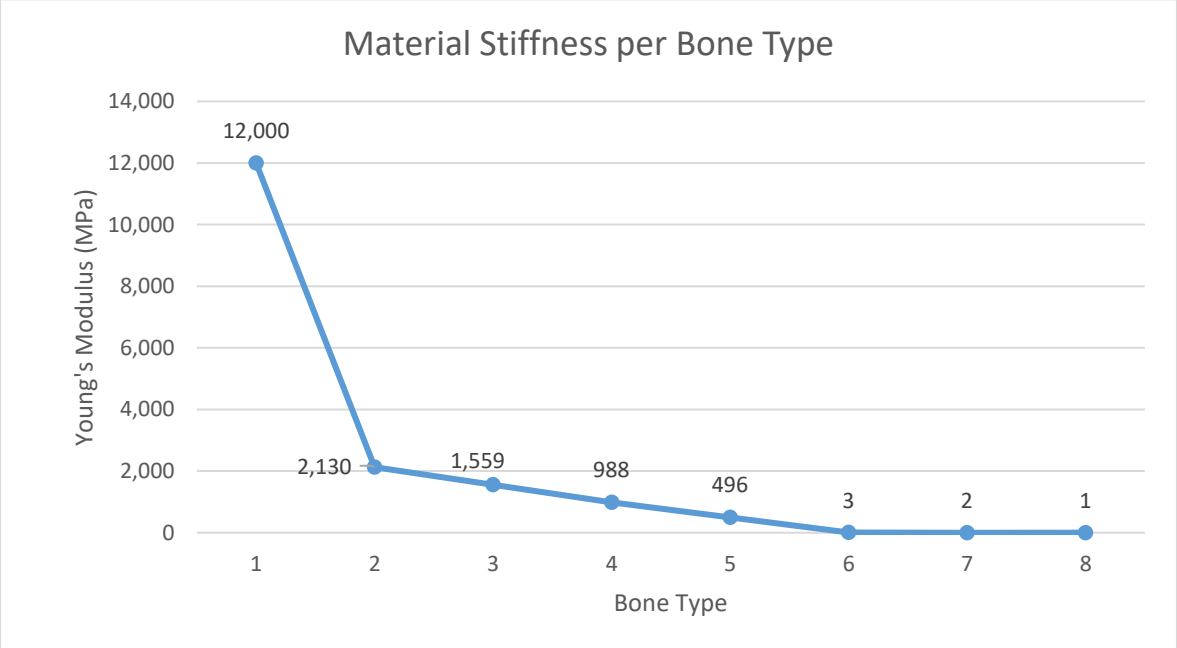

Figure 8.15: Graphical display of the changes in bone stiffness.

8.4.5 Refined Advanced Model Outcomes

Analysis of the results for the refined Advanced model were identical to the previous iteration of this model. The trends observed were the same: as bone stiffness in the BHZ increased, the stress and strain response of the spinal rods (both types) decreased. The primary differences in response of this model were that the softer tissue types (soft callus and granulation tissue) provided almost zero functional support to the loading regime due to their very low stiffnesses. A secondary outcome was the observed difference in strain through the spinal rods. The sensor rod versus the standard 5.5mm spinal rod showed the standard rod bearing more strain as stiffness increased.

The refined Advanced model had a nearly identical strain distribution to the initial model, as expected. The strain observed in the standard spinal rod was greater than the strain in the sensor rod as measured on the housing face (Figure 8.16). This made sense, as the sensor rod has a larger cross-section and therefore was stiffer in bending direction (Figure 8.17).

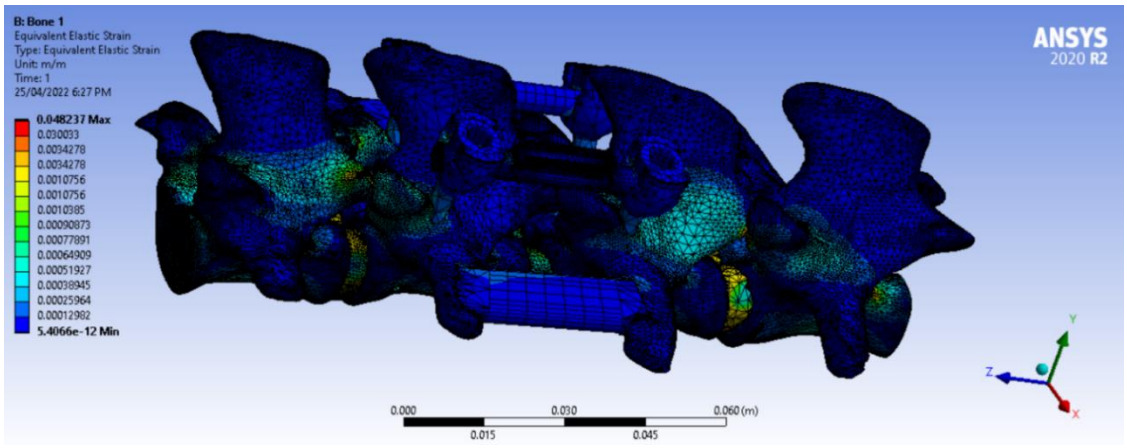

Figure 8.16: Typical strain distribution across entire model.

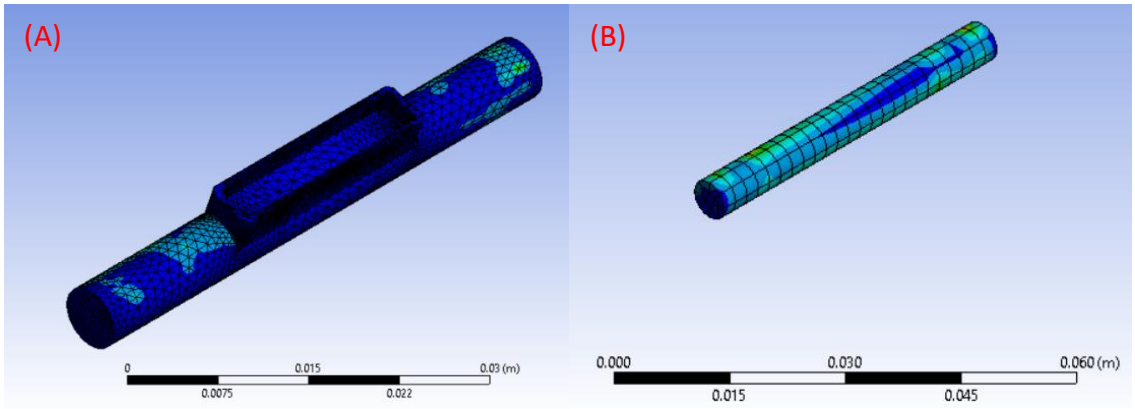

Figure 8.17: A) Typical strain distribution across sensor rod. B) Strain distribution through standard spinal rod used in spinal fusion surgery.

The increase in observed strain from one end of the sensor face compared to the other was due to the cantilever loading and fixed boundary condition applied to the FEA model. Strain on the surface of the standard rod was always greater in magnitude than strain on the housing face of the sensor rod for each bone stiffness type (Figure 8.17 to 8.19). Interestingly, the observed strain in the standard rod decreased slightly with the decrease of bone stiffness while the sensor rod at the housing face saw a slight increase of strain with the same BHZ stiffness change. This was related to the differing shape of the spinal rods and how they responded to the moment load exerted through the spine. The average stress and strain response in the sensor rod increased with a decrease of modelled BHZ stiffness. This showed that the sensor rod transferred a higher load proportion when the BHZ were simulating less stiff tissue types present in early bone healing (Figure 8.20).

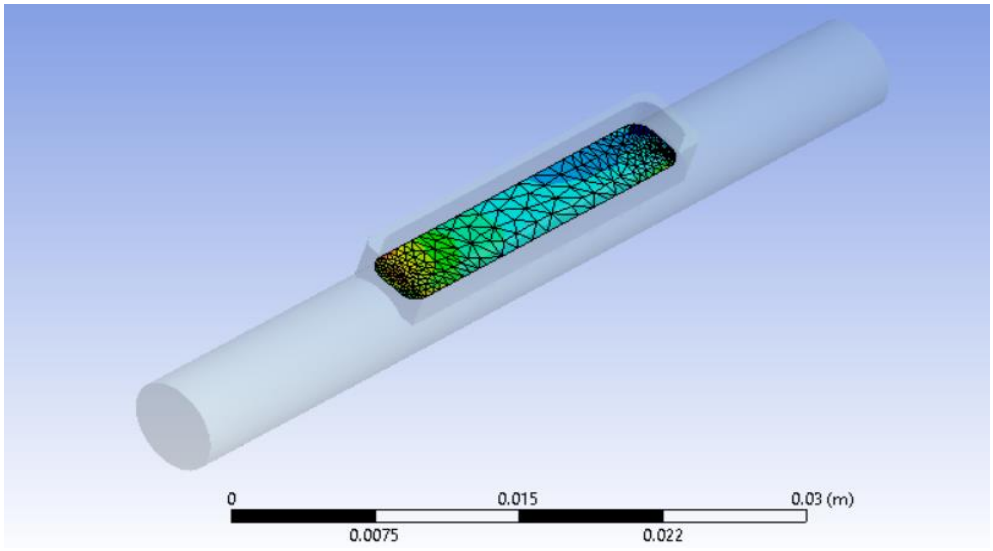

Figure 8.18: Typical strain distribution across sensor housing face.

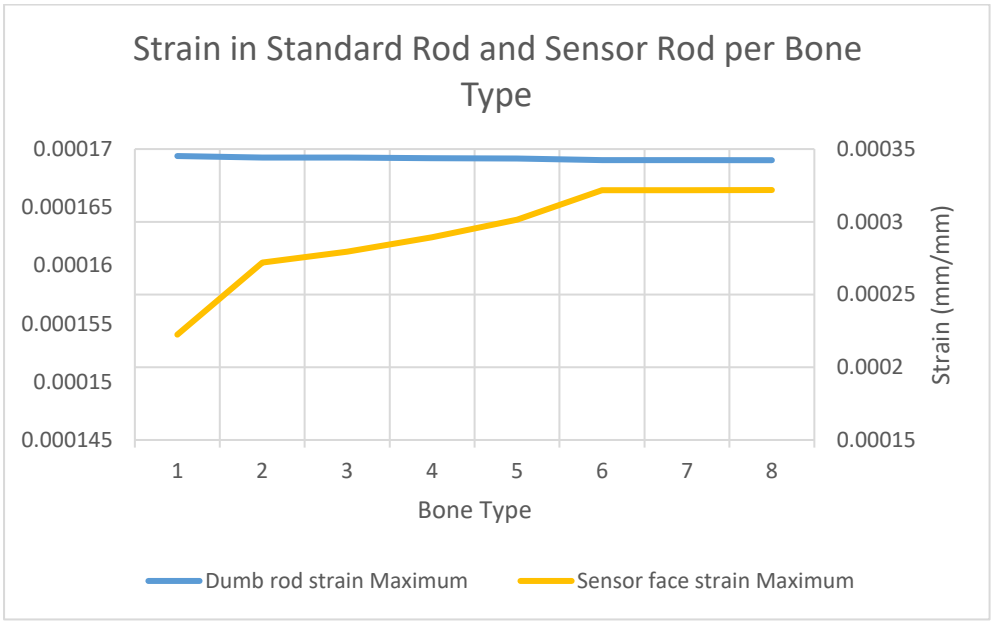

Figure 8.19: Strain through the standard spinal rod and sensor rod with change in bone stiffness.

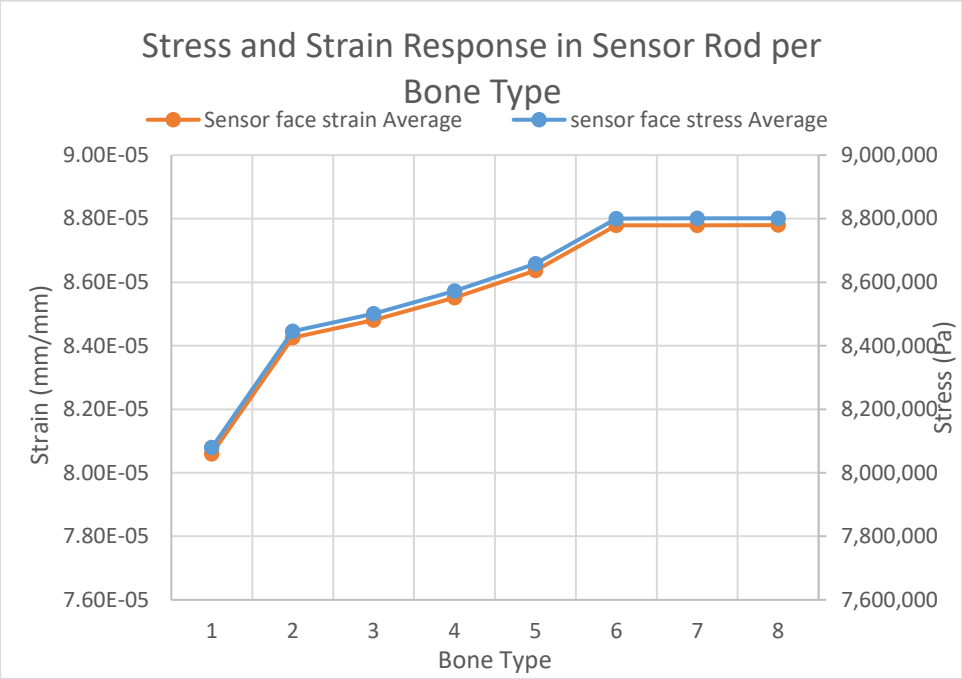

Figure 8.20: Stress and strain response through the sensor rod at the housing face for each bone stiffness.

8.5 Discussion & Conclusions

This set of FEA models succeeded in modelling the ovine lumbar spine and demonstrating how changes in bone stiffness can be modelled. The FEA model was intended to show trends of how the spine reacts mechanically during the spinal fusion process and was successful. As bone in the BHZ heals and increases in stiffness, the model deflects less (becomes stiffer), and the observed stress and strain in the sensor rod decreases. Thus, these models follow the expected result for spinal fusion.

An FEA model is only as good as the data that is input. The accuracy of the geometry and mesh were a direct match to real-life anatomical structures—the CT-to-CAD conversion process assured this. The bone materials used were researched in the literature, then characterised as classically elastic with isotropic properties; however, this is not the case in reality, as bone, ligament, scar tissue-like woven bone, are viscoelastic materials that are strain-rate dependent. The material properties are also directionally-dependent on their strength profiles, and they are stronger in compression than in tension or shear loading. Some of the materials are also hyper-plastic and/or hyper-elastic. Research has shown that variation in material properties will exist even in the same tissue type in the same specimen. As such, this brings great difficulty to the modelling process because of the vast range of material parameters. As such, creating the most accurate material properties for the various tissue types in the model will need to be determined through material testing.

The best way to improve the accuracy of this model would be to test the mechanical material properties of each tissue type at each stage of healing. An initial goal of this research was to conduct a live animal study into spinal fusion on 3 sheep that tested the mechanical properties at 0 weeks and 16-24 weeks, but this animal study was delayed. While mechanical testing was simulated in the lab with artificially-induced changes of stiffness using two-part PMMA (see next chapter on mechanical testing), this will not mimic actual bone healing in specimens collected and tested on different spines at various stages of bone healing.

This model assumed that the effects of ligaments and muscles were statistically irrelevant, as muscles do not contribute to stiffness, and the addition of ligaments only increases stiffness by 7% [58]. With a simulated 3 order of magnitude variation of stiffness in the BHZ (Elastic moduli between 12 GPa and 0.99 MPa), anatomical variation in the spine between individuals, and slight differences in surgical techniques will constitute much more significant differences in strain output than the addition of ligaments. Under identical loading, there can be substantial variation in deflection, stress and strain between seemingly similar specimens [59] [60]. The variations between specimens, and in the modelling process itself regarding materials, makes the use of ligaments and other features less significant to the results of the model.

The developed FEA model used a defined material library and output values in terms of BHZ stiffness Bone Type. A more useful way to display the results would be to display the data and changes in strain relative to healing time. However, the strength of bone relative to time is still unknown.

Chapter 9 Mechanical Testing

9.1 Introduction

A test setup that effectively simulated movement of the spine was necessary for validation of the FEA models. This setup had to fit an existing test jig with rotary encoders within the jaws of a tensile test machine while securely holding an instrumented sheep spine in a way that force was accurately transferred through the spine in a realistic physiological manner. With the vertical movement of the jaws of the tensile machine, compression or flexion was applied to the test jig holding the offset spine segment, creating a physiological moment of 5 Nm. This was measured with a set of rotary encoders (for angular stiffness calculations) and integrated strain gauges mounted on one of the spinal rods. The configuration differed between the intended tensile test machine and a modified drill press setup, but the core of the testing apparatus remained the same regardless of the tensile setup.

This chapter highlights the development of a mechanical testing apparatus for the testing of ovine lumbar spines. Two main testing apparatuses were planned to be used: a modified drill press for manual loading of the spine and an Instron ElectroPuls E3000 for automated testing. The modified drill press setup was used for development of the software and hardware systems and methods and was actuated by hand movement. The Instron was planned for automated mechanical spine testing with programmable force and displacement actuation and the ability to run cyclic testing with preload.

Both devices used the same existing test jig and shared the same developed instrumentation: a pair of rotary encoders, the method of securing (potting) the spine, a strain gauge sensor, and National Instruments' (NI) LabVIEW data logging software and DAQ modules. Test fittings, methods of measuring load and displacement, and instrumentation were developed and tested on the modified drill press with the intention to move the instrumentation to the Instron tensile testing machine once fully commissioned. The digital nature of the test equipment allowed direct transfer of equipment and methods from the drill press apparatus to the Instron.

The testing regime on the modified drill press involved simulating compression, which induced an axial load and slight flexion on a spine across the spinal hardware secured to it. This was first performed with wooden blocks simulating the spine that was spanned by spinal hardware. Testing was then repeated with a lumbar sheep spine using simulated fusion.

Simulated fusion testing was undertaken with a thawed ovine lumbar spine. In a process called potting, the spine segment was secured using M8 machine screws and a fast-setting PMMA plastic epoxy resin typically used for dental moulds into the spine pots (Figure 9.3). PMMA was also used to simulate spinal fusion by sequentially applying it to the spine to represent an increasing strength fusion mass between the transverse processes. This process confirmed that the equipment, software, and sensors for mechanical spine testing were functional, and that the LabVIEW script developed was ready for use (with minor adaptations) with the Instron.

9.2 Drill press apparatus design

To develop methods for mechanical testing, a drill press was modified with custom aluminium and 3D printed components to work with the existing test jig (Figure 9.4) to enable a strain to be exerted through a spinal rod with strain gauges attached to its exterior. The intent was to use instrumentation, such as the rotary encoders on the test jig, that had already been purchased for cyclic mechanical testing with tensile test machines. An existing load cell was also utilised. The hand

controllable vertical motion of the drill rig was useful in producing data for strain, rotation, load, and displacement, but the motion did not replicate physiological loading due to space constraints of the drill rig setup.

9.2.1 Hardware

Measurements were taken with a pair of Dynapar model 2207203440 rotary encoders mounted at either end of the spine specimen, two strain gauges mounted at the midpoint of one of the spinal rods, and a load cell at the bottom of the entire apparatus. Displacement was measured manually at two points: from the depth ruler on the drill press itself, and using a ruler between the lower plate, and the upper surface of the top encoder. All electronic instrumentation was wired and implemented to work with LabVIEW data logging software. This required the use of a 4-slot cDAQ-9174 chassis unit and DAC units NI-9402 and NI-9237. Both encoders were wired into an external power supply providing a 12V current voltage and both single-ended digital encoder outputs were wired into a single NI DAQ unit NI-9402. Each strain gauge (the sensor rod and load cell) was wired to an DA-15 connector which in turn was wired into a RJ45 ethernet port. The RJ45 cable ends were plugged into the NI-9237 DAQ unit. This allowed a full Wheatstone bridge configuration for the strain gauges. The rotary encoders were each wired from their 6-pin connection to a DA-15 port in a single-sided (5 wire) operation. A wiring jig then joined the DA-15 ports and connected both encoders to a shared DE-25 connector, each encoder using a different set of pins. This DE-25 connector was plugged directly into the NI-9402 unit. Separate leads for 12V power and grounding also interfaced at this connector. These were soldered to be common across both encoders (Figure 9.1).

The complete recording system routed all analogue signals through the NI-9237 unit and all digital inputs though the NI-9402 unit. The full wiring schematic is in Figure 9.2.

Frequent solder breakages occurred due to the movement of the wiring during actuation and during setup/pack down. This was largely resolved with the application of heat shrink around connections.

The main device for measuring strain across the spine itself was via two strain gauges bonded to a titanium spinal rod by Dr Munro. The strain gauges were wired to their connector through a shielded, 7-pin serial port which in turn was wired into a NI-9237 DAQ controller via a rj50 connector (Ethernet connector).

Force through the drill rig press was measured with the existing button-type load cell and was wired in an identical fashion to the strain gauge sensors but into port 2 of the NI-9237 DAQ controller. For the purposes of this project, a 3D printed jig was produced to hold the load cell and allow clearance for the wire. This wire was connected into the same NI-9237 controller as the strain gauge sensors and then programmed.

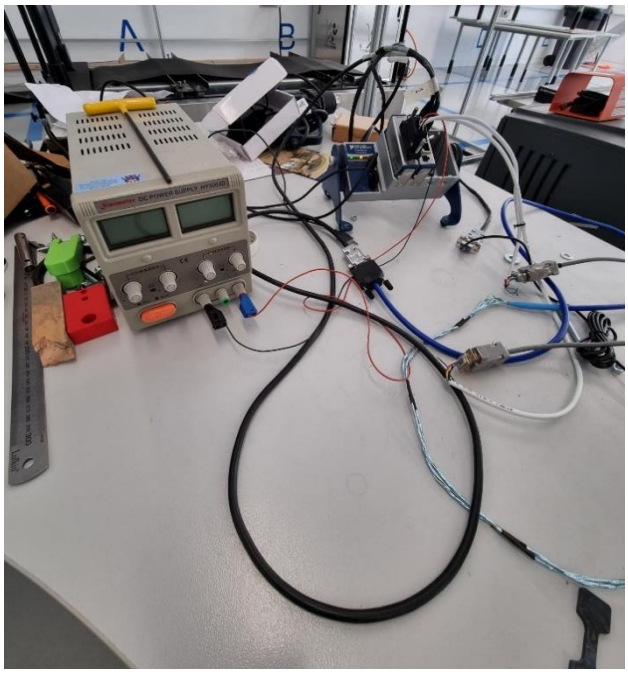

Figure 9.1: Power supply, NI cradle, DAQs and wiring harness with connectors.

9.2.2 Software

The NI instrumentation with LabVIEW was built up and trialled on the drill press rig to ensure it was working and would output the data required. This drill rig was nearly always accessible and thus

troubleshooting test equipment could be done more easily and effectively. The LabVIEW script was designed to graph all sensor outputs (sensor rod strain gauges, load cell, rotary encoder 1, rotary encoder 2) at once. Scaling factors could be input to each sensor channel in order to fine tune the outputs, if required. In recording mode, the script would write all sensor values to a CSV file at the sampling rate of the slowest DAQ unit (NI-9402 unit). In the event of lag when writing, a counter would show the delay of "packets in queue" yet to write. This was coded in as a troubleshooting tool for a "write to cloud" scenario. The script also allowed for inspection of the previous recorded file.

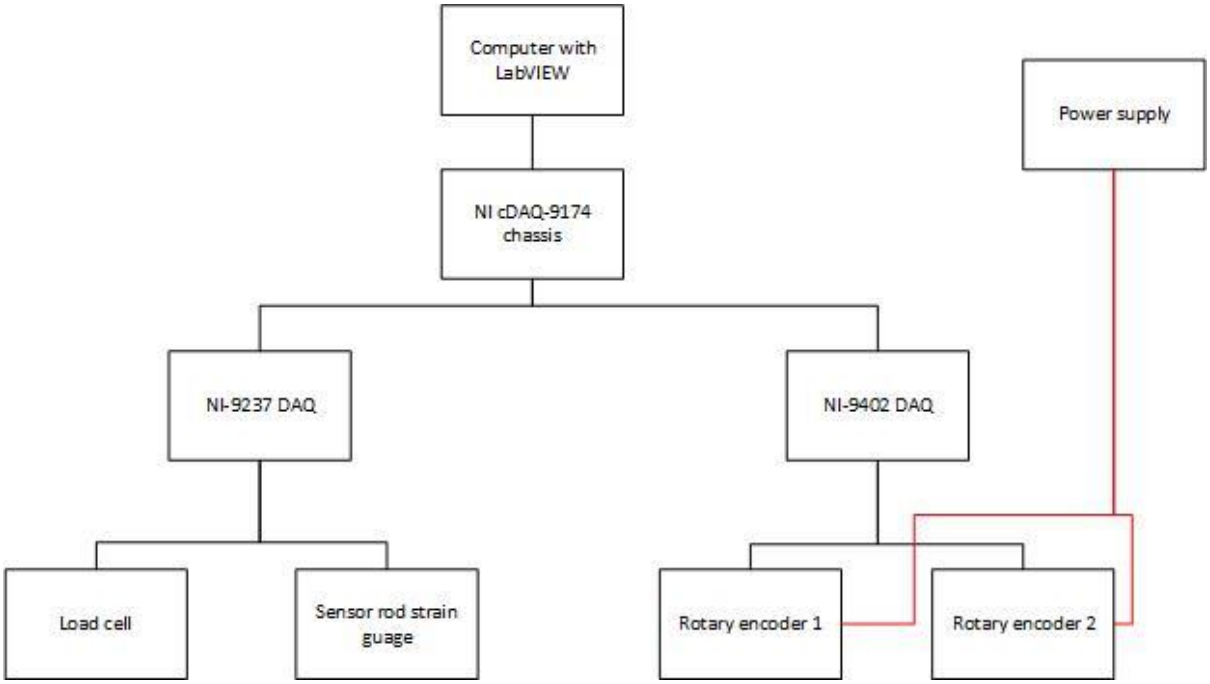

Figure 9.9.2: Wiring outline for data acquisition system used for the drill press apparatus.

The main advantages of the script were flexibility to add additional sensors or make changes to the current sensor setup. This was deemed crucial with the anticipated use of the Instron ElectroPuls E3000. While the Instron uses its onboard systems for programmable tensile testing and recording, an analogue output of each channel would be available for input into the NI system. This was important as the rotary encoders will not integrate with the Instron. For testing of spine specimens, Instron WaveMatrix software will be used for the programming of the Instron and the cyclic action used for load and displacement to obtain the desired flexion and thus physiological moment. The NI hardware and LabVIEW will continue to be used to record all sensor outputs synchronously.

9.2.3 Spine mounting pot design

For mechanical testing, the physical connection needed to be robust between the vertebral lumbar section and the test jig. This interface, in the form of pots, needed to be a high stiffness part with the ability to withstand the force of locking the ends of the vertebral sections into the pots with four M8 bolts. During the potting process, bone cement was poured around the vertebrae being held by the bolts to provide further stiffness. The pots were machined out of aluminium and resembled a box with a fattened X-shaped cavity hollowed out of the centre. This increased the threaded surface area for resisting bending loads in the bolts while reducing the volume needed for bone cement. The whole spine testing pot assembly attached to the test fixtures via two collars (one on each pot) with

4 grub screws and an H6 loose fit at a 25mm diameter. This was the diameter of the existing test fixture bosses on the test jig with rotary encoders designed by Dr Munro. A hole through the bottom of the pots was added to allow the solidified PMMA and spine to be pushed out once mechanical testing was complete, or if the pots needed to be removed for any other reason (Figure 9.3).

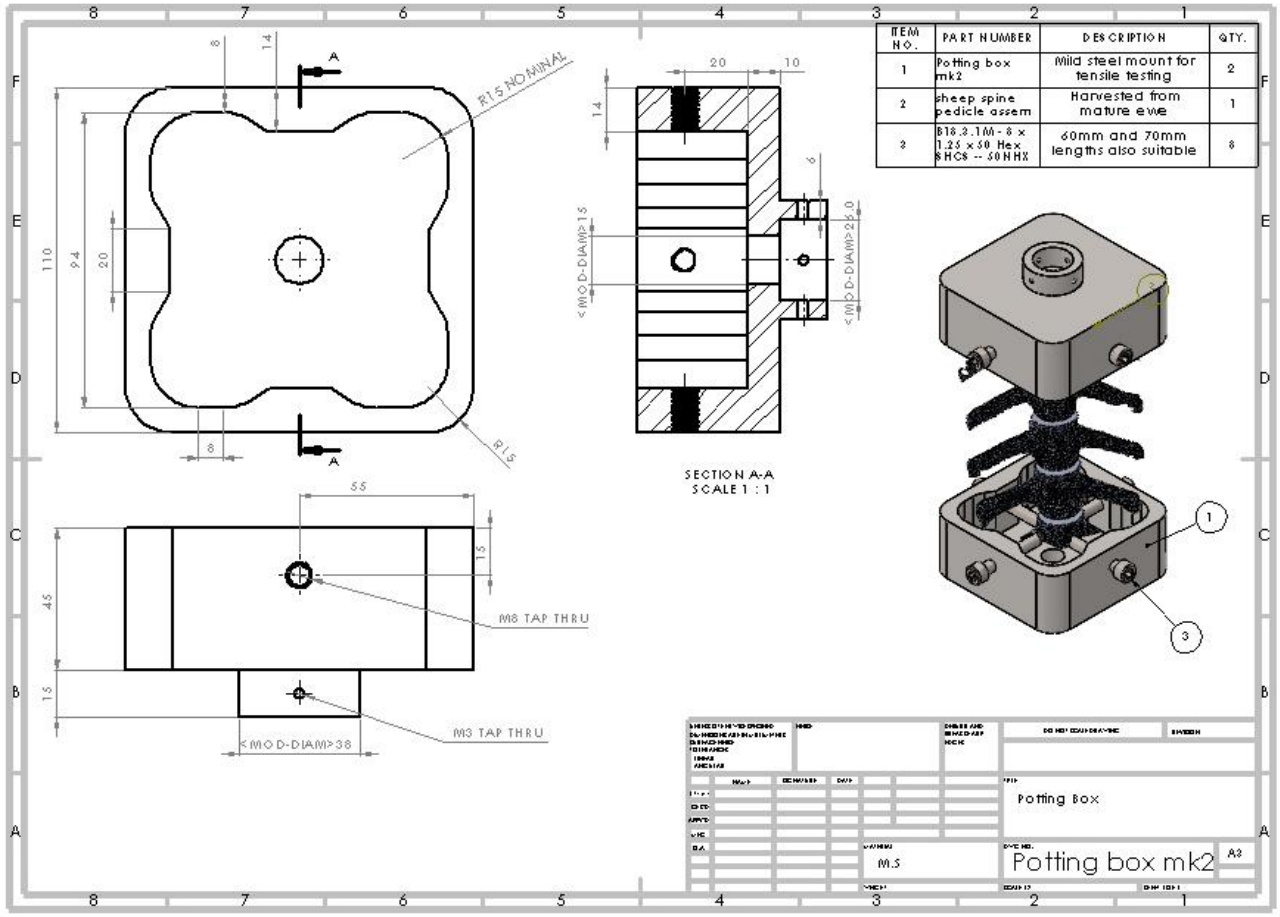

Figure 9.3: Design schematics of the spine securing pots.

This design worked well in practice except for removing the spine specimens from the pots, in spite of attempts at lubrication. Sometimes this required large amounts of force to release. Ideally the pots would have had a slight taper on their side walls to allow easier release, but this would have required the use of a 5-axis CNC machine.

9.2.4 Fixtures

The test apparatus needed to fit the clamps of the Instron as well as be adapted to fit the drill rig apparatus. The rotary encoder mounting plates on the existing test jig were designed and calibrated for use with tensile test machine clamps in a vertical position. To fit the limited confines of the drill press, 3D printed adaptations were used to mount the rotary encoders in a lateral position. The upper adapter was mounted to a rod that the drill chuck could close upon and was secured through a press-fit with screws to provide extra clamping force and locating ability. The adapter slid onto the upper rotary encoder plate. While a tight fit, an M4 screw and nut were used to better secure the encoders' plates. The lower adapter consisted of a baseplate that could be bolted to the drill press. A hinge allowed vertical movement of the lower rotary encoder. The design enabled compressive force to be transferred through the load cell mounted to the baseplate while keeping the lower encoder

level and usable. The lower adapter shared a similar slip-on design with the upper mount; however, it allowed rotation to allow for a vertical load to be transferred from the lower encoder to the load cell (Figure 9.6A and 9.6B).

For calibration purposes, two wooden blocks were used with the pedicle screws inserted. A longer upper adapter rod was used to compensate for the shorter blocks. Applied load and strain could then be calibrated. Exact 200g, 500g and 1kg calibration weights were used to ensure linearity and fine tuning of the scaling factors. The scaling factor for the strain rod was based on a calibration made by Julian Philips.

Table 9.1: Bill of materials for Drill press rig instrumentation and adapters (drill press itself not included)

ITEM NO.	PART NUMBER	QTY.
4	Rotary Encoding Moment Grips	2
5	Potting box mk2	2
6	B18.3.1M - 8 x 1.25 x 50 Hex SHCS -- 50NHX	8
7	Premium Spine - Instrumented	1
8	Chuck Adapter Lower	1
9	Drill Rig Baseplate	1
10	Load Cell	1
11	Upper Chuck Rod	1
12	Chuck Adapter Upper	1

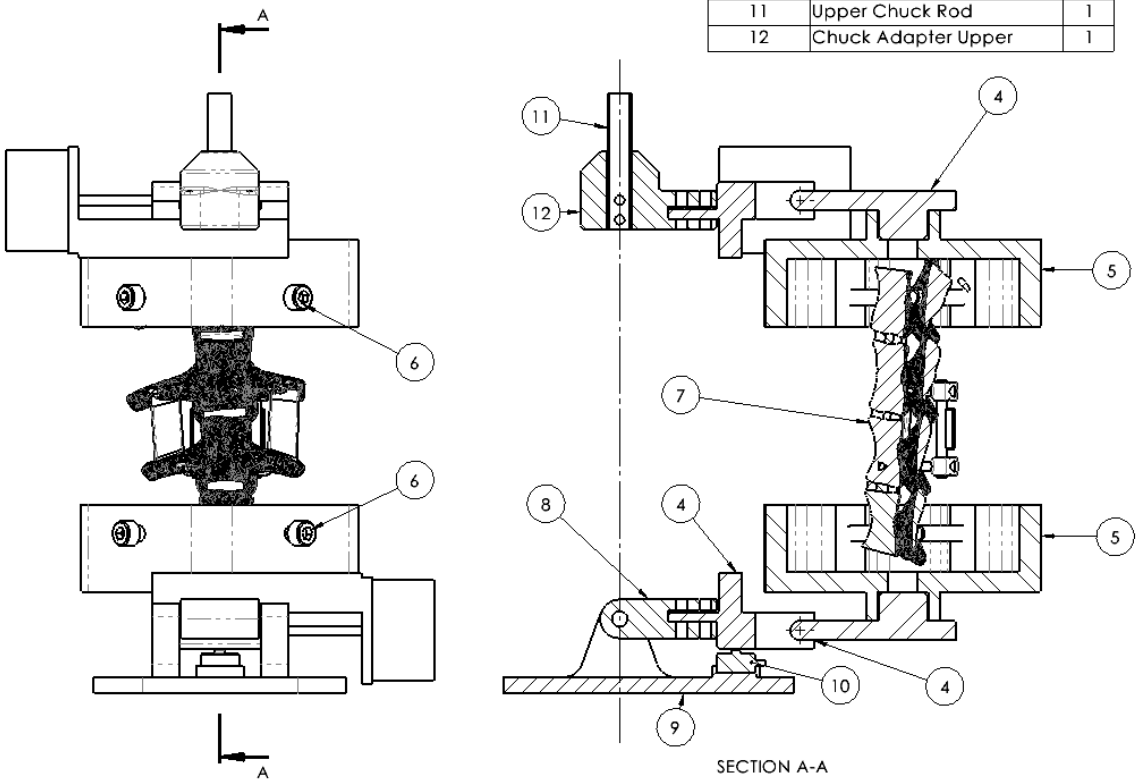

Figure 9.4: Drill press rig apparatus schematic

Several design iterations of the adapters were used. Initial versions made no accommodation for the rotary encoders, which didn't allow for them to be tested for functionality. The load cell mounted directly below the lower spine pot with a loose fit to the baseplate, allowing vertical displacement, but no rotation could be measured. This design was used with the ABS plastic simulated spine (sim spine) testing and was useful for obtaining a rough force-strain response (Figure 9.4 and 9.5).

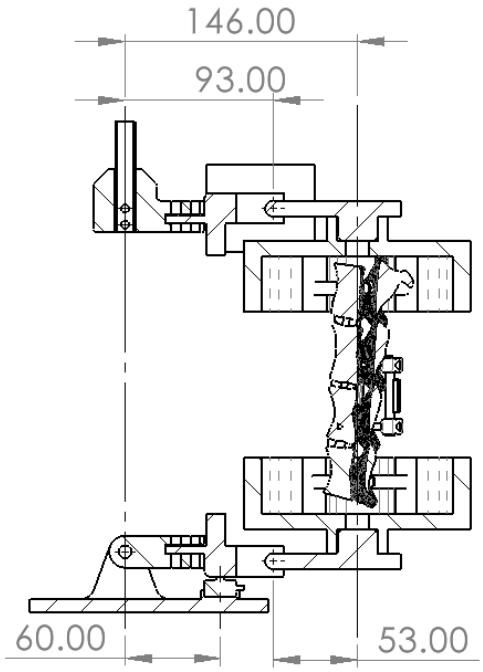

Figure 9.5: Design of adapters including most important dimensions.

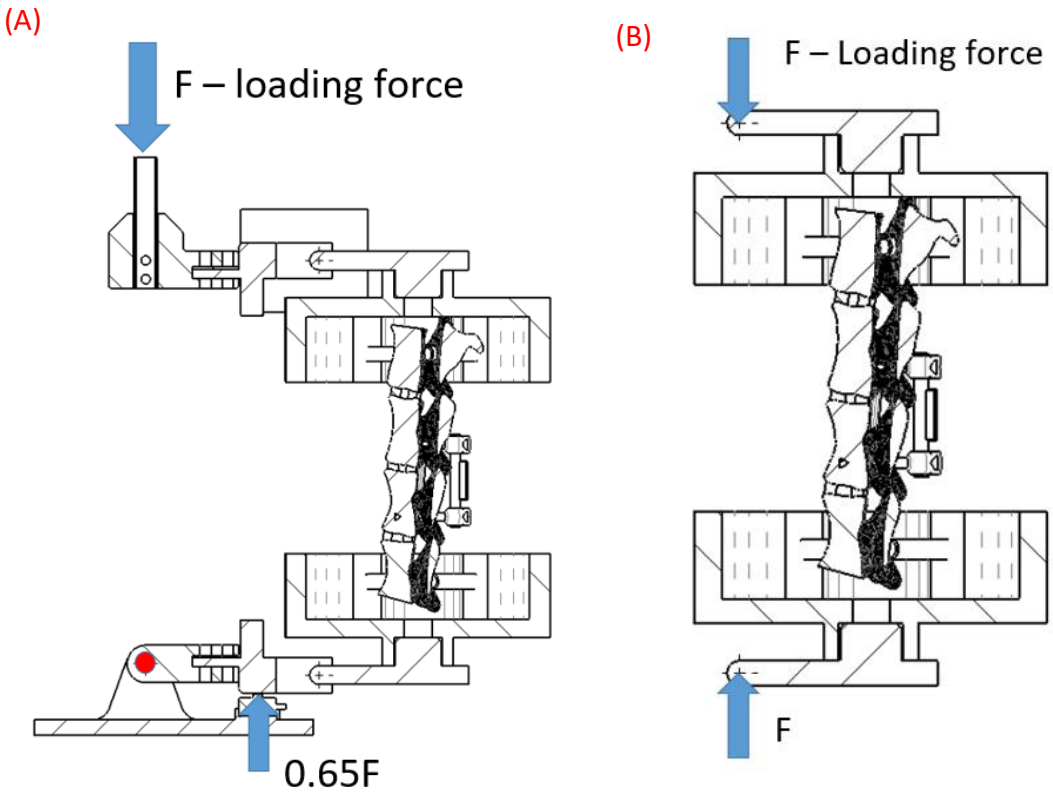

Figure 9.6: (A) FBD for drill press apparatus. (B) FBD for idealised E3000 mounted spine testing apparatus.

9.3 Simulated spine/testbed

A realistic model was required to troubleshoot and test the equipment setup for future Instron testing of sheep spines. The intention was that a sim spine could be surgically prepared and instrumented like a real cadaver ovine spine, thus an ovine lumbar spine from L2 to L5 vertebrae was 3D printed from the Mechanical faculty's Connex Polyjet with digital ABS and digital Shore A40 rubber (Veroblack and VantaRubber materials, respectively). This simulated spine was based on the Basic spine model. It was mounted in the drill press rig for testing (Figure 9.7)

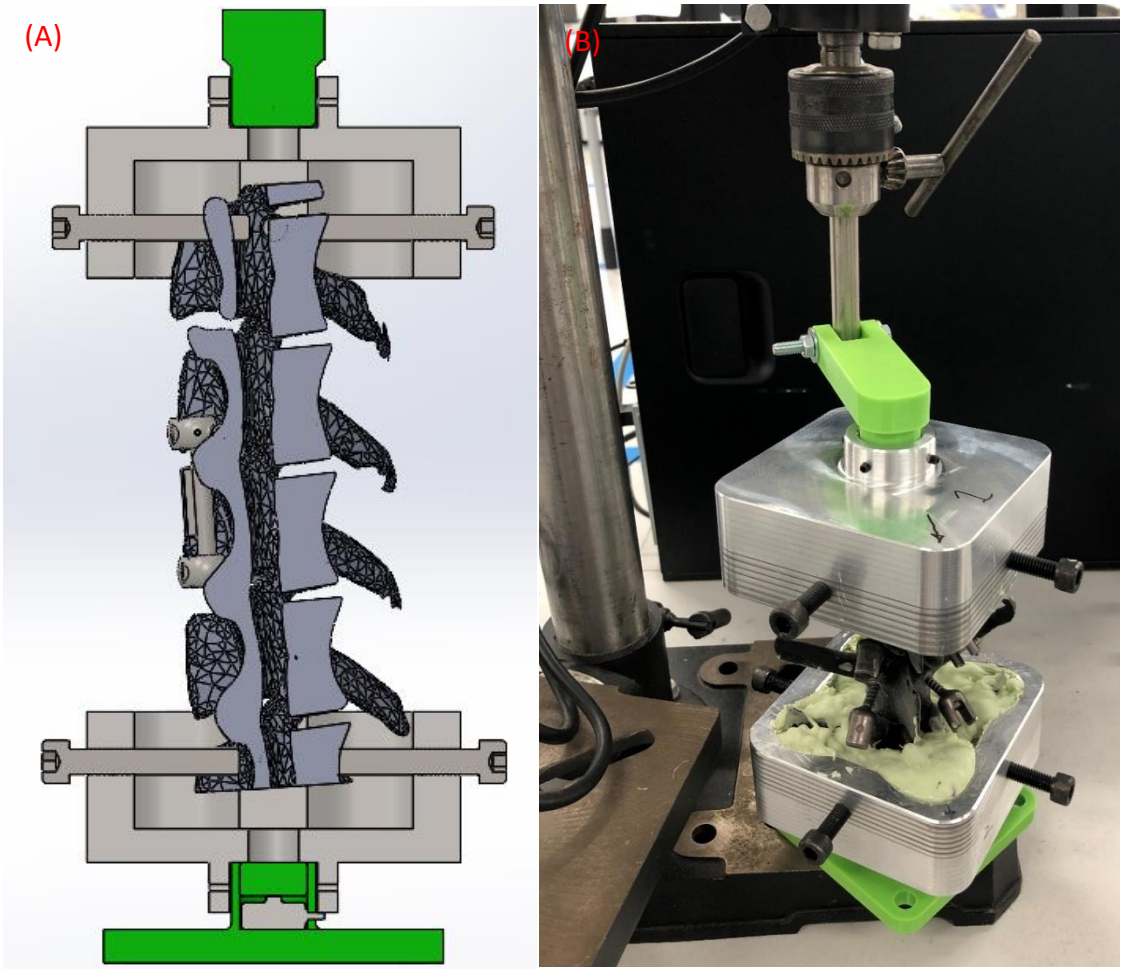

Figure 9.7: Cross – section of early encoder – less drill press adapters (A). Adapters and Simulated spine mounted in the drill press (B).

To prepare the simulated spine for testing, it was drilled at the angles and placement required for pedicle fixation. Pedicle screws were then installed. On installation of the last screw, the sim spine fractured laterally through the L4 vertebrae, indicating the pedicle screw had been driven too deep without accounting for the taper of the pedicle screw threads. The spine was subsequently repaired with Araldite and wire-lashed to compress the fractured vertebrae together. This repair was successful and allowed the spine to be used as intended (Figure 9.8).

The sim spine was used for the first spine potting attempt with some expired bone cement. This involved securing the sim spine in the spine pots and filling the lowest pot with a 2:1 mixture of bone

cement liquid resin to powder. The spine and pots were set into a spine potting rig, filling one pot at a time and allowing it to harden before flipping the spine assembly over to fill the other pot. The potting rig kept the alignment of the two pots correct for mounting in the drill press rig (Figure 9.8 A). The sim spine was then instrumented with the strain gauge rod and a second standard spinal rod and mounted to the drill press rig for flexion and compression testing.

After extensive use as test fixture spine, the rubber disc portions of the sim spine began to separate from their ABS vertebrae. This first showed as cracking at the rubber-ABS interface and culminated in complete separation of vertebrae and disc at the L4-L5 interface. This was glued back together with the flexible adhesive ADOS but soon separated again after light use (Figure 9.8 B).

The simulated spine could be considered a success for increasing the understanding of what was required for the test rig and the process of potting the spine. However, as a test piece, it deteriorated too fast and was too easy to break for use in replicating a cadaveric ovine lumber spine. Thus an actual lumbar sheep spine was used for further testing.

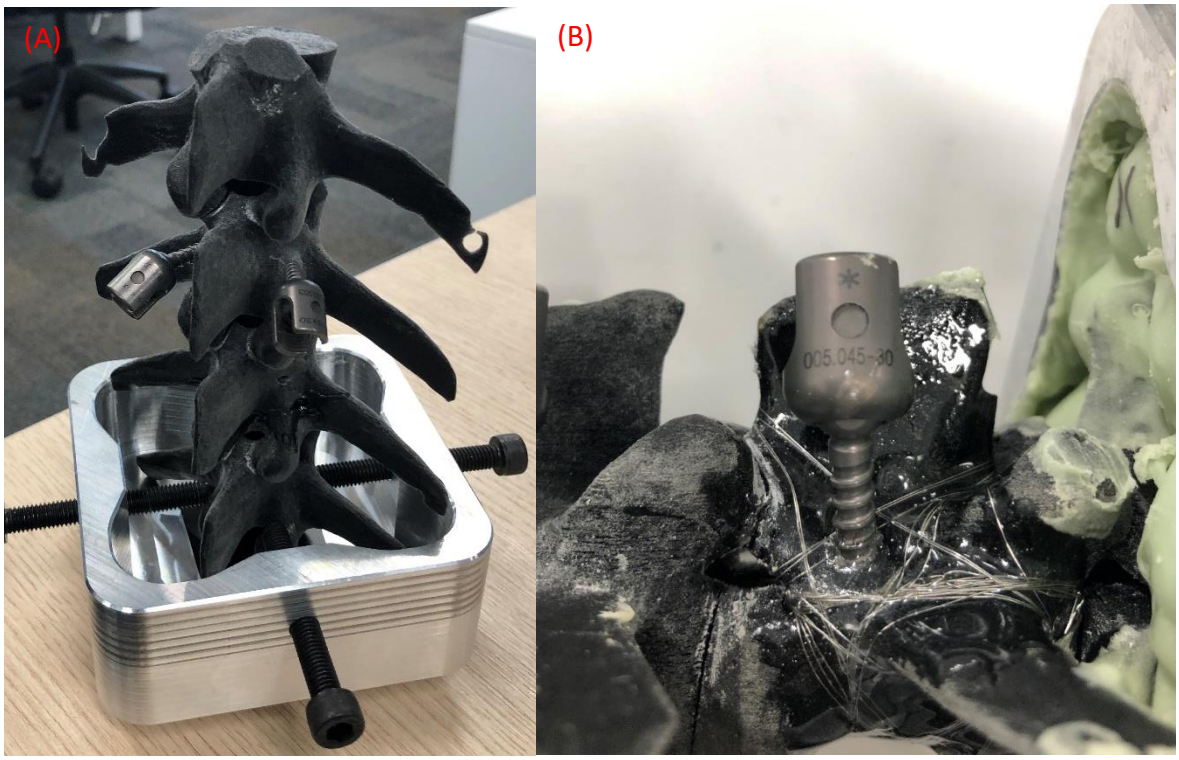

Figure 9.8: Simulated spine in spine securing pot (A). Close up of repair and pedicle screw (B).

9.4 Spine preparation

A few 4-vertebrae lumbar spine segments were potted and secured in a similar manner to the sim spine. Each ovine spine provided by Lincoln University was thawed, dissected to a useful size and appropriate vertebral count. The end vertebrae (L2 and L5) were bolted into the spine pots and then set in place with bone cement or similar (PMMA). This process was done one end at a time using the alignment jig as before. Once potted and set, the spines were fitted with pedicle screws, CT scanned at Lincoln to verify the position of these, then put in frozen storage until needed for use for mechanical testing.

9.4.1 Dissection

Most sheep spines provided by Lincoln were loosely bagged and frozen. They usually consisted of the lower thoracic and lumbar spine regions. In spite of being pre-dissected to remove most of the excess tissue, some cleaning and trimming were required to bring the sheep spines up to a usable state for tensile experimentation.

To process the spines for further use and potting, they were first thawed out from frozen. Unnecessary vertebrae were then removed so that the vertebrae of interest, L2-L5, were clean and ready. The spine was separated between vertebrae with an incision through the intervertebral discs. Any muscle between wanted and unwanted vertebrae was cut through. After cutting, the vertebrae still took some force to separate. This was likely due to the tight-fitting nature of the facet joints.

With a scalpel, fat and muscle beyond the vertebral and transverse processes was removed. 1cm diameter areas were cleared of tissue up to the bone for access to the vertebrae for drilling of pedicle screw holes (L3-L4) and to create recesses for engaging the potting screws (L2 and L5). Major ligaments were left intact where possible. Muscles located between the vertebral processes were also left intact (Figure 9.9).

9.4.2 Drilling and screw fixation

The sheep spines also needed to have holes pre-drilled for installation of the pedicle screws used for fixation of the vertebrae. This was done to better replicate surgical procedures for spinal fusion and to avoid cracking of the bone during pedicle screw insertion. These holes were drilled at a roughly 30-degree angle from vertical with entry holes located at the beginning of the facet joint rise. To initiate the drill holes, a conical burr was used to remove the hardest outermost layer of bone. A 4mm drill bit was used to drill the pilot hole and a 5mm drill bit was used to provide a wider width bore to better fit the upper end of the tapered pedicle screws.

Spine 1 was drilled with the assistance Dr Munro. On inspection with CT scanning at Lincoln University, the pedicle screws installed during this attempt intersected spinal column and were reinstalled at the correct angles. Spines 2 and 3 were drilled without supervisory assistance. Due to all pedicle screws being in use in the sim spine or Spine 1, 3.56mm diameter wood screws were inserted temporarily to provide an X-ray opaque reference to ensure the drilled holes were in the correct orientation in order to make use of Lincoln University's GE Prospeed CT machine at the Johnstone Research Station (Figure 9.9).

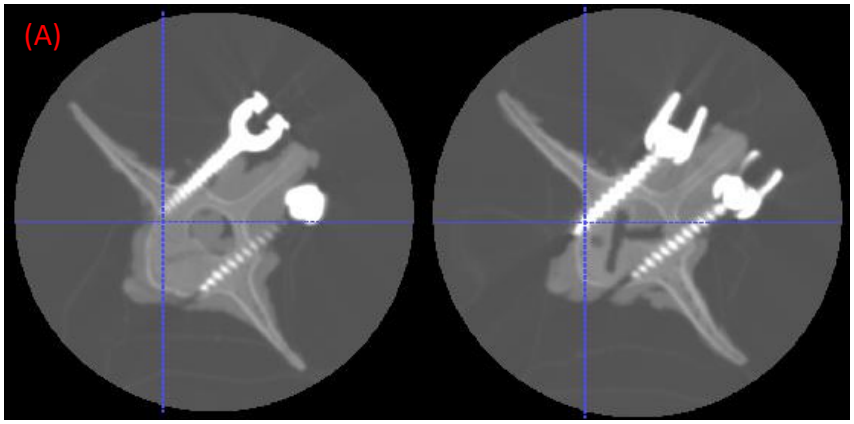

Figure 9.9A: CT scans verifying pedicle screw location for spine testing. Note failed initial hole location.

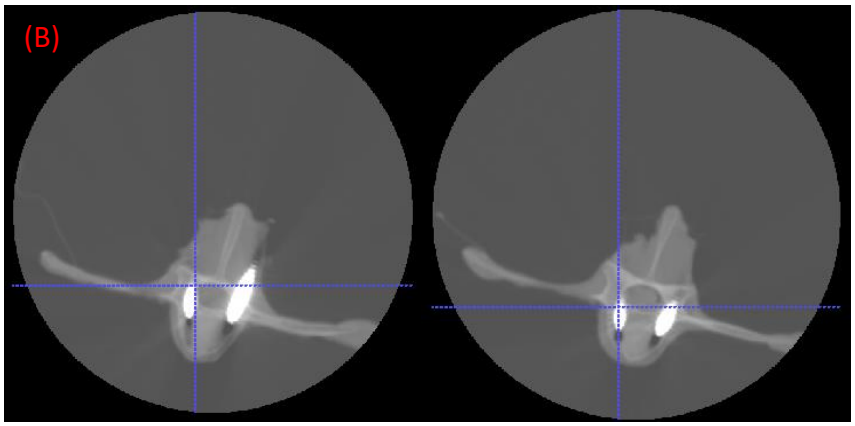

Figure 9.9B: Placeholder screw position in test spine 2 verified with CT.

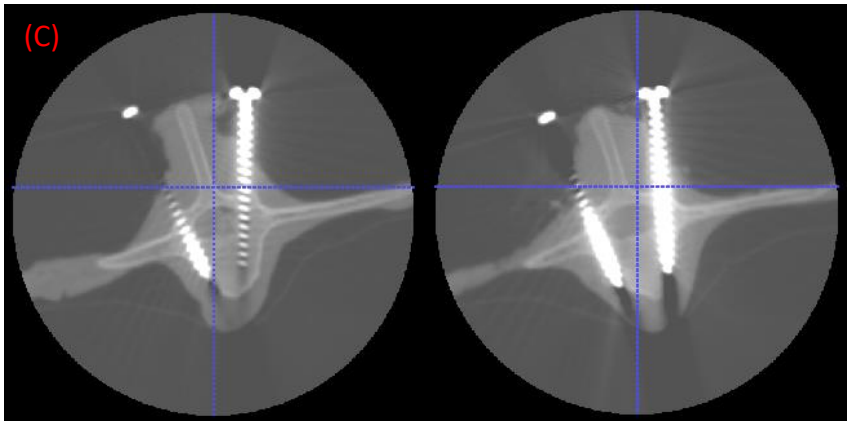

Figure 9.9C: Placeholder screw position in test spine 3 verified with CT.

9.4.3 Potting

The potting of ovine spines was required to add additional stiffness to the test assembly and ensure the only movement to the spine was due to actuation during testing.

Potting was undertaken within a fume hood with the ovine lumbar spine secured with screws in the spine pots and these pots subsequently secured to the potting alignment jig shown in Figure 9.10. The process of potting the ovine spine had to be done in two stages to allow for the pouring and setting of each mix of PMMA dental resin in each pot. After the first of the spine pots was set, the entire spine and both upper and lower spine pots were inverted and remounted. A second batch of PMMA was then mixed and poured in the now lower spine pot as shown in Figure 9.11. The alignment jig ensured that the upper and lower pots were perfectly aligned and thus would align for accurate spine flexion/compression testing on both the Instron and drill rig.

Two potting mixtures were used: a medical grade bone cement, and denture repair/production mix. Both these formulations were a two-part PMMA mix with a hardener liquid and monomer powder. The bone cement was acquired as expired stock from a medical equipment importer and the dental PMMA was purchased from a dental wholesaler. The sim spine was potted in a two-part bone cement product at a 2:3 ratio of powder to liquid hardening agent for the lower pot (1) and 1:2 ratio for the upper pot (2), as a more liquid mixture was needed to manipulate the bone cement before it cured. Sheep spines were potted with an approximate 1:1.25 mass ratio of dental PMMA powder to hardener. This was equivalent to a volume ratio of liquid to powder of approximately 1:1. More information on precise mixing ratios are given in Table 9.2.

Figure 9.10: Spine potting jig.

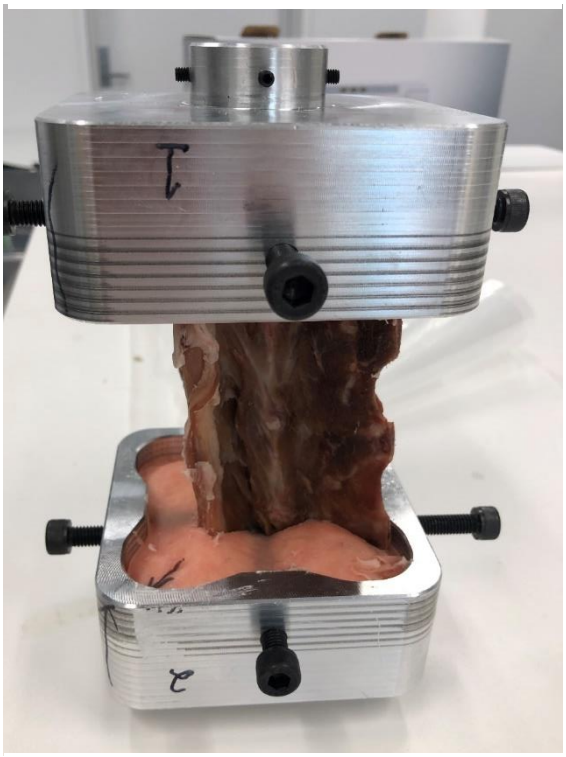

Figure 9.11: Freshly potted spine.

Table 9.2: Spine potting PMMA mix quantities and ratios.

Spine	*PMMA type*	*Upper pot Mg of powder*	*Mg of liquid*	*Ratio*	*Lower pot Mg of powder*	*Mg of liquid*	*Ratio*
Sim spine	Bone cement	Two packets 100g	Three Vials 150ml	2:3	Two packets 100g	4 vials 200ml	1:2
Spine 1	Diamond D dental	121.8g	98.4g	1:1.24	118.3g	93.2g	1:1.27
Spine 2	Not potted						
Spine 3	Not potted						

The Diamond D dental PMMA set within half an hour. Normally the dental compound is used under compression to ensure tighter bonding and thus a stronger bulk plastic. However, it worked perfectly with the free-pour method used to apply the compound around the spine(s). Resulting potted spines are shown in Figure 9.12.

9.4.4 Storage

Spines were collected from Lincoln University and stored in the PID lab freezer at -20C. Initially spines were loosely wrapped in unsealed plastic. For the process of dissection, they were allowed to thaw out either at room temperature for 3-5 hours or thawed overnight in the PID lab fridge. After dissection, spines were vacuum-sealed in food-grade plastic, and stored again at -20C. The vacuum bagging prevented freezer burn, and it is known that freezing maintains normal tissue properties for testing purposes. For the process of potting, the spine was allowed to thaw out again, then removed from the vacuum bagging. Post potting, the entire spine and PMMA structure were vacuum bagged and frozen once more. For mechanical testing the spine was thawed out once more. The spine was kept cold at 4C for each round of adding simulated bone fusion and was followed by mechanical testing. This process limited the thaw/freeze process to 3 times per spine. Once mechanical testing was complete the ovine spines were vacuum bagged and discarded.

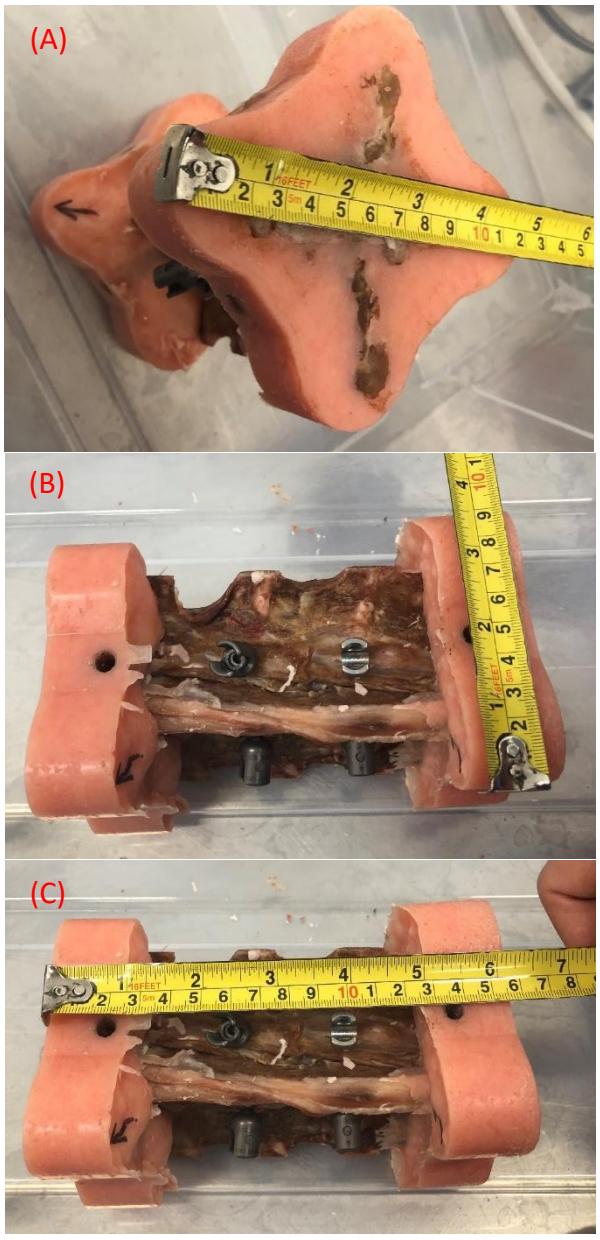

Figure 9.12: (A, B, C) Freshly potted spine with spine pots removed. Note arrow denoting lower front corner for anignment purposes.

9.5 Drill rig setup

With all elements of the drill rig test apparatus finalised and functional, mechanical testing could begin. Steps were completed in the following order.

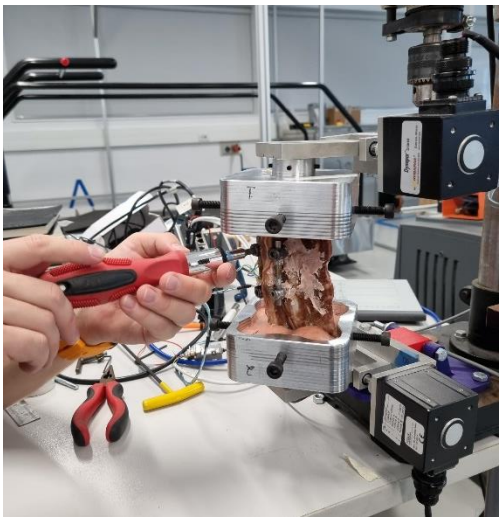

Figure 9.13: Tensioning the pedicle nuts.

1. Spine 1 was retrieved from the freezer and thawed out.
2. The prepared spine was fitted into the pots.
3. Adapter jigs were mounted to the drill press. The upper one was fastened into the chuck while the lower adapter was bolted though the slots on the drill press baseplate.
4. The drill rig was secured to the bench with two G-clamps.
5. The strain sensing rod and standard spinal rod were installed on the spine (Figure 9.13).
6. All cables were connected, both to the power supply and DAQ cradle.
7. The LabVIEW virtual instrument was opened, and a file selected or created for recording.
8. The power supply was set to 12V then turned on.
9. All measurement streams were zeroed.
10. Recording commenced.

Prior to using prepared Spine 1, wooden blocks were used to calibrate the measurement process (Figure 9.14). Because of concerns with deflection in the upper adapter, displacement measurements were taken by hand. The inbuilt depth-of-bore gauge was used for determining displacement at the chuck. Displacement was also measured immediately between the upper encoder and baseplate. The measurement was taken as the vertical distance from the upper surface of the encoder immediately behind the main pivot to the baseplate. This measured the level of deflection with load.

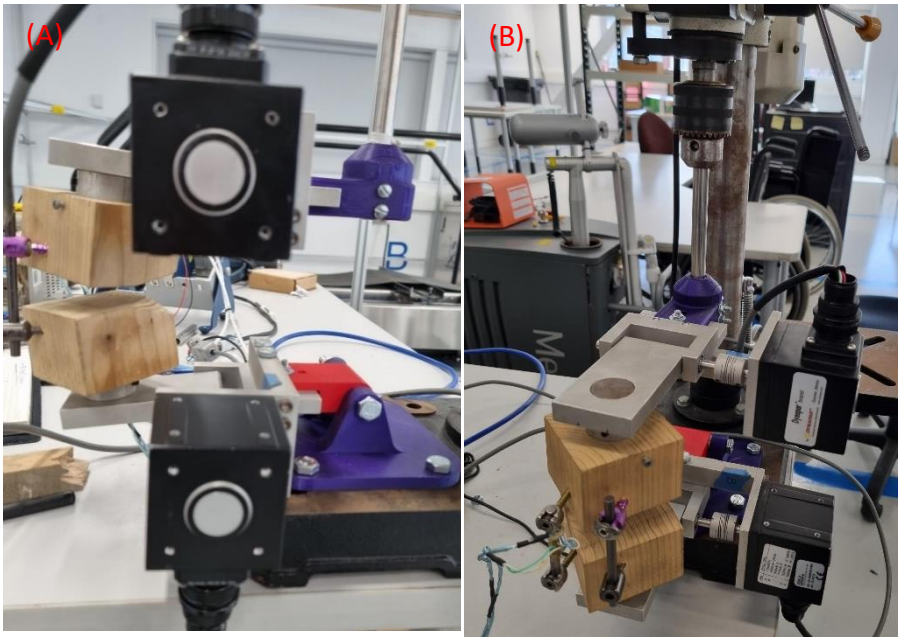

Figure 9.14: (A & B) Wooden blocks were used for calibration of the sensor rod.

Measurements taken automatically were: strain through the pedicle rod, load through the entire test apparatus, and the rotary encoder angles 1 and 2 (upper and lower respectively). Measurements taken manually were the displacement changes (Figure 9.19).

Between tests, the spine was dismounted, the strain sensing rod was removed, and approximately 12.6 g of

bone cement (5ml liquid, 7.6 g – 7.63 g powder) was added to simulate fusion around the transverse processes (Figure 9.15). This was done with all other fixation hardware and the spine pots still attached. Setup steps 5 to 10 were then repeated. This process was done twice to gain three data sets, once without bone cement and two with bone cement to simulate the expected increase of bone stiffness with bone healing.

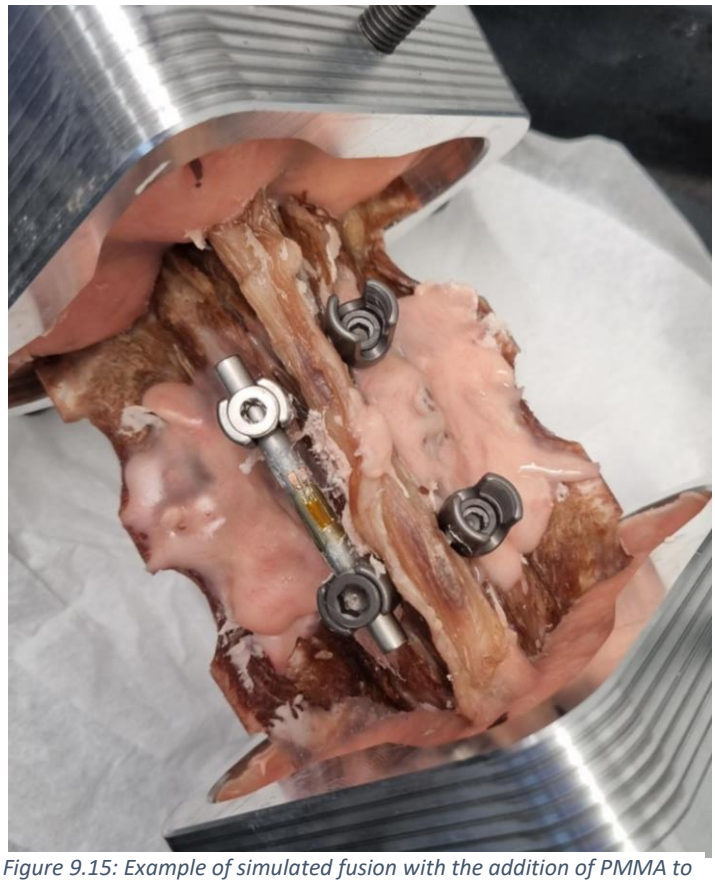

Figure 9.15: Example of simulated fusion with the addition of PMMA to add stiffness to the vertebral group. The sensor rod remained in place to ensure zero change in preload.

9.6 Drill rig testing

Testing of the spine on the drill rig press involved applying incremental 3mm displacements to the drill rig chuck, and taking measurements of upper encoder displacement, strain through the sensor rod and load through the load cell at each displacement step. This was repeated for each level of bone cement applied. Results of this are shown in four graphs, Figures 9.16 through 9.19. With the need to "pause" displacement to take measurements, strain relieving was observed. This strain relieving can be seen in Figures 9.16 and 9.18. The addition of PMMA in the same manner as a developing fusion resulted in a larger strain being observed through the sensor rod with each increment of PMMA. If the drill rig had worked like the Instron with a 5 Nm physiological moment across the spinal rods, a decrease in strain would have been observed at each increase of simulated PMMA fusion.

The rotary encoders have mounting plates that attach to the potted spine ends. Since each spine varies, there is no way to control the starting angle of the pots or their subsequent rotation. Because of the drill rig limitations, these angular anomalies were exaggerated in the drill rig data (Figure 9.17).

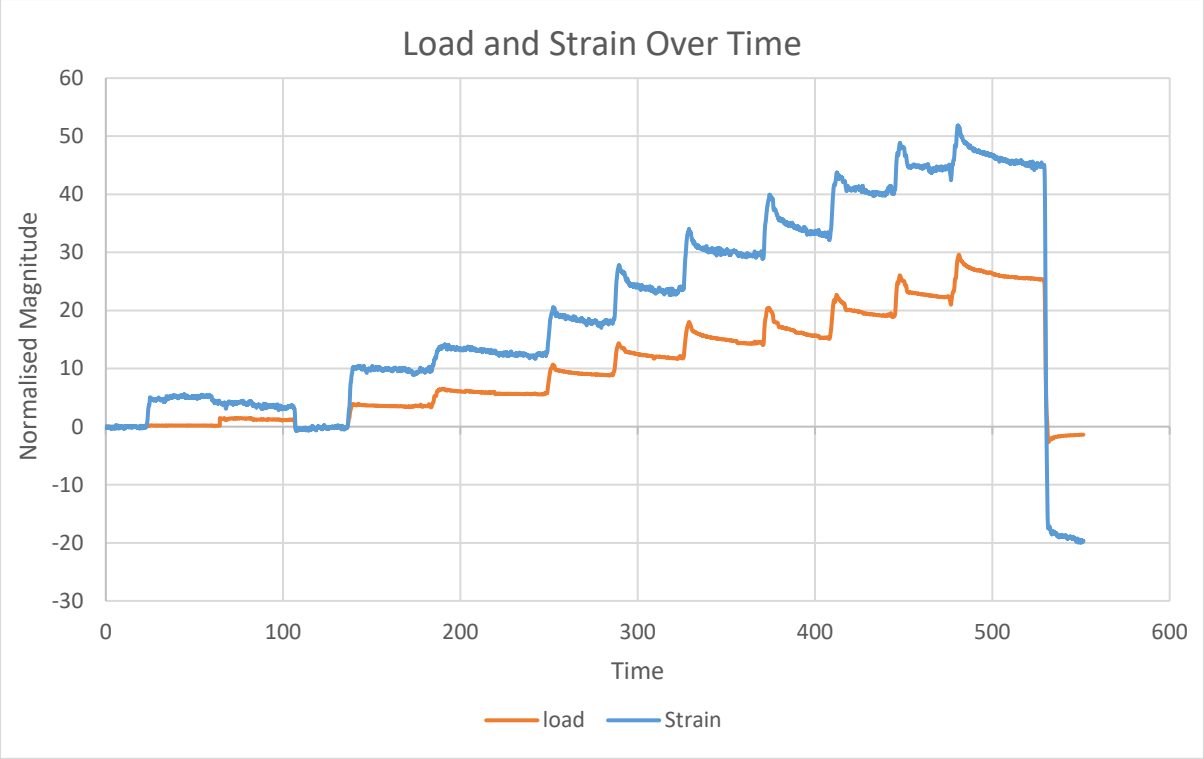

Figure 9.16: Load and stain over time. Note strain relief during each hold.

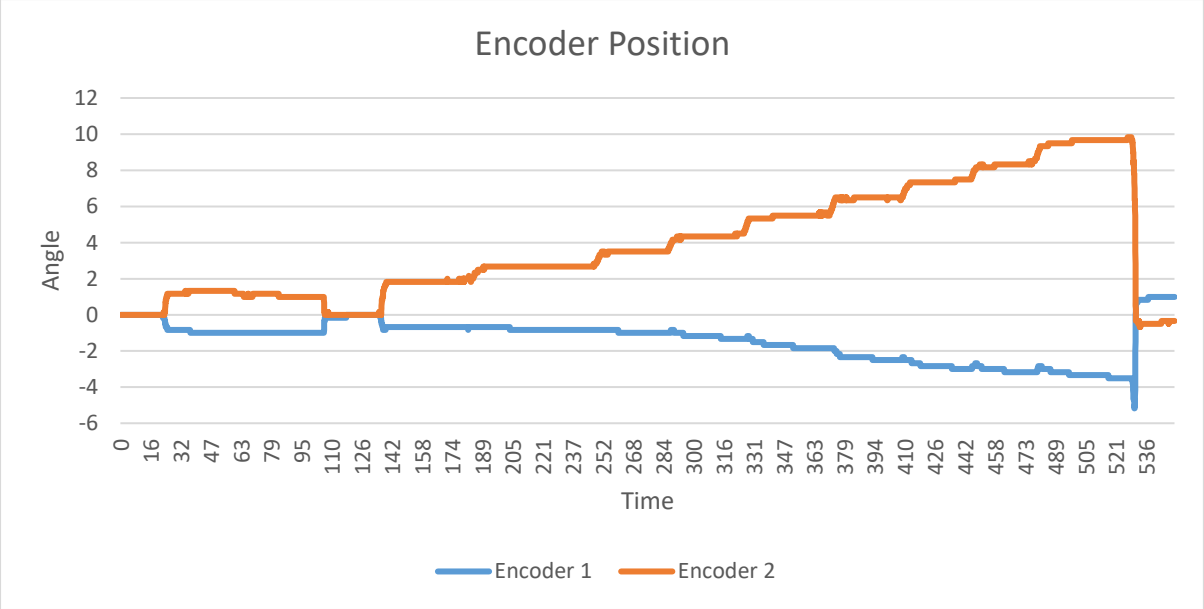

Figure 9.17: Encoder position over the same time trial. Theoretically these would show equal magnitude, but each spine is potted somewhat differently, giving an initial non-zero angle. In addition, the drill rig setup prevented the lower encoder from moving as much.

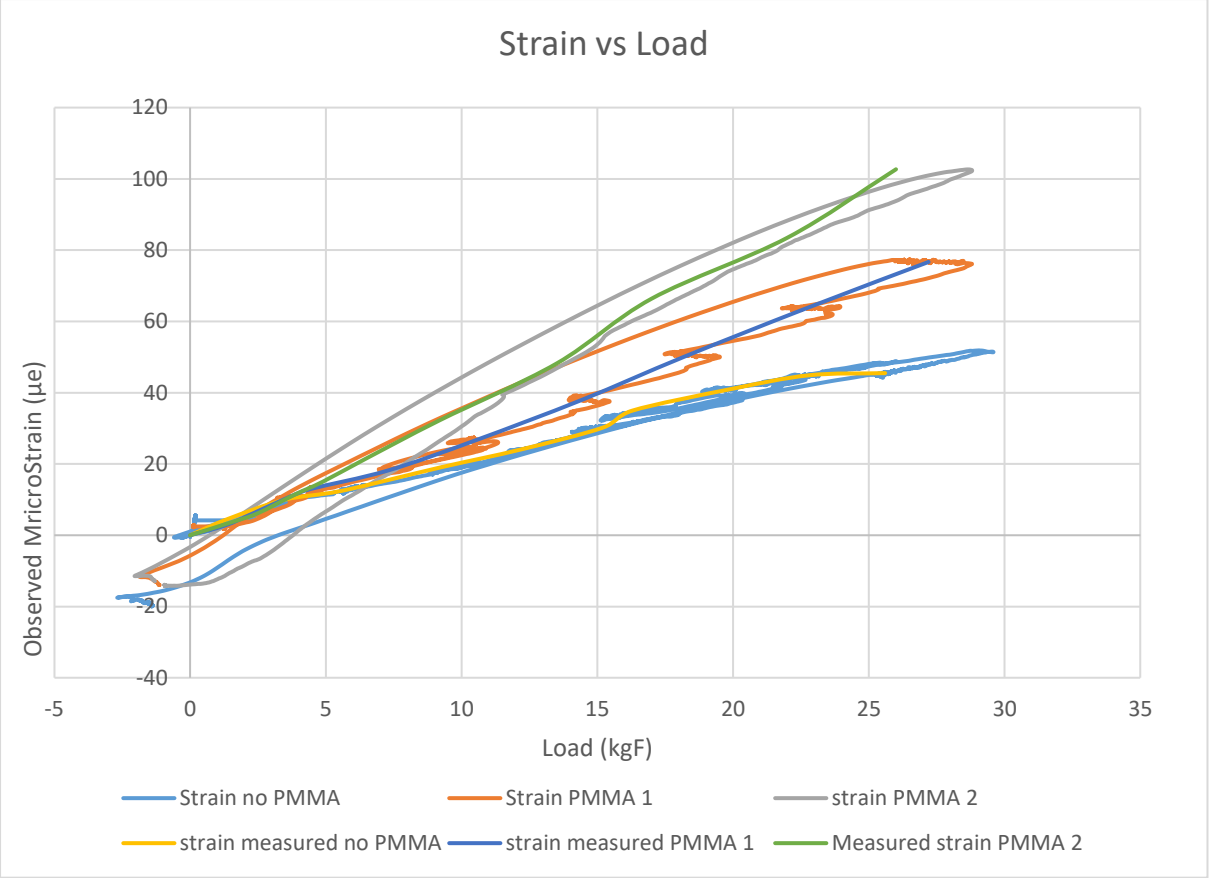

Figure 9.18: Increases of stiffness with the addition of PMMA during simulated fusion.

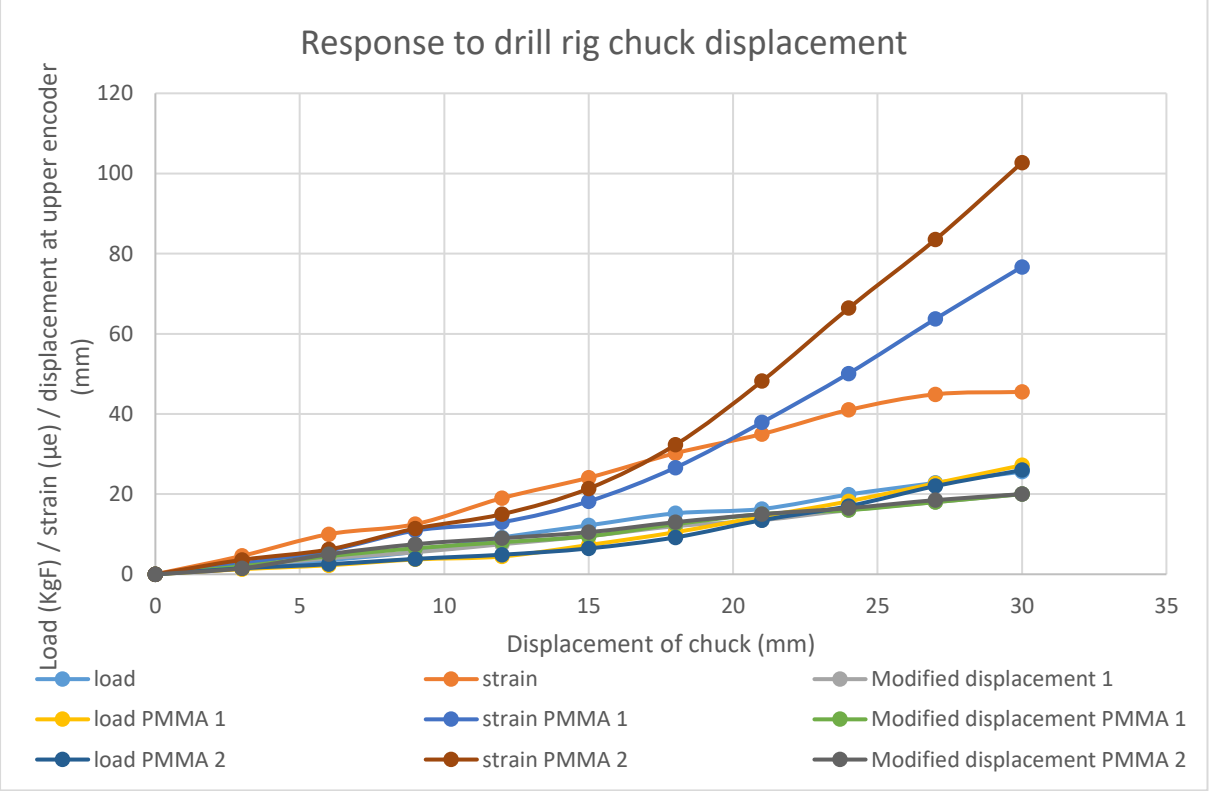

Figure 9.19: compound graph showing the spine response to set displacements.

Figure 9.20: The author performing spine flexion and measuring chuck displacement.

9.7 Outcomes

The drill rig proved useful for the setup and method development of the potting, instrumentation, and testing processes. All methods from the potting to the software were successful. However, as a lower tech substitute to the Instron E3000, the drill rig setup failed in this regard. The amount of clearance in the drill rig as well as the material used in the 3D printed adapters gave low tolerance results, and strain observed in the sensor rod increased with additional PMMA. This was the opposite trend observed in the FEA models where strain decreased with the addition of BHZ stiffness. The tendency for spine specimens to remain in compression, only switching to a bending mode past a certain displacement also presented issues as the observed strain would increase in one magnitude then switch sign to the opposite. This was generally observed around 30mm displacement. Based on the drill rig free body diagram, this was to be expected, as there were additional modes of rotation present that would not exist for the Instron. However, the setup used with the drill rig did prove reliable and with limited effort could be transferred to the Instron for actual biomechanical testing. The Instron would also provide digital displacement data and higher stiffness of the system, as well as an ability to do preloading (a method used to reduce hysteresis in biological tissues).

Chapter 10 Discussion

While the modelling efforts resulted in good repeatable trends, there were limitations to the FEA model. These included issues arising from the CAD process and errors involving the facet joints, material selection, boundary and loading conditions applied, and issues with the mechanical testing and thus verification of the FEA model.

One of the earliest issues to occur was the fusing of the facet joints between vertebrae in the CT-to-CAD conversion process. The segmenting program used could not discern between two separate vertebrae because of their very close proximity to each other at the facet joints, thus they would be interpreted as one solid body, and all 4 vertebrae would be fused as one body. The tapered barrel-like shape of the facet joints meant that separating the joints in CAD was extremely difficult if the anatomical shape of the joints was to be preserved. The solution used was to break the spine into its constituent vertebrae, take CT scans, process and then reconstruct the model in CAD against a shadow mesh of an intact spine. With the Advanced model, this meant that one spine was reconstructed against the vertebral spacing of a different individual and thus, would not be as accurate as it could be; however, slight inaccuracies in spacing are probably not significant to the outcome of the model. If the spine of interest had been scanned in full before dissection, reconstruction differences would not have been present. With a skilled user on 3D Slicer, the facet joints may have remained separate during segmentation, especially if more manual methods were used during segmentation. ITK Snap used for this model did not have the same level of functionality for manual segmentation.

The material types used and placement in the model were satisfactory. All material types were accurate to their source material(s). The intervertebral disc, BHZ, and the geometry of the model had enough complexity in shape and structure to sufficiently replicate the structure of the ovine lumbar spine. The use of compact (cortical) bone as the only bone type in the actual vertebrae resulted in a bone structure stiffer than reality. As compact bone is generally only located within the first few millimetres of the bone surface, a modelled vertebral structure of compact bone externally and softer spongy bone internally may have been a better match for reality. Creating such structures in CAD is a fairly simple process that can be achieved with shell operations or hollowing. This would create two nested bodies per vertebrae. Unfortunately, the use of MARS institute-derived CT scans resulted in models being inseparable this way due to the internal structure revealed by the inherently high resolution of the process.

Related to this is how the maximum healed strength and stiffness of the BHZ were specified as being equivalent to compact bone. This likely is not the correct material to specify a fusion mass for several reasons: Firstly, the maximum strength of compact bone is usually determined from long bones, traditionally the femur, the strongest bone in the body [23]. The femur is generally one of the easiest bones to analyse. Compact bone in this situation is highly directional and very dense due to the large dynamic loads the bone experiences. The fusion mass is not likely to reach this strength. However, no data exists for the properties of the BHZ. This will require a sheep study with multiple sacrifice points so that biomechanical, histological, and/or composition testing of material properties can be performed. When available from future research, the FEA model could be used with more representative materials.

Lack of research into the mechanical strengths of transitional healing tissue properties (hard callus/woven bone, soft callus, granulation tissue) and how the strength of these materials transition over time was one of the leading limitations of this model. This research gap led to the need to create a materials database and then average material properties across species for each tissue type due to the limited research into the area. Across large (rabbit-sized and above) mammalian species,

the fracture healing process is essentially the same, so studies involving other animals than sheep were used to help fill this data gap. The lack of data also led to the need to apply interpolation across BHZ mechanical properties to generate better-spaced inputs to the FEA models.

Strain changes observed in the spinal rods were highly dependent on the shape of the rods. The sensor rod showed a lower magnitude of change compared to the standard rod. This was related to the raised shape of the sensor rod compared to the cylindrical shape of the normal rod. Any sensor rod design for clinical applications will need to be sensitive to strain changes. The more sensitive the rod is to load; the less amplification of signal is required and the less noise will be produced. However, for regulatory purposes and safety requirements, the sensor rod must have, at a minimum, the same diameter as a standard rod; therefore, it is likely the sensor rod will always be larger, and thus stiffer, than a standard spinal rod.

The loading scenario used in the FEA assumed one end of the spinal unit was fully constrained at the lower end (L5) due to its attachment to the (assumed stable) hindquarters, and the upper end free in all axes. The applied moment on the upper free end of the spine was intended to replicate the load of the sheep's upper body. Reality is more complex. The load though the spine depends on the position of the animal, its current action and thus what muscle activations pull on the spine. In addition to the self-weight of the tissues anchored to each individual vertebrae, these combined loads would result in a distributed load and moment that changes with gait and other activities. This is partly why the cadaver study and future planned sheep study will be crucial to the understanding of what aspects of ovine spine loading are important to include in future models.

Loads in the spine increase over time as a patient returns to full activity (especially if heavy lifting is involved), thus static axial loads and bending moments used in FEA are probably not representative of typical activity during healing. At a minimum, a cyclic or step loading that represents the gait cycle might be advisable if the model needs to take account of the strain rate-dependent nature of bone and other tissues. This would also require alterations to the material library developed. The static regime of loading used in the FEA models did not represent the recommended methods of measuring flexion and extension of a lumbar spine. However, it depends on how the sensor would actual be used in clinical practice—will the patient be asked to hold a static position, or will there be continuous monitoring of their activity over time?

The viscoelastic nature of the spine requires that a spine is run through a preload cycle of 40-50 iterations at the intended rate of extension[26]. This is done to reduce hysteresis incurred through strain relaxation. The drill press apparatus did not allow for steady strain rate or an even preload cycle and exhibited too much deflection in the adapter fittings for accurate measurement. It is anticipated that use of the Instron would resolve many of these issues.

Chapter 11 Conclusions

The research completed proves that an FEA model of an ovine lumbar spine can be made that considers the material changes that occur in a healing fusion mass. Like any FEA model, the quality of the results are dependent on the quality of the input information. The model of the lumbar spine during fusion was a success. It showed a proportional relieving of strain in the spinal rods as bone increased in strength. This process showed that load over time transitioned from being transferred through the pedicle fixation to being transferred through the bone healing zones.

The FEA model built during this thesis relied on simplified material assumptions such as homogenous bone material for the vertebrae and treating the BHZ as a linear-elastic material no matter the healing stage and material strength. For better results and a more anatomically correct model, elements in the vertebrae could be assigned their own strengths based on CT density. Intervertebral discs should be treated as hyper-elastic with multiple annulus fibrosis layers and hyper-elastic nucleus pulposus regions. Healing tissue in the BHZ could be better represented with softer tissue categories represented as hyper-elastic. However, the model built for this thesis ran successfully and was able to complete a solve in a reasonable period. Any area of interest such as the BHZ required a high level of mesh refinement and needed filleted edges to obtain adequate strain results, but it is a sufficient baseline for further research once better loading and material properties are known from animal testing.

The process of converting a set of CT images to a CAD model was successful. Semi-automated segmentation methods as used in 3D Slicer and ITK Snap were highly useful and produced great output geometry, even if a clean-up processing was required. Higher resolution CT imagery was not necessarily better as a large portion of processing the MARS images was down-sampling the resultant STL mesh. While a high-resolution geometric mesh may be useful for some applications, in the case of FEA of whole spine sections, it did not offer any benefits. Separation of the facet joints and then CT scanning vertebrae individually worked well. However, preliminary CT scans of the spine specimen before dissection or virtual separation in 3D slicer though manual segmentation by a skilled operator would yield better (and quicker) CAD models, and thus FEA.

Mechanical testing proved to be semi-successful in that the methods, hardware, and data acquisition methods were designed and tested in a low consequence environment. Using National Instruments equipment and software a versatile system was developed for the drill press and the Instron. Spine potting methods and tooling was successful. The addition of PMMA to simulate the increase of stiffness due to spinal fusion showed a change in force-strain response. This validated the sensitivity of the sensors but highlighted flaws in the drill press testing methods, predominantly deflection of the adapters between the rotary encoders and the drill press chuck and loading changes that were necessary to fit the existing test jig in the drill press. These issues are expected to be resolved with use of the Instron.

Chapter 12 Future Work

The largest issue preventing better results for the FEA spine model was the lack of well-characterised material properties for the tissues that make up the bone healing process, including granulation tissue, soft callus, hard callus, woven bone, and hematoma tissue. As the bone healing process involves transition from one tissue type to another, information on how the strength changes over time would be crucial to the further understanding of spinal fusion.

The early stages or this project involved the planning of a sheep study to educate and verify the findings of this FEA study. This sheep study was intended to be a test study for implantable wireless sensors used to measure the state of spinal fusion. A continuation of the body of work discussed in this thesis would require the sheep study to commence to allow verification of the lumbar sheep spine FEA model.

The FEA model could be improved upon with better structuring of the CAD in the model. Using a program such as BoneMat or similar, mechanical properties could be assigned element-wise based on CT data. Combined with improvements to the intervertebral disc area, this would result in a more accurate model. Best modelling results would be obtained through CT-to-CAD conversion of an ovine lumbar spine that has completed fusion because a fusion mass could be directly used in the models. This would require completion of the sheep study, however, and it may not result in a better model, as all individual sheep will fuse differently and have anatomical differences. Therefore, the biggest improvements to the FEA model would come from better material properties for tissues, an understanding of how the fusion mass forms and mineralises, and an accurate loading scenario that represents lumbar spine loading as seen in a sheep.

Chapter 13 Works Cited

1. Hnat KMWJFNWP, Inventor. Strain Sensing System. 2006.
2. Muschler GF, Lane JM, Dawson EG. The Biology of Spinal Fusion. In: Cotler JM, Cotler HB, eds. *Spinal Fusion: Science and Technique.* New York, NY: Springer New York; 1990:9-21.
3. Pelham H, Benza D, Millhouse PW, et al. Implantable strain sensor to monitor fracture healing with standard radiography. *Scientific Reports.* 2017;7(1).
4. Zhong Z-C, Wei S-H, Wang J-P, Feng C-K, Chen C-S, Yu C-h. Finite element analysis of the lumbar spine with a new cage using a topology optimization method. *Medical Engineering & Physics.* 2006;28(1):90-98.
5. Jiang H, Carter NM, Zareei A, et al. A Wireless Implantable Strain Sensing Scheme Using Ultrasound Imaging of Highly Stretchable Zinc Oxide/Poly Dimethylacrylamide Nanocomposite Hydrogel. *ACS Applied Bio Materials.* 2020;3(7):4012-4024.
6. Willems P. Decision Making in Surgical Treatment of Chronic Low Back Pain: The performance of prognostic tests to select patients for lumbar spinal fusion. *Acta Orthopaedica.* 2013;84(sup349):1-37.
7. Closkey RF, Parsons JR, Lee CK, Blacksin MF, Zimmerman MC. Mechanics of interbody spinal fusion. Analysis of critical bone graft area. *Spine (Phila Pa 1976).* 1993;18(8):1011-1015.
8. Peter Ullrich M. Posterior Lumbar Interbody Fusion (PLIF) Surgery. Spine-health.com. Spinal Fusion Web site. https://www.spine-health.com/treatment/spinal-fusion/posterior-lumbar-interbody-fusion-plif-surgery. Published 2012. Accessed 10/06/2022, 2022.
9. Peter Ullrich M. Posterolateral Gutter Spine Fusion Surgery. Spine-health.com. Spinal fusion Web site. https://www.spine-health.com/treatment/spinal-fusion/posterolateral-gutter-spine-fusion-surgery. Published 2009. Accessed 10/06/2022, 2022.
10. Daniell JR, Osti OL. Failed Back Surgery Syndrome: A Review Article. *Asian Spine Journal.* 2018;12(2):372-379.
11. El Bojairami I, El-Monajjed K, Driscoll M. Development and validation of a timely and representative finite element human spine model for biomechanical simulations. *Scientific Reports.* 2020;10(1).
12. Jin YJ, Kim YE, Seo JH, Choi HW, Jahng T-A. Effects of rod stiffness and fusion mass on the adjacent segments after floating mono-segmental fusion: a study using finite element analysis. *European Spine Journal.* 2013;22(5):1066-1077.
13. Bai X, Liu G, Xu C, et al. Morphometry Research of Deer, Sheep, and Human Lumbar Spine: Feasibility of Using Deerand Sheep in Spinal Animal Models. *International Journal of Morphology.* 2012;30:510-520.
14. Schmidt H, Reitmaier S. Is the ovine intervertebral disc a small human one? A finite element model study. *J Mech Behav Biomed Mater.* 2013;17:229-241.
15. Hadjidakis DJ, Androulakis II. Bone Remodeling. *Annals of the New York Academy of Sciences.* 2006;1092(1):385-396.
16. Kanayama MC, Bryan W; Weis, James C; Parker, Larry M. Maturation of the Posterolateral Spinal Fusion and Its Effect on load-Sharing of Spinal Instrumentation. *The Journal of Bone and Joint Surgery.* 1997;79-A.
17. Wang L, Wang Y, Shi L, et al. Can the sheep model fully represent the human model for the functional evaluation of cervical interbody fusion cages? *Biomechanics and Modeling in Mechanobiology.* 2019;18(3):607-616.
18. Xu M, Yang J, Lieberman IH, Haddas R. Lumbar spine finite element model for healthy subjects: development and validation. *Computer Methods in Biomechanics and Biomedical Engineering.* 2017;20(1):1-15.
19. Munish Gupta DS, Eunice Lee, Amjad Ramahi, Inventor; Deborah Schenberger, assignee. STRAIN MONITORING SYSTEM AND APPARATUS. 9/12/2011, 2011.

20. Sheen JR GW. Fracture Healing Overview. NCBI. https://www.ncbi.nlm.nih.gov/books/NBK551678/. Published 2021. Updated 12/05/2021. Accessed 04/2022, 2021.
21. Sandberg OH, Aspenberg P. Inter-trabecular bone formation: a specific mechanism for healing of cancellous bone. *Acta orthopaedica.* 2016;87(5):459-465.
22. Aiyer A. Fracture healing In: healing F, ed. OrthoBullets2020:Stages of bone healing.
23. Curry JD. The Mechanical Properties of Bone. 1970.
24. al RJKe. Biomechanics of bone fusion. *Neurosurgical Focus.* 2001.
25. al YWe. Anatomical Characteristics of Deer and Sheep Lumbar Spines: Comparison to the Human Lumbar Spine. *Int J Morphol.* 2015.
26. Schenberger DS. *Dissertation-Schenberger* [PhD Dissertation]: Biological Systems Engineering, UNIVERSITY OF CALIFORNIA DAVIS; 2006.
27. Drew K. Deer and deer farming - Deer management. In. *Te Ara: The Encyclopedia of New Zealand.* Vol Settled Landscape: Te Ara: The Encyclopedia of New Zealand; 2008:1-12.
28. Long RG, Torre OM, Hom WW, Assael DJ, Iatridis JC. Design Requirements for Annulus Fibrosus Repair: Review of Forces, Displacements, and Material Properties of the Intervertebral Disk and a Summary of Candidate Hydrogels for Repair. *J Biomech Eng.* 2016;138(2):021007.
29. Boskey AL. Bone composition: relationship to bone fragility and antiosteoporotic drug effects. *BoneKEy Reports.* 2013;2.
30. Ott SM. Cortical or Trabecular Bone: What's the Difference? *American Journal of Nephrology.* 2018;47(6):373-375.
31. C. M. Schoenfeld EPLaPRM, Jun. Mechanical properties of human cancellous bone in the femoral head. 1974.
32. Ghiasi MS, Chen JE, Rodriguez EK, Vaziri A, Nazarian A. Computational modeling of human bone fracture healing affected by different conditions of initial healing stage. *BMC Musculoskeletal Disorders.* 2019;20(1).
33. *BoneMat* [computer program]. Medical engineering & physics2007.
34. Inglis B, Schwarzenberg P, Klein K, Von Rechenberg B, Darwiche S, Dailey HL. Biomechanical duality of fracture healing captured using virtual mechanical testing and validated in ovine bones. *Scientific Reports.* 2022;12(1).
35. Moreira CA DD, Baron R. Anatomy and Ultrastructure of Bone – Histogenesis, Growth and Remodeling. MDText.com. https://www.ncbi.nlm.nih.gov/books/NBK279149/. Published 2000. Updated 2019 Jun 5. Accessed2022.
36. Leong PL, Morgan EF. Measurement of fracture callus material properties via nanoindentation. *Acta Biomaterialia.* 2008;4(5):1569-1575.
37. Hsieh Y-Y, Tsuang F-Y, Kuo Y-J, Chen C-H, Chiang C-J, Lin C-L. Biomechanical analysis of single-level interbody fusion with different internal fixation rod materials: a finite element analysis. *BMC Musculoskeletal Disorders.* 2020;21(1).
38. David W. L. Hukins JRM. Relationship Between Structure and Mechanical Function of the Tissues of the Intervertebral Joint. 2000.
39. Nerurkar NL, Elliott DM, Mauck RL. Mechanical design criteria for intervertebral disc tissue engineering. *Journal of Biomechanics.* 2010;43(6):1017-1030.
40. Casaroli G, Galbusera F, Jonas R, Schlager B, Wilke H-J, Villa T. A novel finite element model of the ovine lumbar intervertebral disc with anisotropic hyperelastic material properties. *PLOS ONE.* 2017;12(5):e0177088.
41. Hukins DWL, Meakin JR. Relationship Between Structure and Mechanical Function of the Tissues of the Intervertebral Joint. *American Zoologist.* 2000;40(1):42-052.
42. Wang Y, Yi XD, Li CD. The influence of artificial nucleus pulposus replacement on stress distribution in the cartilaginous endplate in a 3-dimensional finite element model of the lumbar intervertebral disc. *Medicine (Baltimore).* 2017;96(50):e9149.

43. G.J. Rogers BKM, A. Muratore and K. Schindhelm. Measurement of the mechanical properties of the ovine anterior cruciate ligament bone-ligament-bone complex: a basis for prosthetic evaluatio. *Biomaterials.* 1989;1990 Vol 11.
44. Gregory DE, Callaghan JP. A comparison of uniaxial and biaxial mechanical properties of the annulus fibrosus: a porcine model. *J Biomech Eng.* 2011;133(2):024503.
45. ANSYS. ANSYS Granta EduPack 2021 R1. In: ANSYS; 2022.
46. MARS Institute. Multi-spectral CT imaging In: MARS Institute, ed2021.
47. *3D Slicer as an Image Computing Platform for the Quantitative Imaging Network. Magnetic Resonance Imaging* [computer program]. 2021.
48. *ITK Snap* [computer program]. 2018.
49. *MeshLab: an Open-Source Mesh Processing Tool* [computer program]. Sixth Eurographics Italian Chapter Conference, page 129-136, 2008.
50. *MeshMixer* [computer program]. 2021.
51. *Geomagic Freeform* [computer program]. 3Dsystems; 2021.
52. *SolidWorks* [computer program]. 2021.
53. *ANSYS 2020 R3* [computer program]. 2020.
54. GE Healthcare, Inventor. GE Prospeed CT scanning machine. 1997.
55. MARS Institute. Information for researchers - MARS Microlab 5X120. https://www.marsbioimaging.com/mars-for-researchers/. Published 2022. Accessed2022.
56. GrabCAD. GrabCAD Library. https://grabcad.com/library. Published 2022. Accessed.
57. embodi3D. embodi3D medical CAD libary and CT conversion database. https://www.embodi3d.com/. Published 2022. Accessed.
58. Kang I, Choi M, Lee D, Noh G. Effect of Passive Support of the Spinal Muscles on the Biomechanics of a Lumbar Finite Element Model. *Applied Sciences.* 2020;10(18):6278.
59. Williams SA, Middleton ER, Villamil CI, Shattuck MR. Vertebral numbers and human evolution. *American Journal of Physical Anthropology.* 2016;159:19-36.
60. Busscher I, Ploegmakers JJW, Verkerke GJ, Veldhuizen AG. Comparative anatomical dimensions of the complete human and porcine spine. *European Spine Journal.* 2010;19(7):1104-1114.